BIOCHEMICAL AND PHYSIOLOGICAL CHARACTERIZATION OF SECRETED PROTEINS REGULATING WHOLE-BODY ENERGY HOMEOSTASIS

By
Ashley Nicole Stewart

A dissertation submitted to Johns Hopkins University in conformity with the requirements for the degree of Doctor of Philosophy

Baltimore, Maryland
October 2020

Abstract

Interorgan communication mediated by secreted proteins is often disrupted in obesity, leading to insulin resistance, dyslipidemia, and cardiovascular disease. To further our understanding of the complex systems that regulate metabolic homeostasis, we investigated the biochemical and physiological properties of three secreted proteins. In our first two studies, we elucidated the role of posttranslational modifications (PTMs) in regulating the expression of two members of the C1q/TNF-Related Protein (CTRP) family. CTRP12 is a secreted regulator of glucose and lipid metabolism, and circulates in plasma as two distinct isoforms—a full-length protein and a cleaved, globular isoform—each of which preferentially activates different signaling pathways. We demonstrated that *N*-linked glycosylation found on one of three conserved asparagine residues regulates CTRP12 cleavage and stability. When *N*-linked glycosylation was inhibited by tunicamycin, glucosamine supplementation, or by mutation of the asparagine residue to glutamine, CTRP12 cleavage was enhanced. Lastly, cycloheximide chase analysis indicated reduced protein stability for under-glycosylated CTRP12. We next explored how PTMs impact secretion and multimerization of CTRP15, a secreted glycoprotein with metabolic function. We showed that abolishing N-linked glycosylation by tunicamycin, glucosamine supplementation, or asparagine to glutamine substitutions blocks myonectin secretion. Of CTRP15's four conserved cysteines, alanine substitution of either Cys-273 and Cys-278 inhibits protein secretion, while alanine substitutions of Cys-142 and Cys-194 markedly enhanced protein secretion. Formation of higher-

order structures via inter-molecular disulfide bonds critically depends on Cys-142 and Cys-194, as C142A and C194A mutations disrupted formation of high molecular weight oligomers. Finally, secretion of mutant lacking the highly hydroxylated collagen domain is strikingly reduced. In our final study, we describe the function of PRADC1, an enigmatic secretory protein widely expressed in humans and mice. Obese PRADC1-deficient female mice have reduced weight gain and adiposity due to increased metabolic rate, physical activity, and energy expenditure, but do not show improved systemic glucose and lipid metabolism. Thus, in PRADC1-deficient animals, decreased fat mass and enhanced physical activity are insufficient to confer a healthy metabolic phenotype in the context of an obesogenic diet. Taken together, our studies highlight novel functions of posttranslational modifications and a secreted protein in regulating systemic energy homeostasis.

Primary Reader and Advisor: Dr. G. William Wong

Secondary Reader: Dr. Steven Farber

Thesis Committee: Dr. G. William Wong

Dr. Paul Watkins

Dr. Steven Farber

Dr. Natasha Kralli

Acknowledgements

I would like to thank the person who first mentored me and fostered my passion for research. Dr. Peter Berget welcomed me into his lab when I was just a first-year college student. For nearly four years, he encouraged me, challenged me, and helped me realize my own potential. I am incredibly grateful to have had him as a part of my support system throughout my early years as a scientist.

I next want to thank my current advisor, Dr. William Wong. I am very fortunate to have received my training from such a driven and passionate scientist. Will's enthusiasm for science and excitement about our projects have pushed me forward throughout my graduate education. He trusted me to explore the scientific questions that interest me while still providing guidance when I needed it. I greatly appreciate Will's support of my professional development outside of the lab as well, which has allowed me to feel fulfilled as a member of the Johns Hopkins and Baltimore communities.

Dr. Damani Piggott and Dr. Steven Claypool have also been incredible mentors during my time at Hopkins. Both Damani and Steve have provided invaluable advice and support, and have helped me persist through my greatest challenges.

To my lab mates—Hannah, Susie, Dylan, Shelley, and Gel—I am grateful to have had you by my side over the past several years. I could always count on each of you for help when thinking through experiments, for teaching me new skills in the lab, and for laughs when I needed it.

I would like to thank my friends, Allatah Mekile, Amber DeGroot, and Helen Clark, who have inspired and encouraged me during the past several years. Thank you to José P Llongueras, who has made graduate school more fun than I could have thought possible.

I am so lucky to have such a large, loving and supportive family, who have all provided encouragement, inspiration, enthusiasm, and respite every step of the way. I would particularly like to thank my mom, my dad, and my sister, whose confidence in me and unconditional love carried me through.

Finally, I would like to thank my partner, Linda Marchlewski, whose unwavering love and support has meant so much to me. You've helped me more than I can put into words, and for that, I am incredibly grateful.

Dedication

This thesis is dedicated to my parents, Ena A. Stewart and Anthony T. Stewart, for their generous encouragement, support, and love.

Table of Contents

LIST OF TABLES

CHAPTER FOUR: PRADC1: A novel metabolic-responsive secretory protein that modulates physical activity and adiposity

LIST OF FIGURES

CHAPTER TWO: *N*-linked glycosylation dependent and independent mechanisms regulating CTRP12 cleavage, secretion, and stability

CHAPTER THREE: Protein modifications critical for myonectin/erythroferrone secretion and oligomer assembly

CHAPTER FOUR: PRADC1: A novel metabolic-responsive secretory protein that modulates physical activity and adiposity

CHAPTER 1:
Introduction

Secreted proteins play a critical role in maintaining proper energy balance in mammals. These proteins are dynamically regulated and mediate inter-organ crosstalk between tissues in order to coordinate responses to metabolic stress. Regulation of these hormones is often disrupted in the context of obesity, leading to insulin resistance, type 2 diabetes, dyslipidemia, and cardiovascular diseases (1–4) .

Our ability to prevent, treat, and cure these metabolic diseases is impeded by our incomplete understanding of the complex metabolic pathways that work to maintain glucose and lipid homeostasis. To address this challenge, we have characterized a highly conserved family of secreted proteins based on their homology to adiponectin, an adipose-derived anti-diabetic hormone. First described in 2004 (5) , the members of this protein family, designated C1q/TNF-Related Proteins (CTRP) 1-15, share the same domain structure as adiponectin. With the exception of CTRP4 (6) , each protein consists of an N-terminal domain with a signal peptide that promotes secretion, a collagen domain containing multiple Gly-X-Y repeats, and a C1q domain that is homologous to the C1q complement protein and structurally similar to TNF-α (7) .

CTRPs are collectively expressed in a wide range of tissues. Most are found circulating in plasma, and their levels change with the metabolic and nutritional state of an animal. Several functional studies have demonstrated important roles for CTRPs in metabolism (6, 8–16) , immunology (17–19) , the cardiovascular system, (20–26) ophthalmology (27–32) , and pulmonary physiology (33) . All CTRPs form trimers, mediated by disulfide bonds formed between conserved

cysteine residues found within their N-terminal domains (34) . Many also form higher order homo- and hetero- oligomers with adiponectin and other CTRPs (34–38) . In addition to disulfide bonds that enable multimerization, CTRPs contain various post-translational modifications (PTMs), including glycosylation and hydroxylation (34) . It is well understood that PTMs found on adiponectin are critical for the hormone's oligomerization (39–41) , stability (42, 43) , and secretion (40, 44, 45) . Furthermore, adiponectin's biological activity varies with its PTM and oligomeric state (46–48) , and disrupted ratios of circulating adiponectin oligomers are associated with obesity and type 2 diabetes (49–59) .

Despite clear ties between adiponectin PTMs and the hormone's bioactivity, the significance of PTMs in regulating CTRP expression, processing, and function remains largely unexplored. Given the important role CTRPs play in maintaining whole-body energy homeostasis, we sought to determine how various PTMs, including *N*-linked glycosylation, disulfide bonds, and hydroxylation, influence the expression, multimerization, and function of CTRPs. The following work focuses on PTM regulation of two members of this family, CTRP12 and CTRP15. In addition, we have also characterized a novel, metabolic-responsive secreted glycoprotein, PRADC1, in order to further our understanding of how secreted proteins work to maintain energy balance.

CTRP12

CTRP12 as a regulator of glucose metabolism and insulin sensitivity

CTRP12, also known as adipolin, is an antidiabetic, adipose-derived secreted protein that regulates glucose and lipid metabolism. Its expression is responsive to insulin. In cultured 3T3-L1 adipocytes, CTRP12 expression increased following insulin supplementation in a dose-dependent manner (60) . Insulin infusion in healthy, lean human subjects also increases circulating CTRP12 levels (61) . Treating cultured adipocytes, human adipose tissue explants, or human subjects with the insulin-sensitizing drugs rosiglitazone and metformin similarly increased CTRP12 transcript and protein levels (60–64) . These effects appear to be mediated by activation of AMPK, a key downstream target of insulin signaling, as treating human adipose tissue explants with an AMPK inhibitor blocks this increase in expression (63) . In both genetic and diet-induced mouse models of obesity, and in patients with type 2 diabetes, CTRP12 expression is decreased (60, 62, 65, 66) , suggesting that CTRP12 may be a useful biomarker for the prediction and early diagnosis of type 2 diabetes (66) . Taken together, these results illustrate the role of insulin signaling in regulating CTRP12 expression, and demonstrate that this regulation may be disrupted by obesity.

Once expressed and secreted into the bloodstream, CTRP12 improves glucose handling and insulin sensitivity. Increasing circulating CTRP12 levels through either acute adenovirus-mediated overexpression or by administering recombinant CTRP12 leads to reduced serum glucose and insulin levels in lean and obese mice (60, 62) . These mice also show improved insulin sensitivity,

demonstrated by faster glucose clearance from serum following injection with a bolus of glucose, lower post-prandial insulin levels, and a reduced homeostatic model assessment-insulin resistance (HOMA-IR) index. CTRP12 promotes glucose uptake in response to insulin by enhancing signaling through the PI3K-Akt pathway. In the livers and adipose tissue of both healthy and insulin-resistant mice, CTRP12 overexpression increased activation of critical insulin signaling molecules; phosphorylation of insulin receptor substrate (IRS-1) and Akt increased significantly in response to CTRP12 overexpression (60) . Enhanced Akt phosphorylation, along with phosphorylation of FOXO-1 and suppression of gluconeogenic genes PEPCK and G6Pase, was also observed in cultured hepatocytes and adipocytes. Use of a PI3K-specific inhibitor abolished these effects (60) . No changes in PI3K-Akt signaling were observed in the skeletal muscle of mice overexpressing CTRP12, or in cultured L6 myotubes. These results illustrate how CTRP12 acts as an anti-diabetic hormone by improving insulin sensitivity in liver and adipose tissue, and demonstrate its potential as a therapeutic for insulin resistance.

CTRP12 and lipid metabolism

Given the impact of obesity on CTRP12 expression we sought to determine whether CTRP12 plays a role in whole body lipid metabolism. Whereas Enomoto *et al.,* reported reduced adipocyte size and suppression of pro-inflammatory genes in cultured mouse macrophages in a CTRP12 overexpression model (62) , our group observed no influence of CTRP12 overexpression on adipocyte size or

adipose tissue inflammation in mice (60) . Interestingly, while overexpression did not modulate serum fatty acid or triglyceride levels (60, 62) , CTRP12 deficiency led to altered lipid homeostasis. In a heterozygous loss-of-function mouse model, losing one copy of CTRP12 resulted in increased hepatic fat oxidation and reduced VLDL-triglyceride secretion from the liver in male mice fed a low-fat diet (67) . Conversely, in the context of metabolic stress induced by high-fat feeding, CTRP12-deficient mice showed impaired lipid handling; serum fatty acid and triglyceride levels remained significantly higher that wildtype littermates after mice were gavaged with a bolus of emulsified lipid (67) . Elevated hepatic triglyceride and cholesterol levels accompanied by reduced hepatic triglyceride secretion in CTRP12-deficient mice resulted in greater liver steatosis than in wildtype littermates, suggesting that CTRP12 promotes mobilization of lipids from the liver (67) . These results differed from those seen in heterozygous female mice, which were indistinguishable from wildtype littermates on a low-fat diet, and showed enhanced hepatic triglyceride secretion and mild insulin resistance on a high-fat diet (67) . Taken together, these observations highlight the complexity of the components that regulate lipid homeostasis, and illustrate how these systems may be differentially disrupted in males and females in the context of obesity.

CTRP12 cleavage

Prior to secretion, CTRP12 is cleaved by furin proprotein convertase within the N-terminal domain, forming a cleaved, globular isoform (65, 68) . Both the globular (gCTRP12) and full-length (fCTRP12) isoforms are secreted (60) , and the ratio of

globular to full-length CTRP12 is disrupted in obesity (65) . In diet-induced obese mice, the proportion of gCTRP12 relative to fCTRP12 is increased (65) , indicating that proteolytic processing of the protein is regulated. Additionally, each isoform appears to have distinct functions. Although insulin treatment increases overall CTRP12 expression in cells (60) , this impact appears to be primarily driven by increased gCTRP12 expression, rather than by fCTRP12 (68) . Furthermore, each isoform activates distinct signaling pathways. In cultured hepatocytes and adipocytes, fCTRP12 treatment enhances IRS-1 and Akt phosphorylation, while gCTRP12 preferentially activates the MAPK signaling pathway (68) . Collectively, these results suggest that regulating CTRP12 cleavage may in turn regulate its function as an anti-diabetic hormone. Given CTRP12's important role as a regulator of glucose metabolism and insulin sensitivity, more work must be done to elucidate how this cleavage is controlled and dysregulated in the context of obesity. Chapter 2 describes my study investigating the role of *N*-linked glycosylation in regulating CTRP12 cleavage.

CTRP12 and cardiovascular disease

In addition to its involvement in maintaining whole body lipid and glucose homeostasis, CTRP12 is also implicated in cardiovascular disease. Patients with coronary artery disease showed significantly reduced serum CTRP12 levels, independent of body mass index and insulin resistance parameters (69) . Mice deficient in CTRP12 show worse recovery outcomes following vascular injury to the femoral artery, results that are mediated by the macrophage inflammatory

response (70) . In another study, Zhou *et al* developed an *in vitro* cardiomyocyte injury system, in which cardiomyocytes were treated with lipopolysaccharide (LPS) to model sepsis-induced cardiac injury (71) . CTRP12 overexpression suppressed hyperinflammation, reduced oxidative stress, and mitigated LPS-induced apoptosis, resulting in improved cardiomyocyte viability (71) . The study suggests that CTRP12 acts by increasing expression of nuclear factor E2-related factor 2 (NRF2), an antioxidant-responsive transcription factor that mitigates oxidative stress, though this mechanism of CTRP12 action has yet to be further explored. Collectively, these results demonstrate the cardioprotective properties of CTRP12.

In summary, CTRP12 is a secreted adipokine with anti-diabetic and anti-inflammatory properties. Several questions remain about the protein's structure and physiological roles in metabolism and cardiovascular health. Like all members of the CTRP family, no known CTRP12 receptor has been identified, precluding a complete understanding of the mechanisms underlying its physiology. With respect to protein structure, future studies should explore how differential *N*-linked glycosylation impacts CTRP12 bioactivity. Furthermore, more work must be done to elucidate the protein's specific role in the prevention of coronary artery disease and other cardiovascular diseases.

CTRP15/Myonectin

Myonectin as a regulator of whole-body lipid homeostasis

CTRP15, also termed myonectin, is expressed and secreted predominantly by the skeletal muscle, and mediates inter-organ crosstalk between three key metabolic tissues—skeletal muscle, liver, and adipose tissue. Myonectin expression is highly responsive to metabolic state, as demonstrated by both *in vitro* and *in vivo* experiments. Treating cultured myotubes with glucose, amino acids, or fatty acids stimulates myonectin expression (8) . Levels of circulating myonectin increase dramatically in response to exercise or feeding, while fasting reduces its expression (8) . In line with these observations, increasing intracellular cAMP or calcium levels in cultured myotubes via treatment with forskolin, epinephrine, or ionomycin also increases myonectin expression. These results suggest that acute fluctuations in nutritional state are sufficient to alter myonectin expression. Once produced, circulating myonectin works post-prandially to increase fatty acid uptake in peripheral tissues by upregulating transcription of proteins critical for fatty acid transport into cells (Cav1, Fabp1, CD36, and Fabp4) (8) . In response to infusion with recombinant myonectin, serum levels of non-esterified fatty acid (NEFA) in wildtype mice drop significantly. Similarly, in the context of metabolic stress induced by high fat feeding, myonectin-deficient mice show elevated NEFA and triglyceride levels in serum following an oral lipid gavage. These mice also show altered lipid storage in peripheral tissues, with reduced hepatic lipid content and larger adipose tissue depots (72) . These observations suggest that myonectin

stimulates lipid clearance in a tissue-specific manner, and plays a role in regulating lipid distribution among tissues.

While several studies associate insulin resistance and obesity with decreased myonectin expression (8, 73) , a few studies show an increase in myonectin expression in patients with type 2 diabetes (74–76) , suggesting a compensatory role for the protein. Thus, further studies must be performed to determine whether myonectin expression is dysregulated and contributes to insulin resistance, or if expression increases to compensate for metabolic dysfunction. Nonetheless, these findings collectively highlight myonectin's function as a nutrient-responsive myokine that integrates skeletal muscle, liver, and adipose tissue lipid metabolism.

Myonectin and exercise

In addition to fluxes in glucose and lipid levels, myonectin expression is also induced by exercise (8, 77–79) . Both acute (8, 77) and chronic (78) exercise result in elevated myonectin expression in mouse serum and skeletal muscle, respectively. These results have been recapitulated in humans. When obese women were subjected to eight weeks of aerobic exercise, their circulating myonectin levels increased significantly (79) , indicating a correlation between elevated myonectin levels and improved metabolic parameters associated with exercise. However, how myonectin contributes to these improved outcomes has yet to be determined. In a knockout mouse model, in response to either maximal sprint or endurance exercise on a treadmill, myonectin-deficient mice showed no

differences in total running distance, no changes in the post-exercise serum levels of glucose, lactate, NEFA, triglyceride, and ketone, and no changes in ability to replenish glycogen stores in their skeletal muscle or liver (72) . Taken together, these results suggest that although myonectin is not required for the improved metabolic response associated with exercise, it may play a role in regulating fatty acid metabolism within skeletal muscle,

Conversely, another group has demonstrated that changes in myonectin expression may directly contribute to the cardioprotective benefits of exercise. Otaka *et al.* found that myonectin acts to improve acute myocardial ischemic injury outcomes. In wildtype mice with exercise-induced, elevated myonectin expression, and in transgenic mice overexpressing myonectin, ischemia reperfusion injury resulted in reduced myocardial infarct size and cardiac dysfunction. Comparatively, myonectin-knockout mice showed worse cardiac outcomes (77) . In cultured myocytes, the authors found that myonectin inhibits apoptosis and reduces proinflammatory gene expression, suggesting a mechanism for these outcomes. This finding is in line with a previous study describing myonectin's role in suppressing autophagy in mouse liver and cultured hepatocytes (16) .

Myonectin and iron metabolism

Since we first identified myonectin/CTRP15 in 2012, it has also been described as erythroferrone, as it is secreted from erythroblasts and regulates iron metabolism following significant blood loss (80) . In response to stress erythropoiesis, myonectin/erythroferrone acts to mobilize iron stores from the liver and spleen by

suppressing expression of hepcidin, a liver-derived hormone that inhibits the cellular iron exporter ferroportin (81) . While several studies have demonstrated a link between imbalances in iron homeostasis and the development of diabetes (82–88) , the role myonectin plays in this observation has yet to be explored.

Despite extensive research on CTRP15, more work must be done to fully elucidate its role in nutrient metabolism, exercise physiology, and iron metabolism. Whether myonectin contributes, directly or indirectly, to improved metabolic outcomes associated with exercise is of particular interest. In addition, the mechanisms underlying myonectin's tissue-specific regulation of fat metabolism remain unknown. Finally, a complete understanding of how myonectin bioactivity is exerted will remain out of reach until the protein's receptor is identified.

PRADC1

Chapter 4 details a study on protease-associated domain-containing 1 (PRADC1), an enigmatic secreted glycoprotein that was first identified in 2004 (89) . Two genetics studies have associated the *Pradc1* gene with metabolism (90) and familial colorectal cancer (91) . Nonetheless, very little is known of this protein's function. Also known as protease-associated domain-containing protein, 21 kDa (PAP21), it is highly expressed in metabolic-responsive tissues (skeletal muscle, heart, and liver), and requires *N*-linked glycosylation for secretion (89) . Given this striking expression pattern, we hypothesized that PRADC1 is involved in regulating

whole-body energy homeostasis, and responds to changes in metabolic state. However, what role this novel secreted protein plays in regulating energy metabolism has not been explored. Thus, in Chapter 4, we describe the first functional study of PRADC1.

References

1. Spiegelman, B., and Flier, J. (2001) Obesity and the Regulation of Energy Balance. *Cell*, 531–543
2. Rosen, E., and Spiegelman, B. (2006) Adipocytes as regulators of energy balance and glucose homeostasis. *Nature*, 847–853
3. Friedman, J., and Halaas, J. (1998) Leptin and the regulation of body weight in mammals. *Nature*, 763–770
4. Trujillo, M., and Scherer, P. (2006) Adipose tissue-derived factors: impact on hea lth and disease. *Endocrine reviews*, 762–78
5. Wong, G. W., Wang, J., Hug, C., Tsao, T.-S. S., and Lodish, H. F. (2004) A family of Acrp30/adiponectin structural and functional paralogs. *Proc. Natl. Acad. Sci. U.S.A.* **101**, 10302–7
6. Byerly, M. S., Petersen, P. S., Ramamurthy, S., Seldin, M. M., Lei, X., Provost, E., Wei, Z., Ronnett, G. V., and Wong, G. W. (2014) C1q/TNF-related protein 4 (CTRP4) is a unique secreted protein with two tandem C1q domains that functions in the hypothalamus to modulate food intake and body weight. *J. Biol. Chem.* **289**, 4055–69
7. Seldin, M. M., Tan, S. Y., and Wong, G. W. (2014) Metabolic function of the CTRP family of hormones. *Rev Endocr Metab Disord* **15**, 111–23
8. Seldin, M. M., Peterson, J. M., Byerly, M. S., Wei, Z., and Wong, G. W. (2012) Myonectin (CTRP15), a novel myokine that links skeletal muscle to systemic lipid homeostasis. *J. Biol. Chem.* **287**, 11968–80
9. Byerly, M. S., Swanson, R., Wei, Z., Seldin, M. M., McCulloh, P. S., and Wong, G. W. (2013) A central role for C1q/TNF-related protein 13 (CTRP13) in modulating food intake and body weight. *PLoS ONE* **8**, e62862
10. Peterson, J. M., Aja, S., Wei, Z., and Wong, G. W. (2012) CTRP1 protein enhances fatty acid oxidation via AMP-activated protein kinase (AMPK) activation and acetyl-CoA carboxylase (ACC) inhibition. *J. Biol. Chem.* **287**, 1576–87
11. Peterson, J. M., Seldin, M. M., Tan, S. Y., and Wong, G. W. (2014) CTRP2 overexpression improves insulin and lipid tolerance in diet-induced obese mice. *PLoS ONE* **9**, e88535
12. Peterson, J. M., Seldin, M. M., Wei, Z., Aja, S., and Wong, G. W. (2013) CTRP3 attenuates diet-induced hepatic steatosis by regulating triglyceride metabolism. *Am. J. Physiol. Gastrointest. Liver Physiol.* **305**, G214–24
13. Lei, X., Rodriguez, S., Petersen, P. S., Seldin, M. M., Bowman, C. E., Wolfgang, M. J., and Wong, G. W. (2016) Loss of CTRP5 improves insulin action and hepatic steatosis. *Am. J. Physiol. Endocrinol. Metab.* **310**, E1036–52
14. Rodriguez, S., Lei, X., Petersen, P. S., Tan, S. Y., Little, H. C., and Wong, G. W. (2016) Loss of CTRP1 disrupts glucose and lipid homeostasis. *Am. J. Physiol. Endocrinol. Metab.* **311**, E678–E697
15. Wei, Z., Lei, X., Petersen, P. S., Aja, S., and Wong, G. W. (2014) Targeted deletion of C1q/TNF-related protein 9 increases food intake, decreases insulin sensitivity, and promotes hepatic steatosis in mice. *Am. J. Physiol. Endocrinol. Metab.* **306**, E779–90
16. Seldin, M. M., Lei, X., Tan, S. Y., Stanson, K. P., Wei, Z., and Wong, G. W. (2013) Skeletal muscle-derived myonectin activates the mammalian target of

rapamycin (mTOR) pathway to suppress autophagy in liver. *J. Biol. Chem.* **288**, 36073–82
17. Lu, L., Zhang, R., Wang, X., Liu, Z., Shen, Y., Ding, F., Meng, H., Wang, L., Yan, X., Yang, K., Wang, H., Pu, L., Zhang, Q., Chen, Q., Caterina, R., and Shen, W. (2015) C1q/TNF-related protein-1: an adipokine marking and promoting atherosclerosis. *European heart journal*, 1762–71
18. Hofmann, C., Chen, N., Obermeier, F., Paul, G., Büchler, C., Kopp, A., Falk, W., and Schäffler, A. (2011) C1q/TNF-related protein-3 (CTRP-3) is secreted by visceral adipose tissue and exerts antiinflammatory and antifibrotic effects in primary human colonic fibroblasts. *Inflammatory Bowel Diseases*, 2462–2471
19. Schäffler, A., and Buechler, C. (2012) CTRP family: linking immunity to metabolism. *Trends Endocrinol. Metab.* **23**, 194–204
20. Akiyama, H., Furukawa, S., Wakisaka, S., and Maeda, T. (2007) CTRP3/cartducin promotes proliferation and migration of endothelial cells. *Mol. Cell. Biochem.* **304**, 243–8
21. Zhu, H., Ding, Y., Zhang, Y., Ding, X., Zhao, J., Ouyang, W., Gong, J., Zou, Y., Liu, X., and Wu, W. (2020) CTRP3 induces an intermediate switch of CD14++CD16+ monocyte subset with anti-inflammatory phenotype. *Exp Ther Med* **19**, 2243–2251
22. Zhang, C.-L. L., Chen, Z.-J. J., Feng, H., Zhao, Q., Cao, Y.-P. P., Li, L., Wang, J.-Y. Y., Zhang, Y., and Wu, L.-L. L. (2017) C1q/tumor necrosis factor-related protein-3 enhances the contractility of cardiomyocyte by increasing calcium sensitivity. *Cell Calcium* **66**, 90–97
23. Kambara, T., Ohashi, K., Shibata, R., Ogura, Y., Maruyama, S., Enomoto, T., Uemura, Y., Shimizu, Y., Yuasa, D., Matsuo, K., Miyabe, M., Kataoka, Y., Murohara, T., and Ouchi, N. (2012) CTRP9 Protein Protects against Myocardial Injury following Ischemia-Reperfusion through AMP-activated Protein Kinase (AMPK)-dependent Mechanism. *Journal of Biological Chemistry*, 18965–18973
24. Zhao, D., Feng, P., Sun, Y., Qin, Z., Zhang, Z., Tan, Y., Gao, E., Lau, W., Ma, X., Yang, J., Yu, S., Xu, X., Yi, D., and Yi, W. (2018) Cardiac-derived CTRP9 protects against myocardial ischemia/reperfusion injury via calreticulin-dependent inhibition of apoptosis. *Cell Death & Disease*, 723
25. Kambara, T., Shibata, R., Ohashi, K., Matsuo, K., Hiramatsu-Ito, M., Enomoto, T., Yuasa, D., Ito, M., Hayakawa, S., Ogawa, H., Aprahamian, T., Walsh, K., Murohara, T., and Ouchi, N. (2015) C1q/Tumor Necrosis Factor-Related Protein 9 Protects against Acute Myocardial Injury through an Adiponectin Receptor I-AMPK-Dependent Mechanism. *Molecular and Cellular Biology*, 2173–2185
26. Liu, F., Tan, A., Yang, R., Xue, Y., Zhang, M., Chen, L., Xiao, L., Yang, X., and Yu, Y. (2017) C1ql1/Ctrp14 and C1ql4/Ctrp11 promote angiogenesis of endothelial cells through activation of ERK1/2 signal pathway. *Mol. Cell. Biochem.* **424**, 57–67
27. Tu, X., and Palczewski, K. (2012) Crystal structure of the globular domain of C1QTNF5: Implications for late-onset retinal macular degeneration. *J. Struct. Biol.* **180**, 439–46
28. Hayward, C., Shu, X., Cideciyan, A., Lennon, A., Barran, P., Zareparsi, S., Sawyer, L., Hendry, G., Dhillon, B., Milam, A., Luthert, P., Swaroop, A., Hastie, N., Jacobson, S., and Wright, A. (2003) Mutation in a short-chain collagen gene, CTRP5 , results in extracellular deposit formation in late-onset retinal degeneration: a genetic model for age-related macular degeneration. *Human Molecular Genetics*, 2657–2667

29. Ayyagari, R., Mandal, M., Karoukis, A., Chen, L., McLaren, N., Lichter, M., Wong, D., Hitchcock, P., Caruso, R., Moroi, S., Maumenee, I., and Sieving, P. (2005) Late-Onset Macular Degeneration and Long Anterior Lens Zonules Result from a CTRP5 Gene Mutation. *Investigative Ophthalmology & Visual Science*, 3363–3371
30. Shu, X., Tulloch, B., Lennon, A., Vlachantoni, D., Zhou, X., Hayward, C., and Wright, A. (2006) Disease mechanisms in late-onset retinal macular degeneration associated with mutation in C1QTNF5. *Human Molecular Genetics*, 1680–1689
31. Stanton, C., Borooah, S., Drake, C., Marsh, J., Campbell, S., Lennon, A., Soares, D., Vallabh, N., Sahni, J., Cideciyan, A., Dhillon, B., Vitart, V., Jacobson, S., Wright, A., and Hayward, C. (2017) Novel pathogenic mutations in C1QTNF5 support a dominant negative disease mechanism in late-onset retinal degeneration. *Scientific Reports*, 12147
32. Chavali, V., Khan, N., Cukras, C., Bartsch, D.-U., Jablonski, M., and Ayyagari, R. (2011) A CTRP5 gene S163R mutation knock-in mouse model for late-onset retinal degeneration. *Human Molecular Genetics*, 2000–2014
33. Li, D., Wu, Y., Tian, P., Zhang, X., Wang, H., Wang, T., Ying, B., Wang, L., Shen, Y., and Wen, F. (2015) Adipokine CTRP-5 as a Potential Novel Inflammatory Biomarker in Chronic Obstructive Pulmonary Disease. *Medicine (Baltimore)* **94**, e1503
34. Wong, G. W., Krawczyk, S. A., Kitidis-Mitrokostas, C., Revett, T., Gimeno, R., and Lodish, H. F. (2008) Molecular, biochemical and functional characterizations of C1q/TNF family members: adipose-tissue-selective expression patterns, regulation by PPAR-gamma agonist, cysteine-mediated oligomerizations, combinatorial associations and metabolic functions. *Biochem. J.* **416**, 161–77
35. Wong, W., Krawczyk, S., Kitidis-Mitrokostas, C., Ge, G., Spooner, E., Hug, C., Gimeno, R., and Lodish, H. (2009) Identification and characterization of CTRP9, a novel secreted glycoprotein, from adipose tissue that reduces serum glucose in mice and forms heterotrimers with adiponectin. *Faseb J* **23**, 241–258
36. Peterson, J., Wei, Z., and Wong, W. (2009) CTRP8 and CTRP9B are novel proteins that hetero-oligomerize with C1q/TNF family members. *Biochemical and Biophysical Research Communications*, 360–365
37. Wei, Z., Seldin, M., Natarajan, N., Djemal, D., Peterson, J., and Wong, W. (2013) C1q/Tumor Necrosis Factor-related Protein 11 (CTRP11), a Novel Adipose Stroma-derived Regulator of Adipogenesis. *Journal of Biological Chemistry*, 10214–10229
38. Wei, Z., Peterson, J., and Wong, W. (2011) Metabolic Regulation by C1q/TNF-related Protein-13 (CTRP13) ACTIVATION OF AMP-ACTIVATED PROTEIN KINASE AND SUPPRESSION OF FATTY ACID-INDUCED JNK SIGNALING. *Journal of Biological Chemistry*, 15652–15665
39. Wang, Y., Lam, K., Chan, L., Chan, K., Lam, J., Lam, M., Hoo, R., Mak, W., Cooper, G., and Xu, A. (2006) Post-translational Modifications of the Four Conserved Lysine Residues within the Collagenous Domain of Adiponectin Are Required for the Formation of Its High Molecular Weight Oligomeric Complex. *Journal of Biological Chemistry*, 16391–16400
40. Ruotsalainen, H., Risteli, M., Wang, C., Wang, Y., Karppinen, M., Bergmann, U., Kvist, A.-P. P., Pospiech, H., Herzig, K.-H. H., and Myllylä, R. (2012) The activities of lysyl hydroxylase 3 (LH3) regulate the amount and oligomerization status of adiponectin. *PLoS ONE* **7**, e50045

41. Richards, A., Stephens, T., Charlton, H., Jones, A., Macdonald, G., Prins, J., and Whitehead, J. (2006) Adiponectin multimerization is dependent on conserved lysines in the collagenous domain: evidence for regulation of multimerization by alterations in posttranslational modifications. *Molecular endocrinology (Baltimore, Md.)*, 1673–87
42. Richards, A., Colgrave, M., Zhang, J., Webster, J., Simpson, F., Preston, E., Wilks, D., Hoehn, K., Stephenson, M., Macdonald, G., Prins, J., Cooney, G., Xu, A., and Whitehead, J. (2009) Sialic acid modification of adiponectin is not required for multimerization or secretion but determines half-life in circulation. *Molecular endocrinology (Baltimore, Md.)*, 229–39
43. Peake, P., Hughes, J., Shen, Y., and Charlesworth, J. (2007) Glycosylation of human adiponectin affects its conformation and stability. *Journal of molecular endocrinology*, 45–52
44. Wang, Z., Schraw, T., Kim, J.-Y., Khan, T., Rajala, M., Follenzi, A., and Scherer, P. (2007) Secretion of the Adipocyte-Specific Secretory Protein Adiponectin Critically Depends on Thiol-Mediated Protein Retention ▿ †. *Molecular and Cellular Biology*, 3716–3731
45. Qiang, L., Wang, H., and Farmer, S. R. (2007) Adiponectin secretion is regulated by SIRT1 and the endoplasmic reticulum oxidoreductase Ero1-L alpha. *Mol. Cell. Biol.* **27**, 4698–707
46. Pajvani, U., Du, X., Combs, T., Berg, A., Rajala, M., Schulthess, T., Engel, J., Brownlee, M., and Scherer, P. (2003) Structure-Function Studies of the Adipocyte-secreted Hormone Acrp30/Adiponectin IMPLICATIONS FOR METABOLIC REGULATION AND BIOACTIVITY. *Journal of Biological Chemistry*, 9073–9085
47. Schraw, T., Wang, Z. V., Halberg, N., Hawkins, M., and Scherer, P. E. (2008) Plasma adiponectin complexes have distinct biochemical characteristics. *Endocrinology* **149**, 2270–82
48. Chen, X., Yuan, Y., Wang, Q., Xie, F., Xia, D., Wang, X., Wei, Y., and Xie, T. (2017) Post-Translational Modification of Adiponectin Affects Lipid Accumulation, Proliferation and Migration of Vascular Smooth Muscle Cells. *Cellular Physiology and Biochemistry*, 172–181
49. De Rosa, A., Monaco, M. L., Capasso, M., Forestieri, P., Pilone, V., Nardelli, C., Buono, P., and Daniele, A. (2013) Adiponectin oligomers as potential indicators of adipose tissue improvement in obese subjects. *Eur. J. Endocrinol.* **169**, 37–43
50. Pajvani, U., Hawkins, M., Combs, T., Rajala, M., Doebber, T., Berger, J., Wagner, J., Wu, M., Knopps, A., Xiang, A., Utzschneider, K., Kahn, S., Olefsky, J., Buchanan, T., and Scherer, P. (2004) Complex Distribution, Not Absolute Amount of Adiponectin, Correlates with Thiazolidinedione-mediated Improvement in Insulin Sensitivity. *Journal of Biological Chemistry*, 12152–12162
51. Bobbert, T., Rochlitz, H., Wegewitz, U., Akpulat, S., Mai, K., Weickert, M., Möhlig, M., Pfeiffer, A., and Spranger, J. (2005) Changes of Adiponectin Oligomer Composition by Moderate Weight Reduction. *Diabetes*, 2712–2719
52. Hara, K., Horikoshi, M., Yamauchi, T., Yago, H., Miyazaki, O., Ebinuma, H., Imai, Y., Nagai, R., and Kadowaki, T. (2006) Measurement of the High–Molecular Weight Form of Adiponectin in Plasma Is Useful for the Prediction of Insulin Resistance and Metabolic Syndrome. *Diabetes Care*, 1357–1362
53. Nakashima, R., Kamei, N., Yamane, K., Nakanishi, S., Nakashima, A., and Kohno, N. (2006) Decreased total and high molecular weight adiponectin are independent risk factors for the development of type 2 diabetes in Japanese-Americans. *The Journal of clinical endocrinology and metabolism*, 3873–7

54. Basu, R., Pajvani, U., Rizza, R., and Scherer, P. (2007) Selective Downregulation of the High–Molecular Weight Form of Adiponectin in Hyperinsulinemia and in Type 2 Diabetes Differential Regulation From Nondiabetic Subjects. *Diabetes*, 2174–2177
55. Liu, Y., Retnakaran, R., Hanley, A., Tungtrongchitr, R., Shaw, C., and Sweeney, G. (2007) Total and high molecular weight but not trimeric or hexameric forms of adiponectin correlate with markers of the metabolic syndrome and liver injury in Thai subjects. *The Journal of clinical endocrinology and metabolism*, 4313–8
56. Aso, Yamamoto, Suetsugu, Matsumoto, Wakabayashi, Matsutomo, Takebayashi, and Inukai (2007) Comparison of the effects of pioglitazone and voglibose on circulating total and high-molecular-weight adiponectin, and on two fibrinolysis inhibitors, in patients with Type 2 diabetes. *Diabetic Medicine*, 962–968
57. Seino, Y., Hirose, H., Saito, I., and Itoh, H. (2007) High molecular weight multimer form of adiponectin as a useful marker to evaluate insulin resistance and metabolic syndrome in Japanese men. *Metabolism*, 1493–1499
58. Heidemann, C., Sun, Q., van Dam, R., Meigs, J., Zhang, C., Tworoger, S., Mantzoros, C., and Hu, F. (2008) Total and high-molecular-weight adiponectin and resistin in relation to the risk for type 2 diabetes in women. *Annals of internal medicine*, 307–16
59. F Fisher, f., Trujillo, Hanif, Barnett, McTernan, Scherer, and Kumar (2005) Serum high molecular weight complex of adiponectin correlates better with glucose tolerance than total serum adiponectin in Indo-Asian males. *Diabetologia*, 1084–1087
60. Wei, Z., Peterson, J. M., Lei, X., Cebotaru, L., Wolfgang, M. J., Baldeviano, G. C., and Wong, G. W. (2012) C1q/TNF-related protein-12 (CTRP12), a novel adipokine that improves insulin sensitivity and glycemic control in mouse models of obesity and diabetes. *J. Biol. Chem.* **287**, 10301–15
61. Tan, B. K., Lewandowski, K. C., O'Hare, J. P., and Randeva, H. S. (2014) Insulin regulates the novel adipokine adipolin/CTRP12: in vivo and ex vivo effects. *J. Endocrinol.* **221**, 111–9
62. Enomoto, T., Ohashi, K., Shibata, R., Higuchi, A., Maruyama, S., Izumiya, Y., Walsh, K., Murohara, T., and Ouchi, N. (2011) Adipolin/C1qdc2/CTRP12 protein functions as an adipokine that improves glucose metabolism. *J. Biol. Chem.* **286**, 34552–8
63. Tan, B. K., Chen, J., Adya, R., Ramanjaneya, M., Patel, V., and Randeva, H. S. (2013) Metformin increases the novel adipokine adipolin/CTRP12: role of the AMPK pathway. *J. Endocrinol.* **219**, 101–8
64. Tan, B. K., Chen, J., Hu, J., Amar, O., Mattu, H. S., Ramanjaneya, M., Patel, V., Lehnert, H., and Randeva, H. S. (2014) Circulatory changes of the novel adipokine adipolin/CTRP12 in response to metformin treatment and an oral glucose challenge in humans. *Clin. Endocrinol. (Oxf)* **81**, 841–6
65. Enomoto, T., Shibata, R., Ohashi, K., Kambara, T., Kataoka, Y., Uemura, Y., Yuasa, D., Murohara, T., and Ouchi, N. (2012) Regulation of adipolin/CTRP12 cleavage by obesity. *Biochem. Biophys. Res. Commun.* **428**, 155–9
66. Bai, B., Ban, B., Liu, Z., Zhang, M. M., Tan, B. K., and Chen, J. (2017) Circulating C1q complement/TNF-related protein (CTRP) 1, CTRP9, CTRP12 and CTRP13 concentrations in Type 2 diabetes mellitus: In vivo regulation by glucose. *PLoS ONE* **12**, e0172271
67. Tan, S. Y., Little, H. C., Lei, X., Li, S., Rodriguez, S., and Wong, G. W. (2016) Partial deficiency of CTRP12 alters hepatic lipid metabolism. *Physiol. Genomics* **48**, 936–949

68. Wei, Z., Lei, X., Seldin, M. M., and Wong, G. W. (2012) Endopeptidase cleavage generates a functionally distinct isoform of C1q/tumor necrosis factor-related protein-12 (CTRP12) with an altered oligomeric state and signaling specificity. *J. Biol. Chem.* **287**, 35804–14
69. Fadaei, R., Moradi, N., Kazemi, T., Chamani, E., Azdaki, N., Moezibady, S. A., Shahmohamadnejad, S., and Fallah, S. (2019) Decreased serum levels of CTRP12/adipolin in patients with coronary artery disease in relation to inflammatory cytokines and insulin resistance. *Cytokine* **113**, 326–331
70. Ogawa, H., Ohashi, K., Ito, M., Shibata, R., Kanemura, N., Yuasa, D., Kambara, T., Matsuo, K., Hayakawa, S., Hiramatsu-Ito, M., Otaka, N., Kawanishi, H., Yamaguchi, S., Enomoto, T., Abe, T., Kaneko, M., Takefuji, M., Murohara, T., and Ouchi, N. (2020) Adipolin/CTRP12 protects against pathological vascular remodelling through suppression of smooth muscle cell growth and macrophage inflammatory response. *Cardiovasc. Res.* **116**, 237–249
71. Zhou, M.-Q. Q., Jin, E., Wu, J., Ren, F., Yang, Y.-Z. Z., and Duan, D.-D. D. (2020) CTRP12 Ameliorated Lipopolysaccharide-Induced Cardiomyocyte Injury. *Chem. Pharm. Bull.* **68**, 133–139
72. Little, H. C., Rodriguez, S., Lei, X., Tan, S. Y., Stewart, A. N., Sahagun, A., Sarver, D. C., and Wong, G. W. (2019) Myonectin deletion promotes adipose fat storage and reduces liver steatosis. *FASEB J.* **33**, 8666–8687
73. Li, Z., Yang, Y.-L. L., Zhu, Y.-J. J., Li, C.-G. G., Tang, Y.-Z. Z., Ni, C.-L. L., Chen, L.-M. M., and Niu, W.-Y. Y. (2019) Circulating Serum Myonectin Levels in Obesity and Type 2 Diabetes Mellitus. *Exp. Clin. Endocrinol. Diabetes*
74. Toloza, F. J. K. J., Mantilla-Rivas, J. O., Pérez-Matos, M. C., Ricardo-Silgado, M. L., Morales-Alvarez, M. C., Pinzón-Cortés, J. A., Pérez-Mayorga, M., Arévalo-Garcia, M. L., Tolosa-González, G., and Mendivil, C. O. (2018) Plasma Levels of Myonectin But Not Myostatin or Fibroblast-Derived Growth Factor 21 Are Associated with Insulin Resistance in Adult Humans without Diabetes Mellitus. *Front Endocrinol (Lausanne)* **9**, 5
75. Li, K., Liao, X., Wang, K., Mi, Q., Zhang, T., Jia, Y., Xu, X., Luo, X., Zhang, C., Liu, H., Zhen, H., Li, L., and Yang, G. (2018) Myonectin Predicts the Development of Type 2 Diabetes. *J. Clin. Endocrinol. Metab.* **103**, 139–147
76. Gamas, L., Matafome, P., and Seiça, R. (2015) Irisin and Myonectin Regulation in the Insulin Resistant Muscle: Implications to Adipose Tissue: Muscle Crosstalk. *J Diabetes Res* **2015**, 359159
77. Otaka, N., Shibata, R., Ohashi, K., Uemura, Y., Kambara, T., Enomoto, T., Ogawa, H., Ito, M., Kawanishi, H., Maruyama, S., Joki, Y., Fujikawa, Y., Narita, S., Unno, K., Kawamoto, Y., Murate, T., Murohara, T., and Ouchi, N. (2018) Myonectin Is an Exercise-Induced Myokine That Protects the Heart From Ischemia-Reperfusion Injury. *Circ. Res.* **123**, 1326–1338
78. Peterson, J. M., Mart, R., and Bond, C. E. (2014) Effect of obesity and exercise on the expression of the novel myokines, Myonectin and Fibronectin type III domain containing 5. *PeerJ* **2**, e605
79. Pourranjbar, M., Arabnejad, N., Naderipour, K., and Rafie, F. (2018) Effects of Aerobic Exercises on Serum Levels of Myonectin and Insulin Resistance in Obese and Overweight Women. *J Med Life* **11**, 381–386
80. Kautz, L., Jung, G., Valore, E. V., Rivella, S., Nemeth, E., and Ganz, T. (2020) Author Correction: Identification of erythroferrone as an erythroid regulator of iron metabolism. *Nat. Genet.*

81. Nemeth, E., Tuttle, M. S., Powelson, J., Vaughn, M. B., Donovan, A., Ward, D. M., Ganz, T., and Kaplan, J. (2004) Hepcidin regulates cellular iron efflux by binding to ferroportin and inducing its internalization. *Science* **306**, 2090–3
82. Jiang, R., Ma, J., Ascherio, A., Stampfer, M. J., Willett, W. C., and Hu, F. B. (2004) Dietary iron intake and blood donations in relation to risk of type 2 diabetes in men: a prospective cohort study. *Am. J. Clin. Nutr.* **79**, 70–5
83. Fernández-Real, J. M. M., López-Bermejo, A., and Ricart, W. (2005) Iron stores, blood donation, and insulin sensitivity and secretion. *Clin. Chem.* **51**, 1201–5
84. Cooksey, R. C., Jouihan, H. A., Ajioka, R. S., Hazel, M. W., Jones, D. L., Kushner, J. P., and McClain, D. A. (2004) Oxidative stress, beta-cell apoptosis, and decreased insulin secretory capacity in mouse models of hemochromatosis. *Endocrinology* **145**, 5305–12
85. Merkel, P. A., Simonson, D. C., Amiel, S. A., Plewe, G., Sherwin, R. S., Pearson, H. A., and Tamborlane, W. V. (1988) Insulin resistance and hyperinsulinemia in patients with thalassemia major treated by hypertransfusion. *N. Engl. J. Med.* **318**, 809–14
86. Lee, H. J., Choi, J. S., Lee, H. J., Kim, W.-H. H., Park, S. I., and Song, J. (2015) Effect of excess iron on oxidative stress and gluconeogenesis through hepcidin during mitochondrial dysfunction. *J. Nutr. Biochem.* **26**, 1414–23
87. Willmann, C., Heni, M., Linder, K., Wagner, R., Stefan, N., Machann, J., Schulze, M. B., Joost, H.-G. G., Häring, H.-U. U., and Fritsche, A. (2019) Potential effects of reduced red meat compared with increased fiber intake on glucose metabolism and liver fat content: a randomized and controlled dietary intervention study. *Am. J. Clin. Nutr.* **109**, 288–296
88. Liang, Y., Bajoria, R., Jiang, Y., Su, H., Pan, H., Xia, N., Chatterjee, R., and Lai, Y. (2017) Prevalence of diabetes mellitus in Chinese children with thalassaemia major. *Trop. Med. Int. Health* **22**, 716–724
89. Zhou, Y.-B. B., Liu, F., Zhu, Z.-D. D., Zhu, H., Zhang, X., Wang, Z.-Q. Q., Liu, J.-H. H., and Han, Z.-G. G. (2004) N-glycosylation is required for efficient secretion of a novel human secreted glycoprotein, hPAP21. *FEBS Lett.* **576**, 401–7
90. Ghosh, S., Hota, M., Chai, X., Kiranya, J., Ghosh, P., He, Z., Ruiz-Ramie, J. J., Sarzynski, M. A., and Bouchard, C. (2019) Exploring the underlying biology of intrinsic cardiorespiratory fitness through integrative analysis of genomic variants and muscle gene expression profiling. *J. Appl. Physiol.* **126**, 1292–1314
91. Gylfe AE, Katainen R, Kondelin J, Tanskanen T, Cajuso T, Hänninen U, Taipale J, Taipale M, Renkonen-Sinisalo L, Järvinen H, Mecklin JP, Kilpivaara O, Pitkänen E, Vahteristo P, Tuupanen S, Karhu A, Aaltonen LA. (2013) Eleven candidate susceptibility genes for common familial colorectal cancer. *PLoS Genet.* **9**, e1003876.

CHAPTER 2:

N-linked glycosylation dependent and independent mechanisms regulating CTRP12 cleavage, secretion, and stability*

*Text and figures in this chapter were published in *Biochemistry* in 2018:

N-Linked Glycosylation-Dependent and -Independent Mechanisms Regulating CTRP12 Cleavage, Secretion, and Stability. Ashley N. Stewart, Stefanie Y. Tan, David J. Clark, Hui Zhang, and G. William Wong, *Biochemistry* 2019 58 (6), 727-741

Ashley Stewart generated data for all figures with the exception of Figure 1A (GWW) and Figure 2A (DJC and HZ).

Abstract

C1q/TNF-related protein 12 (CTRP12) is a secreted regulator of glucose and lipid metabolism. It circulates in plasma as a full-length protein or as a cleaved isoform generated by furin/PCSK3 cleavage. These isoforms preferentially activate different signaling pathways and their ratio in plasma is altered in obesity and diabetes. Here, we show that three conserved asparagine residues (Asn-39, Asn-287, and Asn-297) play important roles in modulating CTRP12 cleavage, secretion, and stability. Mass spectrometry analysis provided direct evidence of Asn-39 glycosylation. When *N*-linked glycosylation was inhibited by tunicamycin or abolished by N39Q, N39A, or T41A mutation, CTRP12 cleavage was enhanced. Complex-type *N*-glycans on CTRP12 blocked cleavage by the Golgi-localized furin. In N-acetyl glucosaminyltransferase I (GnTI)-deficient cells that could not form hybrid and complex-type *N*-glycans in the Golgi, CTRP12 cleavage was enhanced, and re-expressing GnTI reduced cleavage. Replacing the non-glycosylated Asn-297 with glutamine or alanine also increased CTRP12 cleavage. Both Asn-39 and Asn-297 contributed independently to CTRP12 cleavage: maximum cleavage was observed in the double mutant. Further, CTRP12 cleavage was abolished in furin-deficient cells and restored by furin re-expression. Replacing the non-glycosylated Asn-287 with glutamine or alanine resulted in protein misfolding and aggregation, leading to retention in the endoplasmic reticulum. Cycloheximide chase analyses indicated reduced protein stability for N39Q, T41A, and N297Q mutants. Lastly, we show that increasing flux through

the hexosamine biosynthesis pathway by exogenous glucosamine, known to disrupt protein glycosylation, also promoted CTRP12 cleavage. Combined, these data highlight glycosylation-dependent and independent mechanisms regulating CTRP12 cleavage, secretion, and protein stability.

Introduction

CTRPs are a conserved family of secreted plasma proteins (1-9). They belong to the larger C1q family of proteins and each possesses the signature C-terminal globular domain homologous to immune complement C1q (10,11). Recent *in vivo* studies using recombinant protein supplementation or transgenic and knockout mouse models have revealed important functions for multiple CTRP family members in modulating insulin action and glucose and lipid metabolism (7,8,12-23).

We identified CTRP12 (encoded by the *C1QTNF12* gene) on the basis of shared sequence homology with other previously characterized CTRP family members (4,24). Independently, Enomoto et al. also identified CTRP12/adipolin as an adipose-enriched transcript that encodes a novel adipokine (25). CTRP12 expression in mice is modulated by metabolic and physiological states and its transcript level is downregulated in obesity and diabetes (4,25) and upregulated in the context of enhanced insulin sensitivity (26). Insulin infusion in healthy lean humans can acutely increase plasma CTRP12 levels (27). Treatment with anti-

diabetic drugs (e.g., rosiglitazone and metformin) also increases the expression and secretion of CTRP12 in human adipose tissue (27-29).

Using recombinant protein infusion and adenoviral overexpression approaches, we and others have demonstrated an anti-diabetic (4) and anti-inflammatory (25) function for CTRP12 in both genetic (*ob/ob*) and dietary (high-fat feeding) mouse models of obesity and diabetes. CTRP12 regulates glucose metabolism in liver and adipose tissue through insulin-dependent and independent pathways (4). Partial deficiency of CTRP12, resulting from targeted inactivation of a single copy of the *Ctrp12* allele in mice, alters lipid metabolism in liver in a sex-dependent manner (30).

CTRP12 that circulates in plasma and is secreted from adipocytes exists in two natural isoforms. Proteolytic cleavage at the conserved Lys-91 by the proprotein convertase furin/PCSK3 in the Golgi generates a shorter globular gCTRP12 isoform (24). Circulating levels of the cleaved gCTRP12 isoform, relative to the full-length protein, are increased in diet-induced obese and insulin resistant mouse models (31). In cultured 3T3-L1 adipocytes, insulin treatment also promotes the expression and generation of cleaved gCTRP12 (24). The full-length protein (trimer) and globular gCTRP12 (dimer) differ in their oligomeric state. The full-length protein and gCTRP12 isoforms appear to preferentially activate the Akt and MAPK signaling pathways, respectively, in cultured hepatocyte and adipocyte cell lines (24) suggesting that they may have both overlapping and distinct functions. What regulates the secretion and proteolytic cleavage of CTRP12, however, is unknown. In the present study, we reveal the importance of the three

conserved asparagine residues (Asn-39, Asn-287, and Asn-297) in modulating protein secretion and the extent of proteolytic cleavage by furin/PCSK3 endopeptidase. Our data also provides a novel function for *N*-linked glycosylation in modulating protein cleavage by proprotein convertases within the secretory pathway.

Materials and Methods

Materials

Tris(2-carboxyethyl)phosphine (TCEP) was obtained from Thermo Scientific (Rockford, IL). Iodoacetamide, tunicamycin, glucosamine, and mouse monoclonal anti-FLAG M2 antibody were obtained from Sigma-Aldrich (St. Louis, MO). Rabbit polyclonal anti-human GntI/MGAT1 antibody (15103-1-AP) was obtained from Proteintech. Mouse monoclonal anti-CHOP (9C8; MA1-250) was obtained from Thermo Fisher Scientific. Rabbit anti-human/mouse XBP-1 antibody was obtained from Abcam (ab37152). Rabbit monoclonal antibodies against spliced XBP-1s (D2C1F) and ATF-6 (D4Z8V) were obtained from Cell Signaling Technology. Trypsin and chymotrypsin were purchased from Promega (Madison, WI), hydrazine resin was from Bio-Rad (Hercules, CA) and PNGase F and Endoglycosidase H (Endo H) were from New England Biolabs (Ipswich, MA). Furin/PCSK3 inhibitor was obtained from Cayman Chemical. The furin/PCSK3 inhibitor (decanoyl-Arg-Val-Lys-Arg-CMK) was obtained from Cayman Chemical

(catalog # 14965). Cycloheximide was purchased from Calbiochem (catalog # 239764).

Protein digestion and *N*-linked glycopeptide enrichment

To aid protein digestion by proteases, urea was added to 25 µg of protein samples in 25 mM HEPES, 135 mM NaCl, pH 8 to a final concentration of 8 M. Protein was reduced and alkylated with 10 mM TCEP and 15 mM iodoacetamide, respectively. Urea concentration was reduced with 50 mM triethylammonium bicarbonate to a final concentration of 1 M and subjected to serial digestion with trypsin (1:25 enzyme-protein ratio) and chymotrypsin (1:25 enzyme-protein ratio) at 37°C overnight. Glycosylated peptides were enriched using solid-phase extraction of *N*-linked glycoprotein (SPEG) as previously described with minor modifications (32). Briefly, peptides were subjected to C18 Stage Tip clean-up (33), oxidized with 10 mM sodium periodate, and incubated at room temperature for 1 hour. Peptides were desalted using C18 Stage Tip prior to conjugation to hydrazide resin via overnight coupling in 80% acetonitrile, 0.1% TFA (trifluoroacetic acid), and 1% aniline. Non-glycosylated peptides were removed by washing the resin three times each with 1 mL of 50% acetonitrile, 1.5 M NaCl, HPLC-H_2O, and 25 mM triethylammonium bicarbonate. *N*-linked glycosite-containing peptides were released from the resin by incubation overnight with 3 µL of PNGase F in 25 mM triethylammonium bicarbonate. Released glycosite-containing peptides were collected after centrifugation at 3,000 x g. The resin was then rinsed with 50%

acetonitrile twice and pooled. The peptide solution was desalted, dried, and reconstituted in 0.1% formic acid and subjected to MS analysis.

LC-MS/MS analysis and protein identification

Peptides were analyzed via ESI-LC-MS/MS as previously described (34). *N*-linked glycosite-containing peptides (~1 µg) were separated through a Dionex Ultimate 3000 RSLC nano system (Thermo Scientific) with a 75 µm x 15 cm Acclaim PepMap100 separating column (Thermo Scientific) protected by a 2 cm guard column (Thermo Scientific). The mobile phase consisted of 0.1% formic acid in water (A) and 0.1% formic acid/95% acetonitrile (B). Flow rate was 300 nl/min, with a gradient profile as follows: 4-35% B for 70 min, 35-95% B for 5 min, 95% B for 10 min, and equilibrated in 4% B for 15 min. MS analysis was performed using an Orbitrap Velos Pro mass spectrometer (Thermo Scientific). The spray voltage was set at 2.2 kV. Orbitrap spectra (AGC $1x10^6$) were collected from 400-1800 m/z at a resolution of 60K followed by data-dependent HCD MS/MS (at a resolution of 7500, collision energy 35%, activation time 0.1 ms) of the ten most abundance ions using an isolation width of 2.0 Da. Charge state screening was enabled to reject unassigned and singly charged ions. A dynamic exclusion time of 35 sec was used to discriminate against previously selected ions. Peptides were identified using Proteome Discoverer software (Thermo Scientific, ver 1.3). Spectra were searched against the CTRP12/Adipolin protein sequence [UniProtKB – Q8R2Z0, ADIPL_MOUSE)]. The precursor mass tolerance was set at 20 ppm and the MS/MS tolerance at 0.06 Da. Parameters of the search included: variable

modifications such as methionine oxidation (+15.99492) and asparagine deamidation (+0.984016); fixed modification such as cysteine carbamidomethylation (+57.02510); digestion enzymes such as trypsin and chymotrypsin, and a maximum of two missed cleavages were allowed.

cDNA constructs

All C-terminal FLAG epitope-tagged mouse CTRP12 (NCBI GenBank accession no. NP_080401) single, double, and triple mutant constructs (N39Q, N39A, N287Q, N287A, N297Q, N297A, T41A, S289A, S299A, N39Q/N287Q, N39Q/N297Q, N287Q/N297Q, N39Q/N287Q/N297Q) were generated by either site-directed mutagenesis or by GenScript. We also generated an N-terminal FLAG epitope-tagged version of wild-type mouse CTRP12 and the single mutants (N287Q and N297Q). The FLAG tag (DYKDDDDK) was inserted immediately downstream of the signal peptide (amino acid residue 1-22). All cDNA inserts were cloned into the EcoRI restriction site of the mammalian expression vector pCDNA3.1 (Invitrogen) and verified by DNA sequencing. Untagged human GnTI/MGAT1 (NM_002406) and C-terminal FLAG-tagged mouse furin/PCSK3 (NM_001081454) expression plasmids were obtained from Origene and verified by sequencing.

Cell culture and transfection

GripTite™ 293 cells (Invitrogen) and GnTI-deficient HEK293S cells (ATCC; CRL-3022) (35) were cultured in DMEM (Invitrogen) containing 10% fetal bovine serum

(FBS), 4 mM L-glutamine, 100 units/mL penicillin, and 100 µg/mL streptomycin. Transfections were carried out using Lipofectamine (Invitrogen) according to the manufacturer's instructions. Twenty-four hours post transfection, medium was replaced with serum-free Opti-MEM (Invitrogen). Both cell lysates and media from transfected cells were then collected 24 h later. Cell lysates were prepared by solubilizing cells in whole cell extract buffer (20 mM Tris-HCL (pH 7.5), 150 mM NaCl, 1 mM Na_2EDTA, 0.5% NP-40, 10% glycerol) containing SIGMAFAST™ protease inhibitor cocktail (Sigma) and phosSTOP phosphatase inhibitor cocktail (Roche). In our transfection studies, the experiments had been repeated 2-4 times; each time we performed six independent transfections on different dishes of cells. For tunicamycin and glucosamine treatments, GripTite™ 293 cells were cultured in media containing tunicamycin (0.5 µg/mL) or glucosamine (1 or 5 mM) 2 hours before transfection. We used the concentration of glucosamine (5 mM) known to disrupt *N*-glycosylation (36-38). Twenty-four hours post transfection, medium was replaced with serum-free Opti-MEM (Invitrogen). Both cell lysates and media from transfected cells were then collected 24 h later. In the case of furin inhibitor, cells were cultured in the presence of inhibitor (50 µM) from the day of transfection and the inhibitor remained in Opti-MEM media for another 24 hr until cell lysates were harvested. The dose of furin inhibitor used was based on previous studies(39,40). LoVo cells (CCL-229; ATCC), a human colon carcinoma cell line deficient in furin (41), were cultured in F-12K medium (ATCC) supplemented with 10% FBS and penicillin/streptomycin. Transfection of mouse furin cDNA into LoVo cells was carried out as described above for HEK 293 cells.

Western blot analysis

For Western blot analyses, cell lysates in loading buffer (50 mM Tris, 2% SDS, 1% β-ME, 6% glycerol, 0.01% bromophenol blue) were incubated at 94 °C for 5 min. Proteins were separated in 10% or 8-16% pre-cast mini-PROTEAN TGX gel (Bio-Rad), immunoblotted onto nitrocellulose membrane (Bio-Rad), blocked with 5% non-fat milk for 1 h, and probed with mouse anti-FLAG M2 (1:1000), rabbit anti-human MGAT1 primary antibody (1:1000), mouse anti-CHOP monoclonal antibody (1:1000), or rabbit anti-XBP-1 polyclonal antibody (1:1000) overnight. Immunoblots were washed 3X (10 min each) in PBS containing 0.1% Tween-20 and incubated with horseradish perioxidase-conjugated secondary antibody (Amersham Biosciences) (1:2000) for 1 hr. Blots were washed 3X (10 min each) in PBS containing 0.1% Tween 20, developed in ECL reagent (Millipore) for 2-5 min, and visualized with MultiImage III FluorChem ® Q (Alpha Innotech). Quantifications of signal intensity were performed using Image J software. The cleavage index is defined as the ratio of cleaved globular secreted protein to full-length isoform in the supernatant of transfected cells; this describes the extent of proteolytic cleavage of the secreted CTRP12. The secretion index is defined as the ratio of total secreted CTRP12 (full length and globular isoform) to intracellular CTRP12 level.

Cycloheximide chase

We performed cycloheximide chase experiments to determine if N39Q, T41A, N297Q mutation, or glucosamine treatment, affect CTRP12 protein stability. Cycloheximide blocks new protein synthesis; this allows us to determine the rate of protein turnover and hence protein stability. HEK 293 cells were transfected with wild-type mouse CTRP12 or the indicated mutants. The following day (at t=0) cells were harvested. For the remaining cells, the medium was removed and replaced with Opti-MEM containing 100 µg/mL cycloheximide. Cells were harvested 6 hr after treatment and subjected to immunoblot analysis using the anti-FLAG M2 antibody. The ratio of wild-type CTRP12 after a 6 hr cycloheximide chase to its control (harvested at t=0 before cycloheximide treatment) was considered 1. The relative turnover of different mutants were then compared to wild-type CTRP12.

Glycoprotein detection

Experiments were carried as previously described (36). Briefly, HEK 293 cells were treated with 1 or 5 mM glucosamine (GlcN; G4875; Sigma) for 48 hr and harvested as described above. Equal amount of cell lysates were separated by SDS-PAGE. Gels were stained for general glycosylation of proteins using the Pro-Q Emerald 3000 Glycoprotein gel stain kit (P21857; Thermo Scientific). To specifically stain for *N*-glycosylated proteins, proteins were transferred to nitrocellulose membranes, blocked with 5% non-fat milk for 1 hour, and probed overnight with concanavalin A-biotin conjugate (30 µg/mL) (C2272; Sigma). Immunoblots were washed 3X (10 min each) in PBS containing 0.1% Tween-20

and incubated with horseradish perioxidase-conjugated avidin (1:20,000) (1706528; Bio-Rad). Blots were washed 3X (10 min each) in PBS containing 0.1% Tween 20, developed in ECL reagent (Millipore) for 2-5 min, and visualized with MultiImage III FluorChem ® Q (Alpha Innotech). Subsequently, gels and blots were stained for total protein using EZBlue Gel Staining Reagent (G1041; Sigma). Quantifications of signal intensity were performed using Image J software.

RT-PCR analysis

Total RNAs were isolated from HEK 293 cells expressing a wild-type GnTI/MGAT1 and GnTI-deficient HEK 293S using Trizol reagent. Potential genomic DNA was removed by DNAase I digest. Reverse transcription was carried out using random primers and GoScript reverse transcriptase (Promega). The following primers were used to amplify the entire coding region of human *GnTI*/*MGAT1* mRNA: forward, 5'-CTAGGACTGCGGGCAAGGGAGCCG-3', and reverse, 5'-GGGCCCAGGAAGGACAGGCAGGTG-3'. PfuUltra high fedelity polymerase (Agilent) was used in a 36-cycle PCR reactions: denaturing at 95°C for 30 seconds, annealing at 55°C for 30 seconds, and extension at 72°C for 2 min. Amplified PCR product was separated on 1% agarose gel, excised and purified, and verified by DNA sequencing.

Statistical analysis

Comparisons were performed using two-tail Student's *t*-tests. Values were considered significant at $p < 0.05$. All data are presented as mean ± standard error of the mean.

Results

Inhibition of *N*-linked glycosylation enhances CTRP12 cleavage

Mouse CTRP12 possess three potential *N*-linked glycosylation sites at Asn-39, Asn-287, and Asn-297 that conform to the consensus Asn-X-Ser/Thr (where X is any amino acid except proline) (**Fig. 1A**). Two of these sites (Asn-39 and Asn-287) are conserved in human CTRP12. At least one of these sites, Asn-39, was previously suggested to be glycosylated based on changes in the apparent molecular weight of the N39A mutant of CTRP12 relative to wild-type protein on immunoblot (24). *N*-linked glycans are known to play an important role in the quality control of protein folding in the endoplasmic reticulum (42). To assess the impact of glycosylation on CTRP12 expression, we used tunicamycin to block *N*-glycosylation. This aminoglycoside antibiotic inhibits the first step in the lipid-linked oligosaccharide biosynthesis pathway (43,44). In heterologous HEK 293 cells expressing mouse CTRP12, inhibiting *N*-linked glycosylation did not affect protein expression and secretion; however, we observed significantly enhanced cleavage of the protein based on the ratio of cleaved to full length secreted CTRP12 protein (**Fig. 1B,C**).

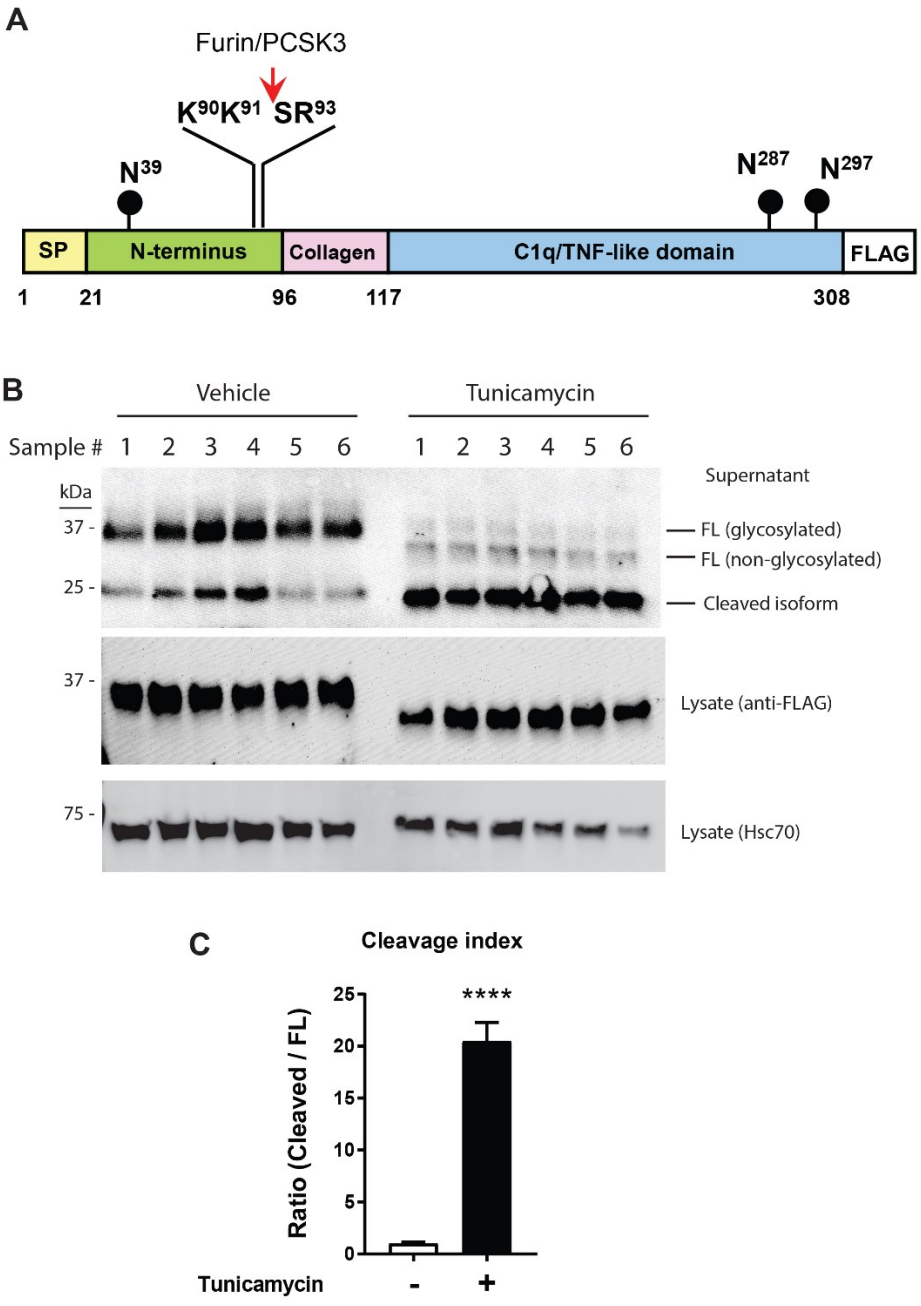

Figure 1. Inhibition of *N*-glycosylation enhances CTRP12 cleavage. ***A***, Domain structure of mouse CTRP12. The conserved furin-cleavage site (Lys-91) and the three potential N-linked glycosylation sites (Asn-39, Asn-287, and Asn-297) that conform to the *N*-X-S/T motif are indicated. The C-terminal FLAG tag is also indicated. ***B***, Western blot analysis (using anti-FLAG M2 antibody) of cell lysate and supernatant of transfected HEK 293 cells treated with vehicle control or tunicamycin, an inhibitor of *N*-glycosylation. ***C***, Quantification of the ratio of cleaved to full-length protein in the supernatant. FL, full-length; N=6 (each lane represents a different sample from an independent transfection); ****p<0.0001

Identification of *N*-glycans on CTRP12 using mass spectrometry

Given that *N*-linked glycosylation influences the extent of CTRP12 proteolytic cleavage, we sought to determine whether Asn-39, Asn-287, and Asn-297 are indeed glycosylated. While previous assessment of *N*-linked glycosylation by PNGase F suggests the presence of glycans on Asn-39 (24), it remains unresolved whether Asn-287 and Asn-297 are also glycosylated. For this reason, we subjected purified recombinant mouse CTRP12 to mass spectrometry analysis. Using this method, we provided direct evidence that Asn-39 is indeed glycosylated (**Fig. 2A**). Whether Asn-287 and Asn-297 are also glycosylated could not be determined by mass spectrometry in the present study; the C-terminal peptide fragment containing Asn-287 and Asn-297 was not detected by mass spectrometry. We therefore used site-directed mutagenesis to assess whether Asn-287 and/or Asn-297 are glycosylated. As expected, replacing Asn-39 with glutamine led to a significant shift in the apparent molecular mass of the secreted protein on immunoblot relative to wild-type protein (**Fig. 2B**). In contrast, replacing Asn-297 with glutamine did not result in a shift of molecular mass of the secreted protein on immunoblot, suggesting that this site is not glycosylated. Replacing Asn-287 with glutamine also did not reduce the apparent molecular weight of the mutant protein relative to wild-type protein on immunoblot, suggesting that Asn-287 is also not glycosylated. To rule out whether the C-terminal FLAG epitope tag affects Asn-287 and Asn-297 glycosylation, we also generated constructs encoding N-terminal FLAG tagged mouse CTRP12. The epitope tag was inserted immediately downstream of the signal peptide. As shown in Fig. 2C, placing the epitope tag at

the N-terminus did not affect the glycosylation outcome for WT, N297Q, and N287Q mutant (Fig. 2C). These results indicate that only Asn-39 is glycosylated.

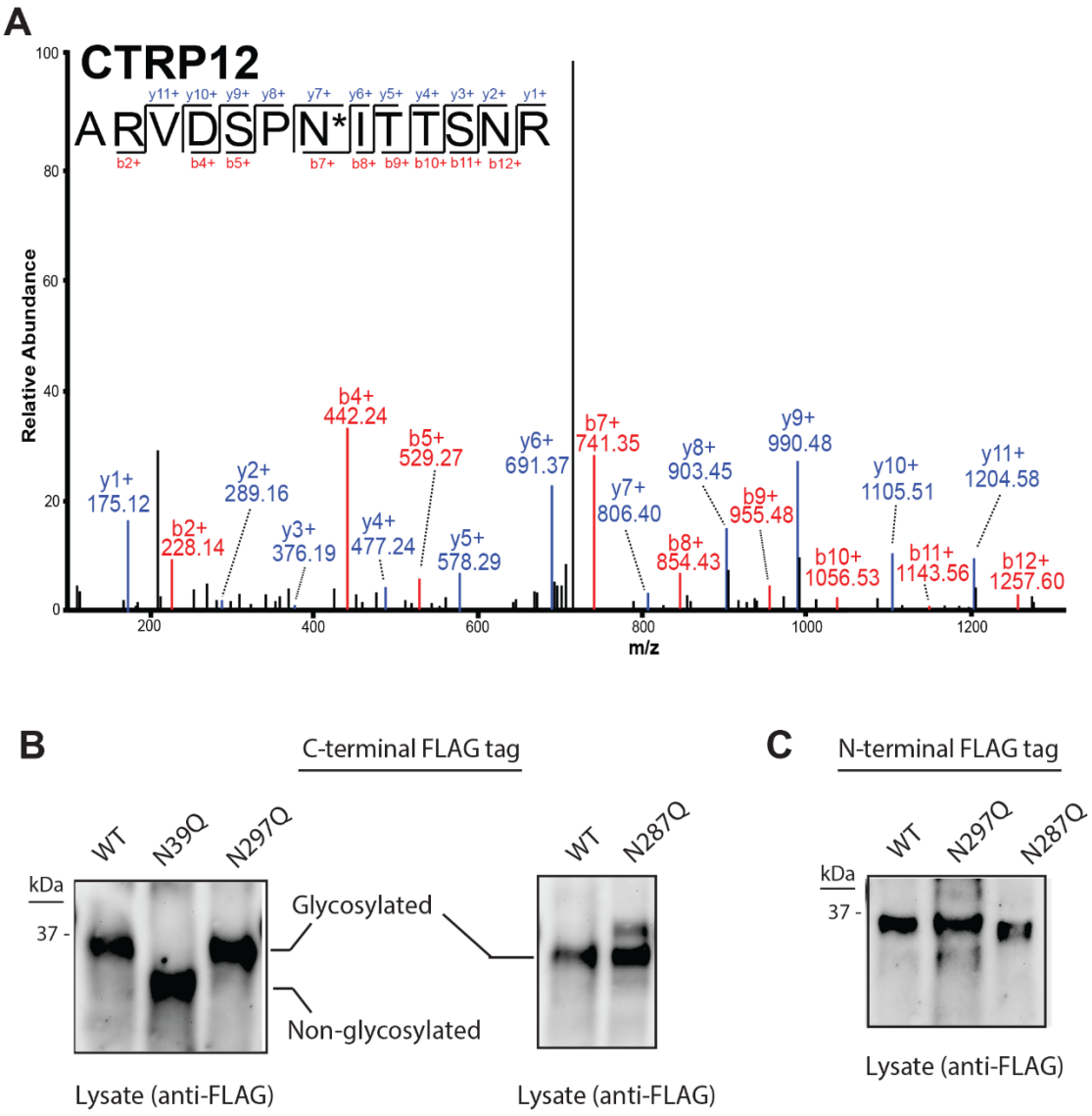

Figure 2. Mass spectrometry and mutational analysis of *N*-glycosylation in CTRP12. ***A***, MS/MS mass spectrum of the glycopeptide ARVDSPNITTSNR derived from CTRP12 identified using Proteome Discoverer. Higher-energy collisional dissociation (HCD) generated b- (red) and y- (blue) peptide fragments that allow for the mapping of the site of glycosylation as indicated by asterisk(*). Cleavage of the glycan structure from the peptide backbone via PNGase F digestion results in deamidation of asparagine and conversion to aspartic acid. Mass spectra indicate that Asn-39 is N-glycosylated. ***B***, Western blot analysis of cell lysates of transfected HEK 293 cells expressing C-terminal FLAG-tagged wild-type (WT) CTRP12 or the single mutants (N39Q, N297Q, or N287Q). ***C***, Western blot analysis of cell lysates of transfected HEK 293 cells expressing N-terminal FLAG-tagged WT CTRP12 or the single mutant (N297Q or N287Q).

Impact of Asn-39 glycosylation on CTRP12 cleavage

We used the N39Q and N39A mutant constructs to determine the role of Asn-39 glycosylation in modulating CTRP12 cleavage. Relative to the wild-type (WT) protein, we observed a significant enhancement of CTRP12 cleavage in the N39Q and N39A mutants when expressed in HEK 293 cells (**Fig. 3A-B, D-E**). The ratio of secreted gCTRP12 to full-length protein indicates a significant increase in proteolytic cleavage. Replacing Asn-39 with either glutamine or alanine did not affect protein secretion (**Fig. 3C,F**). To rule out structural changes due to N39Q or N39A replacements, we also mutated Thr-41 (in the context of N-X-S/T) to Ala. As expected, *N*-glycosylation was abolished in the T41A mutant (**Fig. 3G**). Again, loss of glycosylation resulted in enhanced CTRP12 cleavage (**Fig. 3H**), further confirming that Asn-39 glycosylation is indeed modulating the extent of CTRP12 cleavage. Interestingly, Thr-41 appears to influence protein secretion; replacing Thr-41 with alanine resulted in greater protein secretion (**Fig. 3I**). It is known that *N*-linked glycosylation influences protein stability during synthesis (45). To address whether N39Q and T41A mutations affect protein stability, we performed a cycloheximide chase experiment. Cycloheximide blocks new protein synthesis; this allows us to examine the turnover of mutant CTRP12 and hence their stability relative to wild-type protein. A 6 hr chase with cycloheximide indicated that both the N39Q and T41A mutants were significantly less stable and had faster turnover relative to wild-type CTRP12 (**Fig. 3J-M**).

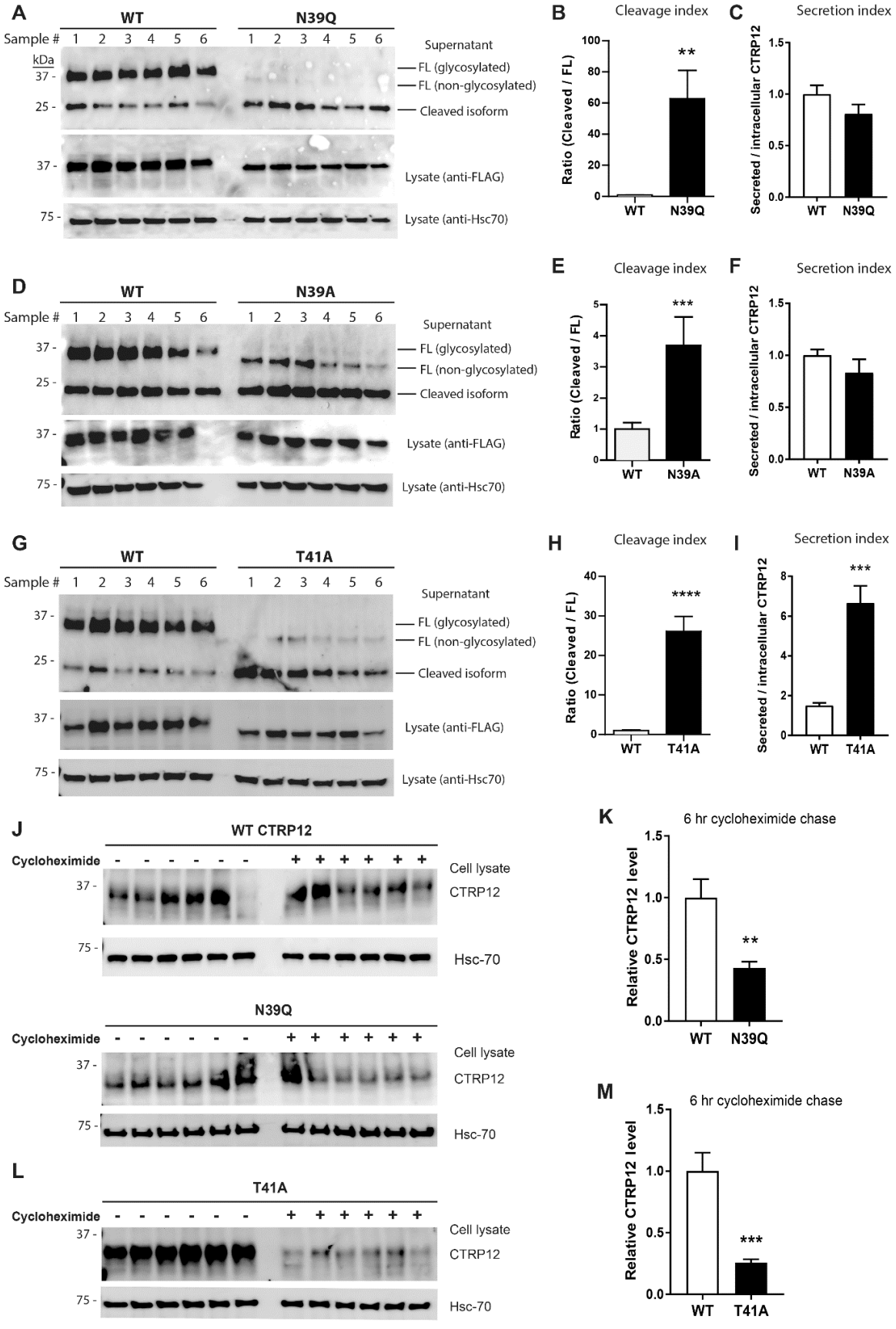
A
WT
N39Q
Sample # 1 2 3 4 5 6 1 2 3 4 5 6
kDa
37 -
25 -
Supernatant
FL (glycosylated)
FL (non-glycosylated)
Cleaved isoform
37 -
Lysate (anti-FLAG)
75 -
Lysate (anti-Hsc70)
B
Cleavage index
Ratio (Cleaved / FL)
100
80
60
40
20
0
**
WT
N39Q
C
Secretion index
Secreted / intracellular CTRP12
1.5
1.0
0.5
0.0
WT
N39Q
D
WT
N39A
Sample # 1 2 3 4 5 6 1 2 3 4 5 6
37 -
25 -
Supernatant
FL (glycosylated)
FL (non-glycosylated)
Cleaved isoform
37 -
Lysate (anti-FLAG)
75 -
Lysate (anti-Hsc70)
E
Cleavage index
Ratio (Cleaved / FL)
5
4
3
2
1
0
***
WT
N39A
F
Secretion index
Secreted / intracellular CTRP12
1.5
1.0
0.5
0.0
WT
N39A
G
WT
T41A
Sample # 1 2 3 4 5 6 1 2 3 4 5 6
37 -
25 -
Supernatant
FL (glycosylated)
FL (non-glycosylated)
Cleaved isoform
37 -
Lysate (anti-FLAG)
75 -
Lysate (anti-Hsc70)
H
Cleavage index
Ratio (Cleaved / FL)
40
30
20
10
0
****
WT
T41A
I
Secretion index
Secreted / intracellular CTRP12
8
6
4
2
0
***
WT
T41A
J
WT CTRP12
Cycloheximide - - - - - - + + + + + +
37 -
Cell lysate
CTRP12
75 -
Hsc-70
N39Q
Cycloheximide - - - - - - + + + + + +
37 -
Cell lysate
CTRP12
75 -
Hsc-70
L
T41A
Cycloheximide - - - - - - + + + + + +
37 -
Cell lysate
CTRP12
75 -
Hsc-70
K
6 hr cycloheximide chase
Relative CTRP12 level
1.5
1.0
0.5
0.0
**
WT
N39Q
M
6 hr cycloheximide chase
Relative CTRP12 level
1.5
1.0
0.5
0.0
***
WT
T41A

Figure 3. Asn-39 glycosylation regulates CTRP12 cleavage and stability. Western blot analysis of cell lysate and supernatant of transfected HEK 293 cells expressing wild-type (WT) CTRP12 or the N39Q (**A**), N39A (**D**), and T41A (**G**) mutants. Quantification of the ratio of cleaved to full-length (FL) protein (the cleavage index) in supernatant for N39Q (**B**), N39A (**E**), and T41A (**H**). Quantification of the ratio of secreted to intracellular CTRP12 (the secretion index) in supernatant for N39Q (**C**), N39A (**F**), and T41A (**I**). (**J**) A 6 hr cycloheximide chase analysis of WT and N39Q mutant. (**K**), Quantification of the relative protein stability of N39Q relative to wild-type CTRP12 protein. (**L**) A 6 hr cycloheximide chase analysis of T41A mutant. (**M**) Quantification of the relative protein stability of T41A relative to wild-type CTRP12 protein. N=6 (each lane represents a different sample from an independent transfection); **p<0.01; ***p<0.001; ****p<0.0001

Complex-type glycans influence CTRP12 cleavage

Increased cleavage of the N39Q mutant suggests that the presence of glycans on Asn-39—located relatively close to the conserved cleavage site at Lys-91—may influence the cleavage efficiency of the Golgi-localized endopeptidase PCSK3/furin (46). To test this, we expressed wild-type CTRP12 protein in *N*-acetylglucosaminyltransferase I-deficient (GnTI) HEK 293 cells (35). We confirmed the absence of GnTI/MGAT1 mRNA and protein in the GnTI-deficient HEK 293 cells (**Fig. 4A-B**). Loss of GnTI enzyme prevents the generation of complex-type glycans in the Golgi (35). Proteins decorated with complex-type N-linked glycans as they transit through the Golgi are resistant to endoglycosidase H (Endo H) digest. As expected, in wild-type HEK 293 cells with intact GnTI activity, CTRP12 protein was susceptible to PNGase F digest and also partially (the pool that acquired complex glycans in the Golgi) resistant to Endo H digest (**Fig. 4C-D**). In contrast, in HEK 293S cells that lack GnTI activity, the entire intracellular pool of CTRP12 (with only high mannose-type glycans) was

susceptible to Endo H digest (**Fig. 4D**). Inability to generate CTRP12 containing complex-type *N*-glycans in the Golgi resulted in enhanced cleavage of the secreted protein (**Fig. 4E-F**). We also observed greater secretion of CTRP12 protein in GnTI-deficient HEK 293S cells (**Fig. 4G**), likely reflecting shorter transit time through the trafficking pathway in the absence of glycan remodeling in the Golgi. We could reverse the enhanced cleavage and secretion in GnTI-deficient cells by re-expressing wild-type human GnTI/MGAT1 (**Fig. 4H-J**).

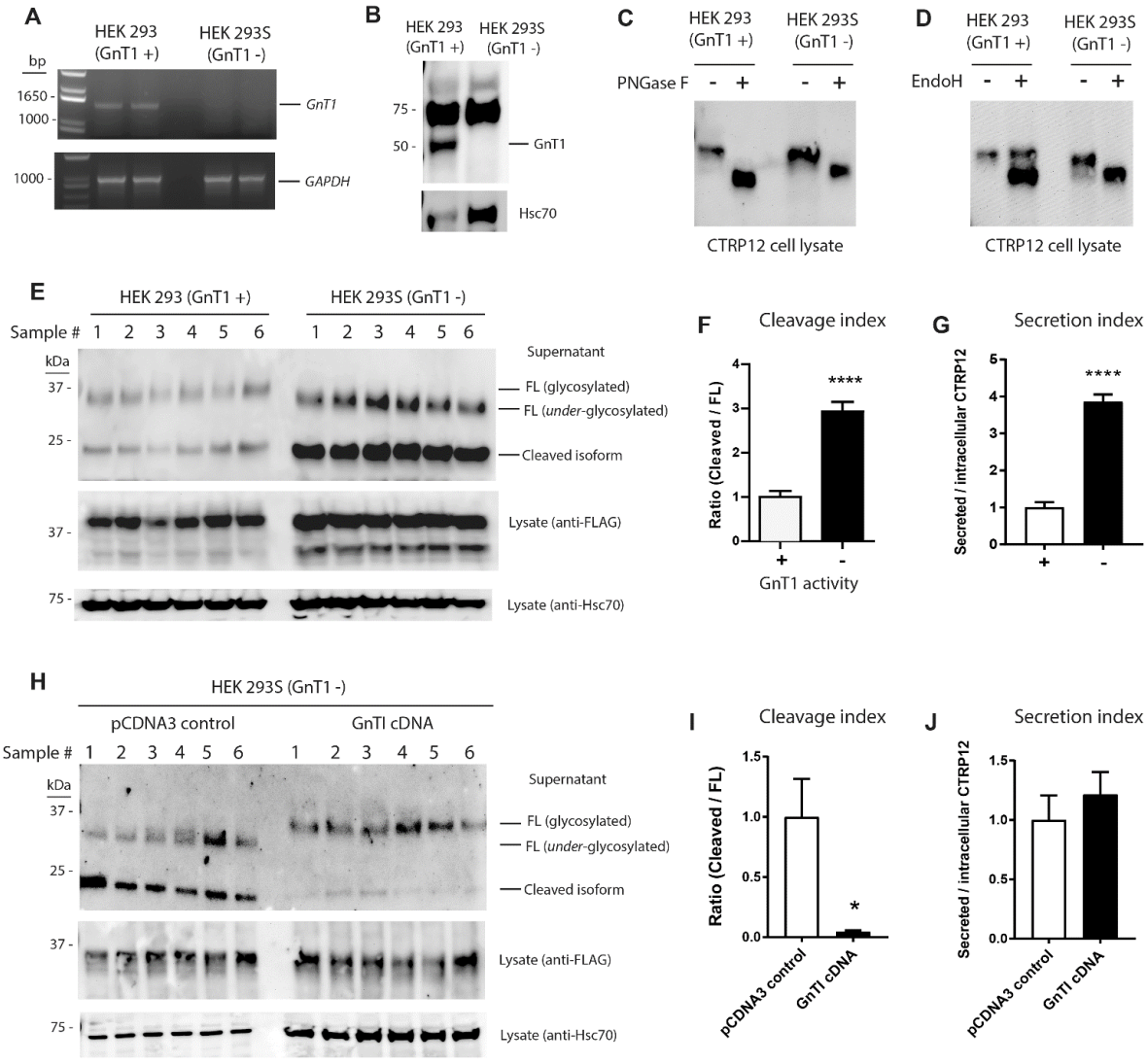

Figure 4. Complex-type glycans influence CTRP12 cleavage. ***A***, PCR amplification of human *GnTI*/*MGAT1* mRNA in wild-type HEK 293 cells and GnTI-deficient HEK 293S cells. The ~1.5 kb amplicon includes the entire coding region of *GnTI*. ***B***, Western blot analysis of endogenous GnTI protein in wild-type (WT) HEK293 cells and GnTI-deficient HEK293S cells. ***C-D***, Immunoblot analysis (using anti-FLAG antibody) of CTRP12 expressed in HEK 293 (GnTI +) and HEK 293S (GnTI -) cells. Cell lysates were subjected to PNGaseF (C) or Endoglycosidase H (D) treatment before Western blot analysis. ***E***, Western blot analysis of cell lysate and supernatant of transfected HEK 293 cells with (+) or without (-) *N*-acetylglucosaminyltransferase I (GnTI) activity involved in *N*-glycan remodeling in the Golgi compartment. ***F***, Quantification of the ratio of cleaved to full-length protein (the cleavage index) in the supernatant. ***G***, Quantification of the ratio of secreted to intracellular CTRP12 (the secretion index). ***H***, Western blot analysis of cell lysate and supernatant of GnTI-deficient HEK 293 cells re-expressing wild-type human

GnTI/MGAT1. ***I***, Quantification of the ratio of cleaved to full-length protein (the cleavage index) in the supernatant. ***J***, Quantification of the ratio of secreted to intracellular CTRP12 (the secretion index). N=6 (each lane represents a different sample from an independent transfection); *p<0.05; ****p<0.0001

Modulation of CTRP12 cleavage, secretion, and protein stability by Asn-297

Although the conserved Asn-297 is not glycosylated, we generated and tested the impact of Asn-297 mutation on CTRP12 cleavage. Surprisingly, either the N297Q or the N297A mutation resulted in enhanced cleavage of the protein (**Fig. 5A-B, D-E**). Interestingly, replacing Asn-297 with alanine, but not glutamine, reduced protein secretion as judged by the ratio of secreted to intracellular CTRP12 protein (**Fig. 5F**). To further ensure that Asn-297 modulates CTRP12 cleavage through a non-glycosylated mechanism distinct from Asn-39, we replaced Ser-299 (within the N^{297}-X-S^{299} glycosylation motif) with alanine. The N-X-S/T is the critical recognition motif needed for *N*-glycosylation (47); mutation of Ser or Thr within this motif will abolish *N*-glycosylation. Because Asn-297 was not glycosylated, we predicted that the S299A mutation would not enhance CTRP12 cleavage as seen in the N297Q mutant. While consistent with our prediction, the S299A mutation unexpectedly abolished protein secretion (**Fig. 5G**). To address whether N297Q mutation affects protein stability, we performed a cycloheximide chase experiment. A 6 hr chase with cycloheximide indicated that N297Q mutant is less stable and has a faster turnover compared to wild-type CTRP12 (**Fig. 5H-I**).

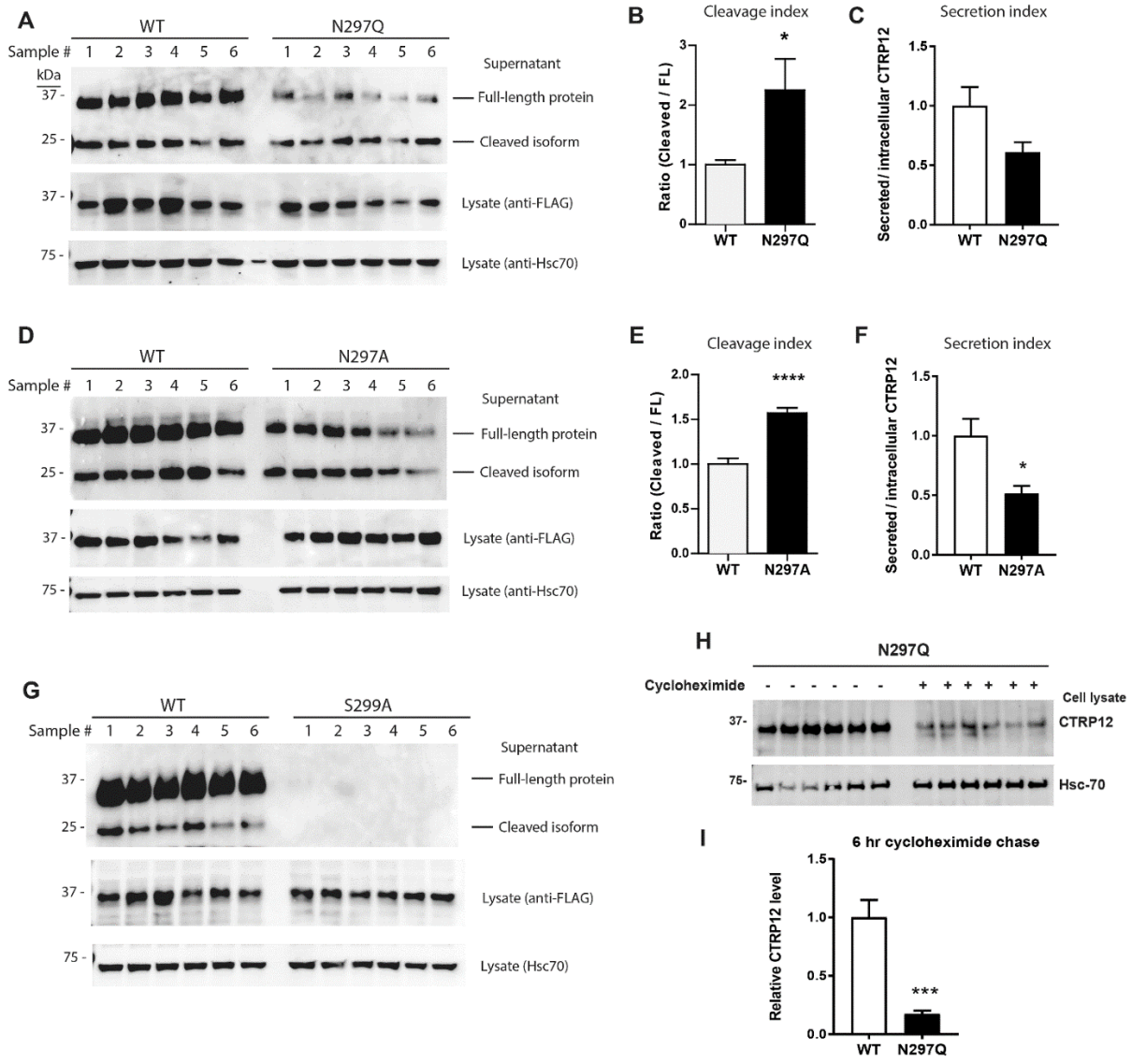

Figure 5. Non-glycosylated Asn-297 independently regulates CTRP12 cleavage and stability. Western blot analysis of cell lysate and supernatant of transfected HEK 293 cells expressing wild-type (WT) CTRP12 or the N297Q (**A**), N297A (**D**), and S299A (**G**) mutants. Quantification of the ratio of cleaved to full-length (FL) protein (the cleavage index) in supernatant for N297Q (**B**) and N297A (**E**). Quantification of the ratio of secreted to intracellular CTRP12 protein (the secretion index) for N297Q (**C**) and N297A (**F**). **H**, A 6 hr cycloheximide chase analysis of N297Q mutant. **I**, Quantification of the relative protein stability of N297Q relative to wild-type CTRP12 protein (WT data shown in Fig. 3J). N=6 (each lane represents a different sample from an independent transfection); *p<0.05; ***p<0.001; ****p<0.0001

Asn-39 and Asn-297 independently modulate CTRP12 cleavage

Since both Asn-39 and Asn-297 affect CTRP12 protein cleavage, we next determined whether the double mutant (N39Q/N297Q) would have an additive effect on cleavage. Indeed, we observed near complete and maximum CTRP12 cleavage in the double mutant (N39Q/N297Q) (**Fig. 6**). Single mutation of Asn-39 and Asn-297 increases cleavage index 10-60-fold (Fig. 3 and 6) and 2.5-fold (Fig. 5), respectively. In the N39Q/N297Q double mutant, we observed >200-fold increase in the cleavage index (Fig. 6). These results suggest that Asn-39 and Asn-297 contribute independently to CTRP12 cleavage. Together, our results suggest that Asn-39 and Asn-297 modulate CTRP12 cleavage via glycosylation-dependent and independent mechanisms.

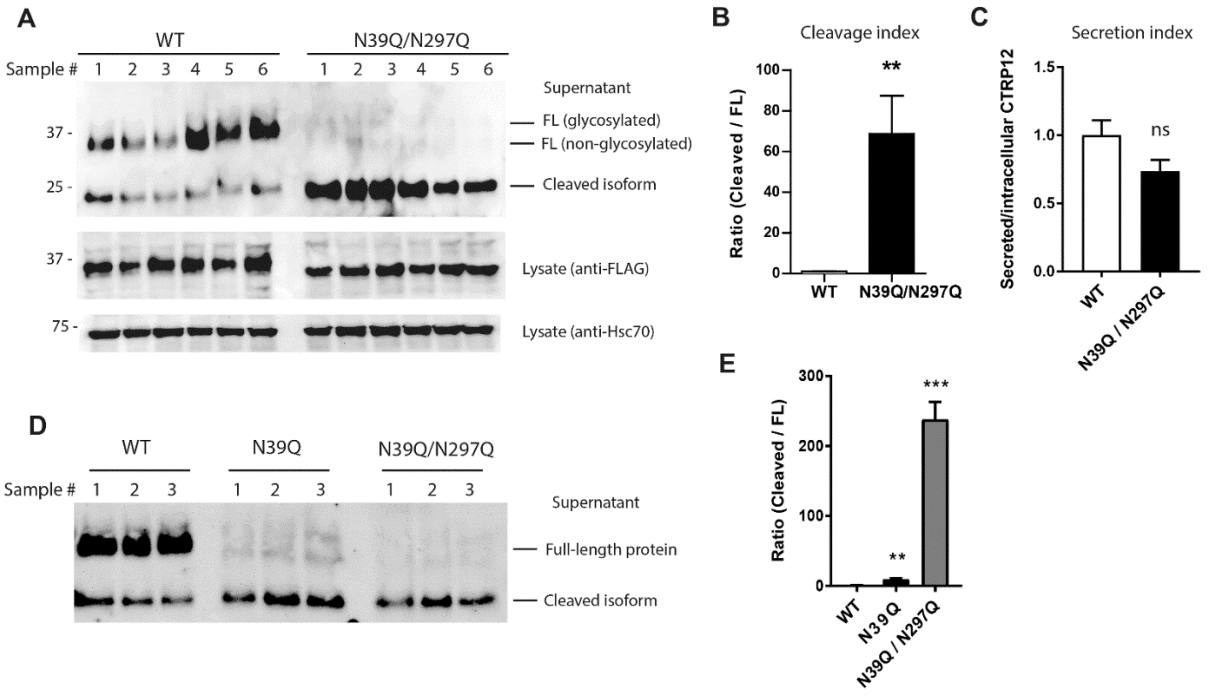

Figure 6. Asn-39 and Asn-297 independently regulate CTRP12 cleavage. ***A,*** Western blot analysis of cell lysate and supernatant of transfected HEK 293 cells expressing wild-type (WT) CTRP12 or the N39Q/N297Q double mutant. ***B***, Quantification of the ratio of cleaved to full-length (FL) protein (the cleavage index) in supernatant for WT and N39Q/N297Q double mutant as shown in A. ***C***, Quantification of the ratio of secreted to intracellular CTRP12 protein (the secretion index) for WT and N39Q/N297Q double mutant as shown in A. ***D***, A side-by-side comparison of WT, N39Q single mutant, and N39Q/N297Q double mutant. ***E***, Quantification of the ratio of cleaved to full-length (FL) protein (the cleavage index) in supernatant for WT, N39Q, and N39Q/N297Q as shown in D. N=6 (each lane represents a different sample from an independent transfection); **p<0.01; ***p<0.001

Furin-mediated cleavage of CTRP12

We previously identified furin/PCSK3 as the proprotein convertase that cleaves CTRP12 at Lys-91 (24). We predicted that CTRP12 cleavage would be largely abolished in cells that lack furin or in which furin activity is pharmacologically inhibited by a furin-specific inhibitor. The peptidyl chloromethylketone (decanoyl-

RVKR-CMK) binds to furin catalytic site and specifically inhibits it enzymatic activity (48-50). Cleavage of N39Q/N297Q (the double mutant with maximum cleavage) was also completely abolished by pharmacological inhibition of furin in HEK 293 cells (**Fig. 7A-B**). Due to a single nucleotide deletion in the furin gene that results in truncation of the protein, the human colon carcinoma cell line LoVo lacks furin endopeptidase activity (41). When we expressed the wild-type CTRP12 protein in LoVo cells, CTRP12 cleavage was abolished (**Fig. 7C**). When we re-expressed mouse furin in LoVo cells that lack a functional furin gene, we restored CTRP12 cleavage (**Fig. 7C-D**). These results indicate that the Golgi-localized furin is indeed the major endopeptidase that cleaves CTRP12.

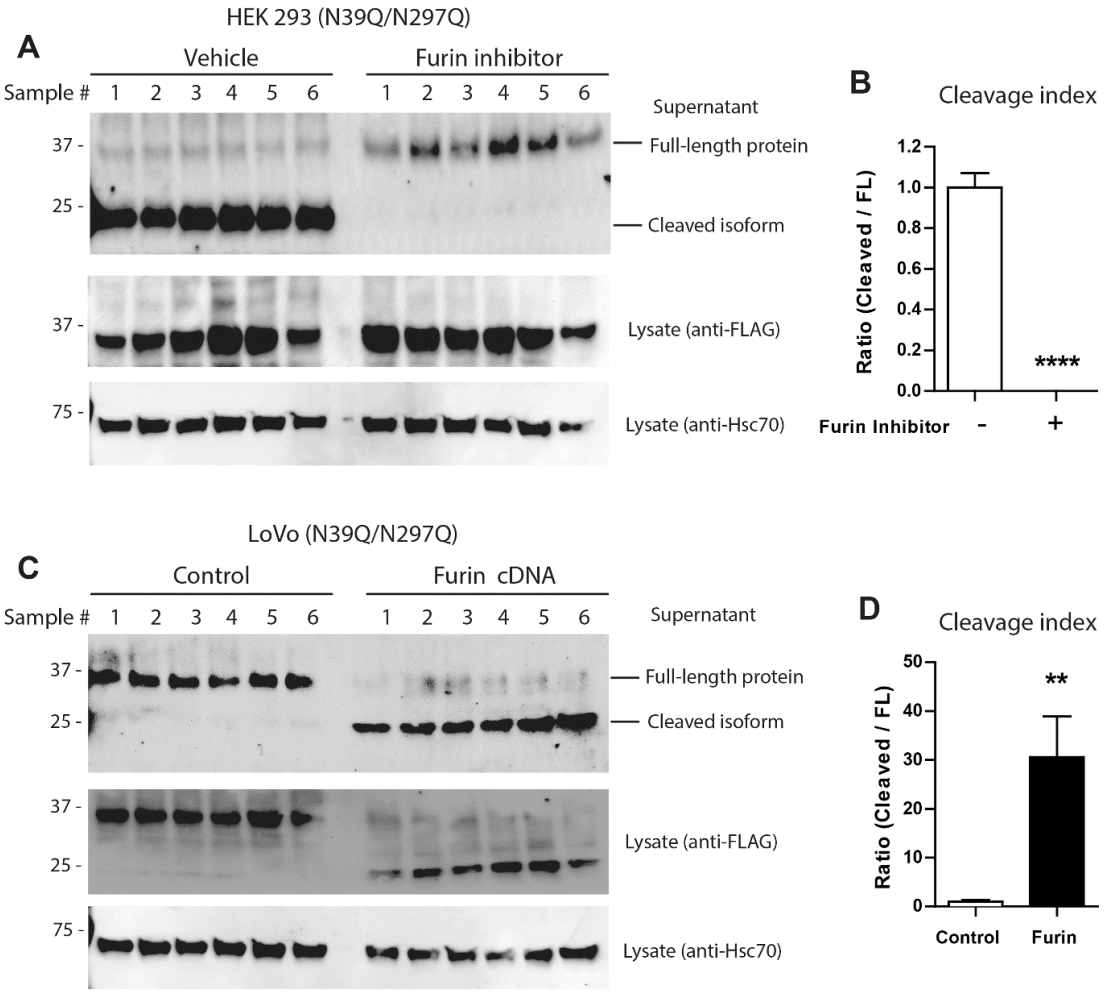

Figure 7. Furin-mediated cleavage of CTRP12. ***A***, Western blot analysis of cell lysate and supernatant of transfected HEK 293 cells expressing the maximally cleaved CTRP12 double mutant (N39Q/N297Q) treated with vehicle control or furin/PCSK3 inhibitor. ***B***, Quantification of the ratio of cleaved to full-length (FL) protein (the cleavage index) in supernatant as shown in A. ***C***, Western blot analysis of cell lysate and supernatant of transfected LoVo cells co-expressing the maximally cleaved CTRP12 double mutant (N39Q/N297) and mouse furin. LoVo cell lacks a functional furin gene and hence the double mutant is not cleaved. Furin re-expression restore maximal cleavage. ***D***, Quantification of the ratio of cleaved to full-length (FL) protein (the cleavage index) in supernatant as shown in C. N=6 (each lane represents a different sample from an independent transfection); **p<0.01; ****p<0.0001

Asn-287 is required for CTRP12 secretion

In contrast to Asn-39 and Asn-297, replacing the non-glycosylated Asn-287 with either glutamine or alanine completely prevented CTRP12 secretion (**Fig. 8A-B**). Endoglycosidase H (Endo H) digestion can be used to assess whether an *N*-glycosylated protein is located in the endoplasmic reticulum (ER; sensitive to Endo H digest) or Gogi (resistant to Endo H digest) (51). Endo H digest followed by immunoblot analysis indicated that the N287Q mutant was retained in the ER (**Fig. 8C**). The mutant protein was misfolded and formed higher molecular weight protein aggregates (**Fig. 8D**). To further ensure that Asn-287 influences protein folding in the ER through a non-glycosylated mechanism, we replaced Ser-289 (within the N^{287}-X-S^{289} motif needed for glycosylation) with alanine. Because Asn-287 is not glycosylated, we predicted that the S289A mutant would not be misfolded and retained in cells as seen in the N287Q or N287A mutant. Indeed, consistent with our hypothesis, the S289A mutant was robustly secreted from cells (**Fig. 8E**). Given that Asn-287 plays a critical role in proper protein folding, we also predicted that the double (N39Q/N287Q) or triple (N39Q/N287Q/N297Q) mutant would also be retained in the cells. Indeed, in the double and triple mutants, CTRP12 failed to be secreted in HEK 293 cells (**Fig. 9**).

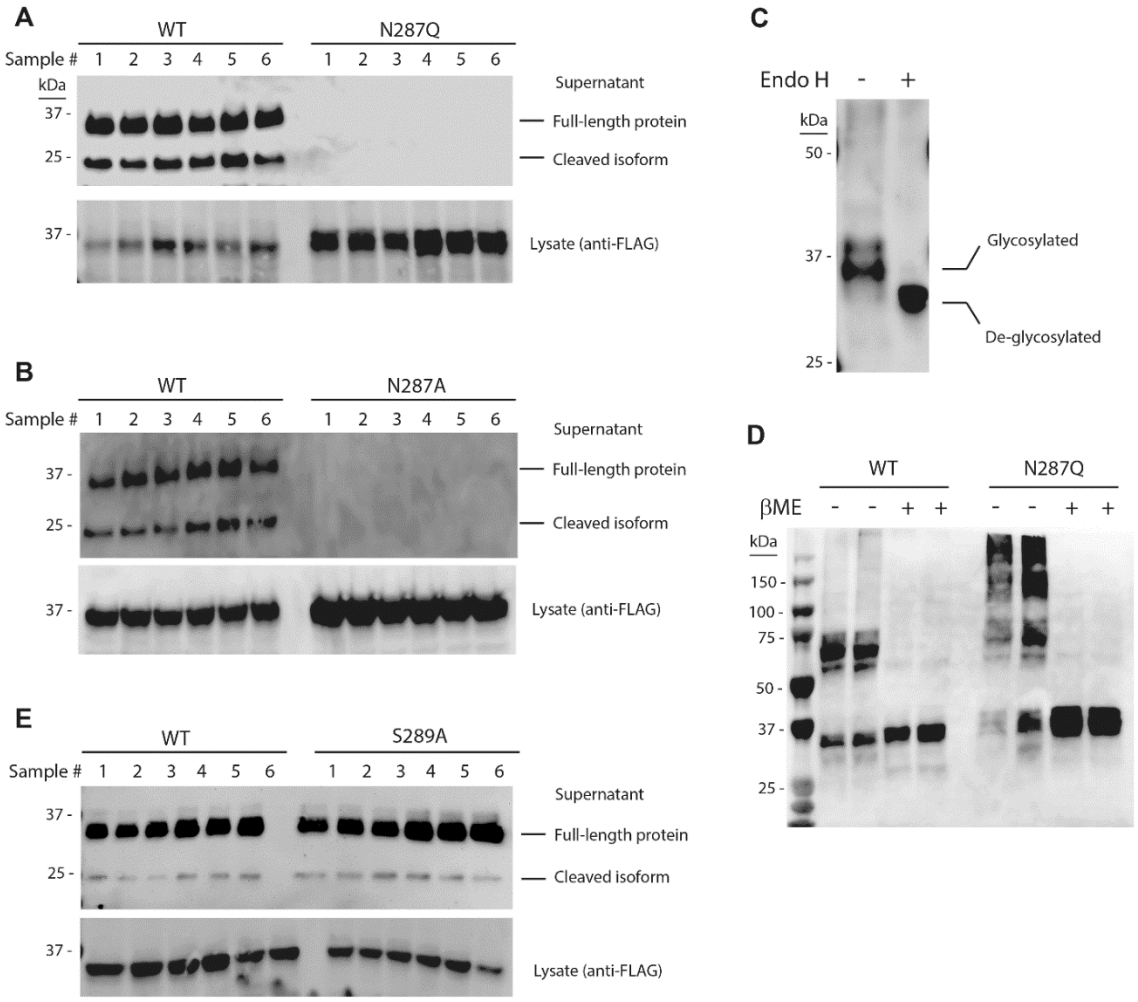

Figure 8. The non-glycosylated Asn-287 is required for proper protein folding and secretion. ***A-B*,** Western blot analysis of cell lysate and supernatant of transfected HEK 293 cells expressing wild-type (WT) CTRP12 or the N287Q (**A**) and N287A (**B**) mutant. ***C***, Western blot analysis of Endo H digested CTRP12 (N287Q mutant) found in transfected cell lysate. ***D***, Formation of higher molecular weight protein aggregate of N287Q mutant in transfected cells. Cell lysates were heated at 95°C for 5 min in the presence (+) or absence (-) of reducing agent β-ME (β-mercaptoethanol) prior to Western blotting. ***E***, Western blot analysis of cell lysate and supernatant of transfected HEK 293 cells expressing S289A mutant. N=6 (each lane represents a different sample from an independent transfection).

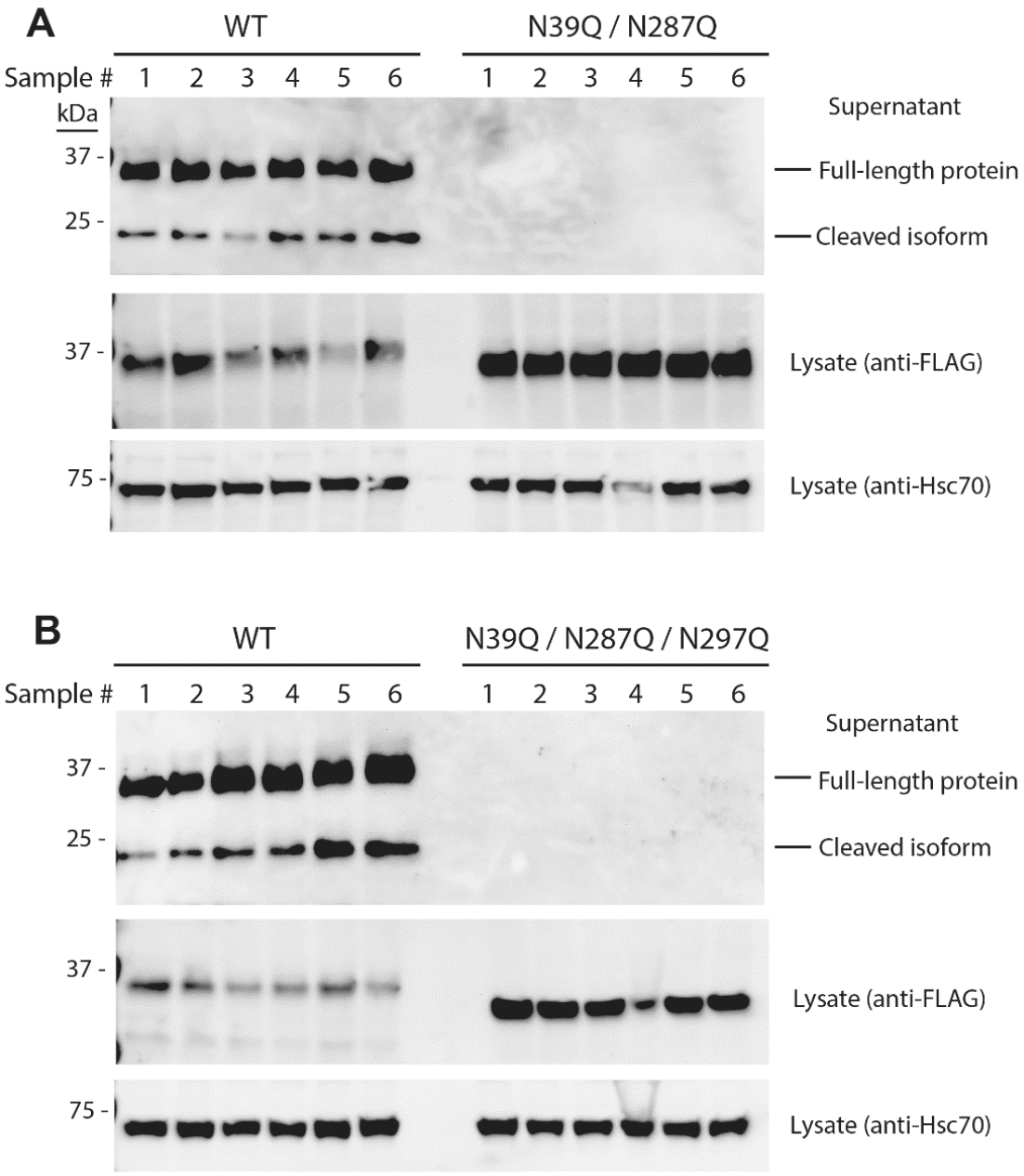

Figure 9. The CTRP12 double and triple mutants also failed to be secreted. ***A-B*,** Western blot analysis of cell lysate and supernatant of transfected HEK 293 cells expressing wild-type (WT) CTRP12 or the double (N39Q/N287Q) and triple (N39Q/N287Q/N297Q) mutants. N=6 (each lane represents a different sample from an independent transfection).

Impact of glucosamine treatment on CTRP12 cleavage

Glucose that fluxes through the hexosamine biosynthesis pathway (HBP) can be used to generate UDP-*N*-acetylglucosamine (UDP-GlcNAc), an essential sugar-nucleotide substrate for protein glycosylation. In the diabetic state characterized by hyperglycemia, the flux through the HBP is greatly enhanced, leading to increased production of UDP-GlcNAc (52,53). Exogenous supplementation of cells with glucosamine can increase intracellular pools of UDP-GlcNAc (53,54), which can, in turn, disrupt *N*-glycosylation of proteins(55) by interfering with the synthesis of dolichol-linked oligosaccharides (36). We previously showed that in obese and diabetic mice, a greater proportion of the cleaved gCTRP12 is found in plasma. We therefore tested whether increasing the intracellular concentration of UDP-GlcNAc by exogenous supplementation of glucosamine affects CTRP12 cleavage. Indeed, when cells were treated with 5 mM of glucosamine, total amount of *N*-linked glycosylated proteins was significantly reduced (**Fig. 10A-B**), consistent with previous studies (36). At 5 mM glucosamine—a dose that affects protein *N*-linked glycosylation—we observed only a modest increase in one of the three major ER stress pathways, as indicated by elevated ATF-6 levels but not that of CHOP and the spliced isoform of XBP-1 (**Fig. 10C**). While 5 mM glucosamine treatment did not affect CTRP12 protein secretion (**Fig. 10F**), it significantly enhanced CTRP12 protein cleavage (**Fig. 10D-E**). At a dose of 1 mM, at which glucosamine has no effects on *N*-glycosylation (36), we did not observe an increase in CTRP12 cleavage (not shown). These results are consistent with the role of *N*-glycosylation in modulating the extent of proteolytic processing. Because

N-linked glycosylation of Asn-39 also affects protein stability during synthesis (**Fig. 3**), we tested if glucosamine treatment would likewise decrease CTRP12 protein stability. Cycloheximide chase experiment indicated that CTRP12 was less stable and had a faster turnover in cells exposed to glucosamine relative to controls (**Fig. 10G-H**).

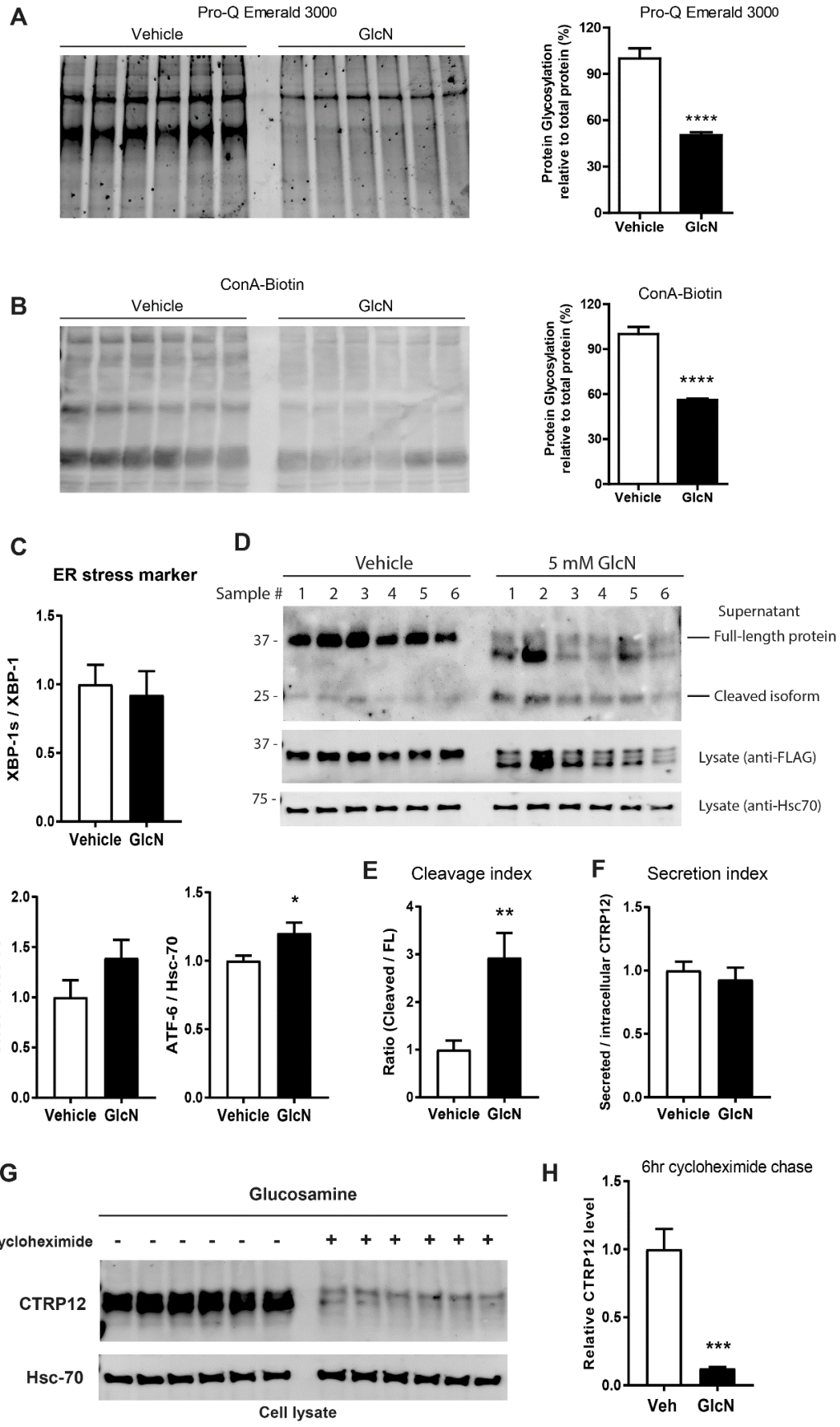
A
Pro-Q Emerald 3000
Vehicle
GlcN
Pro-Q Emerald 3000
Protein Glycosylation relative to total protein (%)
****
Vehicle
GlcN
B
ConA-Biotin
Vehicle
GlcN
ConA-Biotin
Protein Glycosylation relative to total protein (%)
****
Vehicle
GlcN
C
ER stress marker
XBP-1s / XBP-1
Vehicle
GlcN
D
Vehicle
5 mM GlcN
Sample #
1 2 3 4 5 6 1 2 3 4 5 6
Supernatant
37 -
Full-length protein
25 -
Cleaved isoform
37 -
Lysate (anti-FLAG)
75 -
Lysate (anti-Hsc70)
CHOP / Hsc-70
Vehicle
GlcN
ATF-6 / Hsc-70
*
Vehicle
GlcN
E
Cleavage index
Ratio (Cleaved / FL)
**
Vehicle
GlcN
F
Secretion index
Secreted / intracellular CTRP12)
Vehicle
GlcN
G
Glucosamine
Cycloheximide
- - - - - - + + + + + +
CTRP12
Hsc-70
Cell lysate
H
6hr cycloheximide chase
Relative CTRP12 level
***
Veh
GlcN

Figure 10. Impact of hexosamine biosynthesis pathway on CTRP12 cleavage and stability. ***A-B*****,** Quantification of glycosylated proteins (relative to total) in HEK 293 cells treated with 5 mM of glucosamine (GlcN) for 48 hr using Pro-Q emerald 3000 (**A**) or biotin-conjugated concanavalin A (**B**). Each lane represents an independent biological sample. ***C*****,** Western blot quantification of three major ER stress pathways (XBP1, CHOP/GADD153, ATF-6) in HEK 293 cells treated with vehicle control or 5 mM glucosamine. XBP-1s refers to the spliced isoform of XBP-1. ***D*****,** Western blot analysis of cell lysate and supernatant of transfected HEK 293 cells expressing wild-type (WT) CTRP12 treated with 5 mM glucosamine. ***E*****,** Quantification of the ratio of cleaved to full-length (FL) protein (the cleavage index) in supernatant of cells treated with glucosamine. ***F*****,** Quantification of the ratio of secreted to intracellular CTRP12 protein (the secretion index) as shown in D. ***G***, A 6 hr cycloheximide chase experiment of HEK 293 cells treated with 5 mM glucosamine. ***H***, Quantification of the relative protein stability of CTRP12 in glucosamine-treated cells versus non-treated controls (same as the top panel in Fig. 3J). N=6 (each lane represents a different sample from an independent transfection); **p<0.01; ***p<0.001; ****p<0.0001

Discussion

We previously showed that the Golgi-localized endopeptidase furin/PCSK3 cleaves CTRP12 at the conserved Lys-91 to generate the shorter globular gCTRP12 isoform (24). In the present study, we identified *N*-glycosylation as an important posttranslational modification that can modulate the extent of proteolytic processing by furin/PCSK3. Complete inhibition of *N*-linked glycosylation by tunicamycin significantly increased the ratio of cleaved globular isoform to full-length CTRP12 secreted into the conditioned medium. There are three potential *N*-linked glycosylation sites (Asn-39, Asn-287, and Asn-297) that conform to the consensus Asn-X-Ser/Thr motif in mouse CTRP12. Asn-39 and Asn-287 are conserved from zebrafish to human, whereas Asn-297 is conserved in mouse, chicken, xenopus, and zebrafish (24). Each of these conserved Asn residues

appears to play an independent role in modulating either the folding, secretion, stability, or proteolytic cleavage of CTRP12.

For polypeptides that contain *N*-glycosylation sites, addition of glycan is initiated by the en bloc transfer of a 14-sugar moiety, $Glc_3Man_9GlcNAc_2$, from the dolichol lipid carrier to the asparagine residues (within the N-X-S/T sequence) as the polypeptides are co-translationally translocated into the ER (42). The 14-sugar glycans get extensively trimmed by glycosidases in the ER, and the resulting oligomannose-type glycans get further processed and converted to hybrid and complex type oligosaccharides in the Golgi (42). The Golgi-resident glycosyltransferase GnTI (encoded by *MGAT1* gene) converts $Man_5GlcNAc_2$ to $GlcNAcMan_5GlcNAc_2$, a critical initial step needed for all other subsequent glycan processing in the Golgi (56). In the absence of GnTI, only homogenous oligomannosidic type *N*-glycans ($Man_5GlcNAc_2$) are present on glycoproteins (35,57). Since furin/PCSK3 is a Golgi-localized endopeptidase (46,58) responsible for the proteolytic processing of endogenous CTRP12 in adipocytes (24), we took advantage of the HEK 293 cells lacking GnTI to address whether this type of *N*-glycan impacts CTRP12 cleavage. In GnTI-deficient cells, we also observed enhanced cleavage of wild-type CTRP12. These results suggest that the presence of hybrid and complex-type glycans plays a role in modulating furin-mediated cleavage of its substrate, CTRP12, due to *N*-glycan processing and remodeling in the Golgi.

Interestingly, we also observed enhanced cleavage of the N297Q mutant even though Asn-297 is not glycosylated. Asn-297 and Asn-39 are located far apart in the linear sequence of the CTRP12 protein. When we mutated both Asn-39 and Asn-297 to Gln in the double mutant (N39Q/N297Q), nearly all the full-length proteins were cleaved. These results suggest that Asn-39 and Asn-297 act independently to modulate CTRP12 cleavage. Given that Asn-297 is located close to the C-terminus of the protein and Asn-39 is located 54 amino acids upstream of the Lys-91 cleavage site, how these two sites independently modulate furin cleavage of CTRP12 remains unclear. The lack of structural data on CTRP12 precludes a molecular explanation and is a limitation of the present study. Structural information on the C-terminal globular domain (but not full-length protein) exists for CTRP5 (59), CTRP10/C1ql2, CTRP13/C1ql3, CTRP14/C1ql1 (60). The C-terminal globular domain of CTRP12, however, shares only 16-24 % amino acid identity to these related family members, thus precluding molecular modeling of CTRP12 based on these distantly related structures. Despite this limitation, we speculate that in the fully folded state, both Asn-39 and Asn-297 could lie in relative close proximity to the furin cleavage site. The branches of *N*-linked glycans can reach more than 3 nm from the protein surface; further, the bulky and mobile carbohydrate groups are also branched (61). As such, the *N*-glycans could function as independent domains (61). The size and charge of the complex-type glycans on Asn-39 could limit furin access to the Lys-91 cleavage site on CTRP12. Alternatively, complex-type glycans may induce conformational changes in CTRP12 that would make it a poor substrate for furin, causing its

absence to favor a conformation that promotes furin recognition and cleavage within the secretory pathway. Interestingly, Lassa virus glycoprotein GP-C contains eleven *N*-glycosylation sites, six of which are required for proteolytic processing by the proprotein convertase PCSK8 (SK-I/S1P) (62). Opposite to that of CTRP12 described here, abolishing glycosylation at either position 81, 91, 101, 121, 367, or 375 by site-directed mutagenesis in Lassa virus glycoprotein GP-C completely blocked its cleavage by PCSK8 at Arg-260 (62). Based on these results, the authors suggest that *N*-glycosylation may be needed for correct conformation of the viral glycoprotein to be proteolytically processed by PCSK8.

GalNAc type *O*-glycosylation close to the cleavage site plays an important role in modulating proprotein convertase cleavage of secretory proteins (63-67). Specifically, *O*-linked glycans protect the secreted protein from inactivation by proprotein convertase cleavage. In all these cases, the *O*-glycosylated Ser or Thr residue lies within a few amino acids of the cleavage site (63-67). Our current findings represent a novel example of how disruptions in *N*-glycan biosynthesis in the ER and differential processing of *N*-linked glycans in the Golgi can affect the posttranslational cleavage of a secreted protein by proprotein convertases. Rather than inactivating the protein, proteolytic cleavage alters the ratio of full-length to cleaved isoforms of CTRP12 with potentially different biological functions (24). A vast majority of *N*-glycosylation sites are thought to be glycosylated (68) and a large number (~3,500) of secreted proteins are also believed to be processed by proprotein convertases (69). Thus, our results may have broader implications for

understanding crosstalk between complex *N*-linked glycan remodeling and other forms of regulation (e.g., proteolytic cleavage) in the Golgi compartment. Consistent with its importance in *N*-linked glycan remodeling, targeted disruption of the *Mgat1* gene encoding GnTI in mice results in embryonic lethality (70,71).

While Asn-39 and Asn-297 modulate the extent of CTRP12 cleavage, they are not required for protein secretion. Single (N39Q and N287Q) or double (N39Q/N297Q) mutants of CTRP12 are readily secreted from cells. In striking contrast, mutating Asn-287 to Gln completely abolished CTRP12 secretion. The N287Q or N287A mutant was retained in the ER; each still possesses high mannose-type glycans (on Asn-39) that can be acted upon by Endo H glycosidase. Secretory proteins that have exited the ER and transited to the Golgi and trans-Golgi network (TGN) have acquired hybrid or complex-type *N*-glycans that are resistant to Endo H action. Further, the N287Q mutant migrated as a large molecular aggregate compared to wild-type CTRP12 on immunoblot. These results suggest that Asn-287 is required for proper protein folding, and its absence results in protein misfolding, aggregation, and retention in the ER. Consistent with its importance in protein folding, Asn-287 is conserved in zebrafish, frog, chicken, mouse, and human (24).

One of the most important functions of *N*-glycosylation is to assist in protein folding in the ER (42,61). The ER chaperones calnexin and calreticulin recognize and bind to specific *N*-glycan structures (e.g., $Glc_1Man_{9-6}GlcNAc_2$) on glycoproteins;

correctly folded proteins will then be released from the lectin chaperones and transported to the Golgi with the help of other membrane-bound lectins (e.g, ERGIC-53) (72). Incorrectly folded protein will be retained in the ER and be disposed of via several different mechanisms. Although Asn-287 can potentially be glycosylated, site-directed mutagenesis of Asn-287 suggests that this residue is not glycosylated. Further, replacing Ser-289 (within the *N*-X-S glycosylation motif) with Ala did not recapitulate the protein misfolding phenotype of the N287Q mutant, as would be predicted if *N*-linked glycosylation of Asn-287 is important for proper protein folding and secretion. Importantly, complete inhibition of *N*-glycosylation by tunicamycin affected CTRP12 cleavage but not protein secretion. Together, our results point to a critical structural role for Asn-287 in proper protein folding, independent of glycosylation.

In addition to facilitating protein folding in the ER, *N*-linked glycosylation can also influence protein stability (45). Replacing Asn-39 with glutamine or mutating Thr-41 (in the context of *N*-X-T glycosylation motif) not only affects the extent of proteolytic cleavage of CTRP12 by the Golgi-localized furin, it also reduces protein stability and enhances protein turnover during synthesis. Consistent with the role of glycosylated Asn-39 in modulating CTRP12 protein stability, reducing *N*-linked protein glycosylation by exposing cells to exogenous glucosamine also decreases CTRP12 stability and increases its turnover. It appears that the non-glycosylated Asn-297, when mutated to glutamine, also reduces CTRP12 protein stability during synthesis. Unstable or misfolded protein is generally disposed of via the

endoplasmic reticulum associated degradation (ERAD) pathway (73). Thus, only properly folded CTRP12 protein will exit the ER and move to the Golgi where it can be proteolytically processed by the Golgi-localized furin. Given that ERAD occurs in the ER whereas furin cleavage takes place in the Golgi, this suggests that *N*-linked glycosylation can influence both the protein quality control (i.e., stability) and posttranslational processing of CTRP12 as it traverses through the different membrane compartments of the cell.

In the context of obesity and diabetes, high circulating blood glucose increases the generation of UDP-GlcNAc via the hexosamine biosynthesis pathway (52). Excess production of UDP-GlcNAc by exogenous supplementation of glucosamine can disrupt *N*-glycosylation in multiple different cell types *in vitro* and *in vivo* (36-38). Glucosamine ($\geq$5 mM) interferes with the biosynthesis of dolichol-linked oligosaccharides (36), leading to the inhibition of *N*-glycosylation. In animal models of obesity and diabetes, a significantly greater proportion of CTRP12 is cleaved (4,24). For this reason, we sought to address whether increasing the flux through the hexosamine biosynthesis pathway would alter the ratio of full-length protein to cleaved globular isoform secreted from cells. As would be predicted from the deleterious role of glucosamine on protein *N*-glycosylation, exogenous supplementation of glucosamine resulted in enhanced CTRP12 cleavage, an effect comparable to cells treated with tunicamycin. Since the flux through the hexosamine biosynthesis pathway is directly correlated with glucose

concentrations, this pathway may account, at least in part, for the greater CTRP12 cleavage seen in obese and diabetic animal models.

In summary, each of the conserved asparagine residues (Asn-39, Asn-287, and Asn-297) on CTRP12 plays an important role in either regulating proteolytic processing by furin endopeptidase or proper protein folding, stability, and secretion through both glycosylation dependent and independent mechanisms.

References

1. Wong, G. W., Krawczyk, S. A., Kitidis-Mitrokostas, C., Ge, G., Spooner, E., Hug, C., Gimeno, R., and Lodish, H. F. (2009) Identification and characterization of CTRP9, a novel secreted glycoprotein, from adipose tissue that reduces serum glucose in mice and forms heterotrimers with adiponectin. *FASEB J* **23**, 241-258
2. Wong, G. W., Krawczyk, S. A., Kitidis-Mitrokostas, C., Revett, T., Gimeno, R., and Lodish, H. F. (2008) Molecular, biochemical and functional characterizations of C1q/TNF family members: adipose-tissue-selective expression patterns, regulation by PPAR-gamma agonist, cysteine-mediated oligomerizations, combinatorial associations and metabolic functions. *Biochem J* **416**, 161-177
3. Wong, G. W., Wang, J., Hug, C., Tsao, T. S., and Lodish, H. F. (2004) A family of Acrp30/adiponectin structural and functional paralogs. *Proc Natl Acad Sci U S A* **101**, 10302-10307
4. Wei, Z., Peterson, J. M., Lei, X., Cebotaru, L., Wolfgang, M. J., Baldeviano, G. C., and Wong, G. W. (2012) C1q/TNF-related protein-12 (CTRP12), a novel adipokine that improves insulin sensitivity and glycemic control in mouse models of obesity and diabetes. *J Biol Chem* **287**, 10301-10315
5. Wei, Z., Peterson, J. M., and Wong, G. W. (2011) Metabolic regulation by C1q/TNF-related protein-13 (CTRP13): activation of AMP-activated protein kinase and suppression of fatty acid-induced JNK signaling. *J Biol Chem* **286**, 15652-15665
6. Wei, Z., Seldin, M. M., Natarajan, N., Djemal, D. C., Peterson, J. M., and Wong, G. W. (2013) C1q/Tumor Necrosis Factor-related Protein 11 (CTRP11), a Novel Adipose Stroma-derived Regulator of Adipogenesis. *J Biol Chem* **288**, 10214-10229
7. Seldin, M. M., Peterson, J. M., Byerly, M. S., Wei, Z., and Wong, G. W. (2012) Myonectin (CTRP15), a novel myokine that links skeletal muscle to systemic lipid homeostasis. *J Biol Chem* **287**, 11968-11980
8. Byerly, M. S., Petersen, P. S., Ramamurthy, S., Seldin, M. M., Lei, X., Provost, E., Wei, Z., Ronnett, G. V., and Wong, G. W. (2014) C1q/TNF-related Protein 4 (CTRP4) Is a Unique Secreted Protein with Two Tandem C1q Domains That Functions in the Hypothalamus to Modulate Food Intake and Body Weight. *J Biol Chem* **289**, 4055-4069
9. Peterson, J. M., Wei, Z., and Wong, G. W. (2009) CTRP8 and CTRP9B are novel proteins that hetero-oligomerize with C1q/TNF family members. *Biochem Biophys Res Commun* **388**, 360-365
10. Kishore, U., Gaboriaud, C., Waters, P., Shrive, A. K., Greenhough, T. J., Reid, K. B., Sim, R. B., and Arlaud, G. J. (2004) C1q and tumor necrosis factor superfamily: modularity and versatility. *Trends Immunol* **25**, 551-561
11. Seldin, M. M., Tan, S. Y., and Wong, G. W. (2014) Metabolic function of the CTRP family of hormones. *Rev Endocr Metab Disord* **15**, 111-123
12. Byerly, M. S., Swanson, R., Wei, Z., Seldin, M. M., McCulloh, P. S., and Wong, G. W. (2013) A Central Role for C1q/TNF-Related Protein 13 (CTRP13) in Modulating Food Intake and Body Weight. *PLoS One* **8**, e62862
13. Peterson, J. M., Aja, S., Wei, Z., and Wong, G. W. (2012) C1q/TNF-related protein-1 (CTRP1) enhances fatty acid oxidation via AMPK activation and ACC inhibition. *J Biol Chem* **287**, 1576-1587

14. Peterson, J. M., Seldin, M. M., Tan, S. Y., and Wong, G. W. (2014) CTRP2 overexpression improves insulin and lipid tolerance in diet-induced obese mice. *PLoS One* **9**, e88535
15. Peterson, J. M., Seldin, M. M., Wei, Z., Aja, S., and Wong, G. W. (2013) CTRP3 attenuates diet-induced hepatic steatosis by regulating triglyceride metabolism. *Am J Physiol Gastrointest Liver Physiol* **305**, G214-224.
16. Peterson, J. M., Wei, Z., Seldin, M. M., Byerly, M. S., Aja, S., and Wong, G. W. (2013) CTRP9 transgenic mice are protected from diet-induced obesity and metabolic dysfunction. *Am J Physiol Regul Integr Comp Physiol* **305**, R522-533
17. Peterson, J. M., Wei, Z., and Wong, G. W. (2010) C1q/TNF-related Protein-3 (CTRP3), a Novel Adipokine That Regulates Hepatic Glucose Output. *J Biol Chem* **285**, 39691-39701
18. Seldin, M. M., Lei, X., Tan, S. Y., Stanson, K. P., Wei, Z., and Wong, G. W. (2013) Skeletal muscle-derived myonectin activates the mTOR pathway to suppress autophagy in liver. *J Biol Chem* **289**, 36073-36082
19. Wei, Z., Lei, X., Petersen, P. S., Aja, S., and Wong, G. W. (2014) Targeted deletion of C1q/TNF-related protein 9 increases food intake, decreases insulin sensitivity, and promotes hepatic steatosis in mice. *Am J Physiol Endocrinol Metab* **306**, E779-790
20. Rodriguez, S., Lei, X., Petersen, P. S., Tan, S. Y., Little, H. C., and Wong, G. W. (2016) Loss of CTRP1 disrupts glucose and lipid homeostasis. *Am J Physiol Endocrinol Metab* **311**, E678-E697
21. Lei, X., Rodriguez, S., Petersen, P. S., Seldin, M. M., Bowman, C. E., Wolfgang, M. J., and Wong, G. W. (2016) Loss of CTRP5 improves insulin action and hepatic steatosis. *Am J Physiol Endocrinol Metab* **310**, E1036-1052
22. Petersen, P. S., Lei, X., Wolf, R. M., Rodriguez, S., Tan, S. Y., Little, H. C., Schweitzer, M. A., Magnuson, T. H., Steele, K. E., and Wong, G. W. (2017) CTRP7 deletion attenuates obesity-linked glucose intolerance, adipose tissue inflammation, and hepatic stress. *Am J Physiol Endocrinol Metab* **312**, E309-E325
23. Lei, X., Seldin, M. M., Little, H. C., Choy, N., Klonisch, T., and Wong, G. W. (2017) C1q/TNF-related protein 6 (CTRP6) links obesity to adipose tissue inflammation and insulin resistance. *J Biol Chem* **292**, 14836-14850
24. Wei, Z., Lei, X., Seldin, M. M., and Wong, G. W. (2012) Endopeptidase cleavage generates a functionally distinct isoform of C1q/tumor necrosis factor-related protein-12 (CTRP12) with an altered oligomeric state and signaling specificity. *J Biol Chem* **287**, 35804-35814
25. Enomoto, T., Ohashi, K., Shibata, R., Higuchi, A., Maruyama, S., Izumiya, Y., Walsh, K., Murohara, T., and Ouchi, N. (2011) Adipolin/C1qdc2/CTRP12 functions as an adipokine that improves glucose metabolism. *J Biol Chem* **286**, 34552-34558
26. Bell-Anderson, K. S., Funnell, A. P., Williams, H., Mat Jusoh, H., Scully, T., Lim, W. F., Burdach, J. G., Mak, K. S., Knights, A. J., Hoy, A. J., Nicholas, H. R., Sainsbury, A., Turner, N., Pearson, R. C., and Crossley, M. (2013) Loss of Kruppel-like factor 3 (KLF3/BKLF) leads to upregulation of the insulin-sensitizing factor adipolin (FAM132A/CTRP12/C1qdc2). *Diabetes* **62**, 2728-2737
27. Tan, B. K., Lewandowski, K. C., O'Hare, J. P., and Randeva, H. S. (2014) Insulin regulates the novel adipokine adipolin/CTRP12: in vivo and ex vivo effects. *J Endocrinol* **in press**

28. Tan, B. K., Chen, J., Adya, R., Ramanjaneya, M., Patel, V., and Randeva, H. S. (2013) Metformin increases the novel adipokine adipolin/CTRP12: role of the AMPK pathway. *J Endocrinol* **219**, 101-108
29. Tan, B. K., Chen, J., Hu, J., Amar, O., Mattu, H. S., Ramanjaneya, M., Patel, V., Lehnert, H., and Randeva, H. S. (2014) Circulatory changes of the novel adipokine adipolin/CTRP12 in response to metformin treatment and an oral glucose challenge in humans. *Clin Endocrinol (Oxf)* **81**, 841-846
30. Tan, S. Y., Little, H. C., Lei, X., Li, S., Rodriguez, S., and Wong, G. W. (2016) Partial deficiency of CTRP12 alters hepatic lipid metabolism. *Physiol Genomics* **48**, 936-949
31. Enomoto, T., Shibata, R., Ohashi, K., Kambara, T., Kataoka, Y., Uemura, Y., Yuasa, D., Murohara, T., and Ouchi, N. (2012) Regulation of adipolin/CTRP12 cleavage by obesity. *Biochem Biophys Res Commun* **428**, 155-159
32. Tian, Y., Zhou, Y., Elliott, S., Aebersold, R., and Zhang, H. (2007) Solid-phase extraction of N-linked glycopeptides. *Nat Protoc* **2**, 334-339
33. Wisniewski, J. R., Zougman, A., and Mann, M. (2009) Combination of FASP and StageTip-based fractionation allows in-depth analysis of the hippocampal membrane proteome. *J Proteome Res* **8**, 5674-5678
34. Yang, W., Laeyendecker, O., Wendel, S. K., Zhang, B., Sun, S., Zhou, J. Y., Ao, M., Moore, R. D., Jackson, J. B., and Zhang, H. (2014) Glycoproteomic study reveals altered plasma proteins associated with HIV elite suppressors. *Theranostics* **4**, 1153-1163
35. Reeves, P. J., Callewaert, N., Contreras, R., and Khorana, H. G. (2002) Structure and function in rhodopsin: high-level expression of rhodopsin with restricted and homogeneous N-glycosylation by a tetracycline-inducible N-acetylglucosaminyltransferase I-negative HEK293S stable mammalian cell line. *Proc Natl Acad Sci U S A* **99**, 13419-13424
36. Beriault, D. R., Dang, V. T., Zhong, L. H., Petlura, C. I., McAlpine, C. S., Shi, Y., and Werstuck, G. H. (2017) Glucosamine induces ER stress by disrupting lipid-linked oligosaccharide biosynthesis and N-linked protein glycosylation. *Am J Physiol Endocrinol Metab* **312**, E48-E57
37. Chen, C. L., Liang, C. M., Chen, Y. H., Tai, M. C., Lu, D. W., and Chen, J. T. (2012) Glucosamine modulates TNF-alpha-induced ICAM-1 expression and function through O-linked and N-linked glycosylation in human retinal pigment epithelial cells. *Invest Ophthalmol Vis Sci* **53**, 2281-2291
38. Chien, M. W., Lin, M. H., Huang, S. H., Fu, S. H., Hsu, C. Y., Yen, B. L., Chen, J. T., Chang, D. M., and Sytwu, H. K. (2015) Glucosamine Modulates T Cell Differentiation through Down-regulating N-Linked Glycosylation of CD25. *J Biol Chem* **290**, 29329-29344
39. Kato, S., Zhang, R., and Roberts, J. D., Jr. (2013) Proprotein convertases play an important role in regulating PKGI endoproteolytic cleavage and nuclear transport. *Am J Physiol Lung Cell Mol Physiol* **305**, L130-140
40. Wanyiri, J. W., O'Connor, R., Allison, G., Kim, K., Kane, A., Qiu, J., Plaut, A. G., and Ward, H. D. (2007) Proteolytic processing of the Cryptosporidium glycoprotein gp40/15 by human furin and by a parasite-derived furin-like protease activity. *Infect Immun* **75**, 184-192
41. Takahashi, S., Kasai, K., Hatsuzawa, K., Kitamura, N., Misumi, Y., Ikehara, Y., Murakami, K., and Nakayama, K. (1993) A mutation of furin causes the lack of precursor-processing activity in human colon carcinoma LoVo cells. *Biochem Biophys Res Commun* **195**, 1019-1026

42. Helenius, A., and Aebi, M. (2001) Intracellular functions of N-linked glycans. *Science* **291**, 2364-2369
43. Elbein, A. D. (1987) Inhibitors of the biosynthesis and processing of N-linked oligosaccharide chains. *Annu Rev Biochem* **56**, 497-534
44. Tkacz, J. S., and Lampen, O. (1975) Tunicamycin inhibition of polyisoprenyl N-acetylglucosaminyl pyrophosphate formation in calf-liver microsomes. *Biochem Biophys Res Commun* **65**, 248-257
45. Jayaprakash, N. G., and Surolia, A. (2017) Role of glycosylation in nucleating protein folding and stability. *Biochem J* **474**, 2333-2347
46. Molloy, S. S., Thomas, L., VanSlyke, J. K., Stenberg, P. E., and Thomas, G. (1994) Intracellular trafficking and activation of the furin proprotein convertase: localization to the TGN and recycling from the cell surface. *EMBO J* **13**, 18-33
47. Hart, G. W., Brew, K., Grant, G. A., Bradshaw, R. A., and Lennarz, W. J. (1979) Primary structural requirements for the enzymatic formation of the N-glycosidic bond in glycoproteins. Studies with natural and synthetic peptides. *J Biol Chem* **254**, 9747-9753
48. Garten, W., Hallenberger, S., Ortmann, D., Schafer, W., Vey, M., Angliker, H., Shaw, E., and Klenk, H. D. (1994) Processing of viral glycoproteins by the subtilisin-like endoprotease furin and its inhibition by specific peptidylchloroalkylketones. *Biochimie* **76**, 217-225
49. Hallenberger, S., Bosch, V., Angliker, H., Shaw, E., Klenk, H. D., and Garten, W. (1992) Inhibition of furin-mediated cleavage activation of HIV-1 glycoprotein gp160. *Nature* **360**, 358-361
50. Stieneke-Grober, A., Vey, M., Angliker, H., Shaw, E., Thomas, G., Roberts, C., Klenk, H. D., and Garten, W. (1992) Influenza virus hemagglutinin with multibasic cleavage site is activated by furin, a subtilisin-like endoprotease. *EMBO J* **11**, 2407-2414
51. Kornfeld, R., and Kornfeld, S. (1985) Assembly of asparagine-linked oligosaccharides. *Annu Rev Biochem* **54**, 631-664
52. Buse, M. G. (2006) Hexosamines, insulin resistance, and the complications of diabetes: current status. *Am J Physiol Endocrinol Metab* **290**, E1-E8
53. Marshall, S., Nadeau, O., and Yamasaki, K. (2004) Dynamic actions of glucose and glucosamine on hexosamine biosynthesis in isolated adipocytes: differential effects on glucosamine 6-phosphate, UDP-N-acetylglucosamine, and ATP levels. *J Biol Chem* **279**, 35313-35319
54. Jokela, T. A., Jauhiainen, M., Auriola, S., Kauhanen, M., Tiihonen, R., Tammi, M. I., and Tammi, R. H. (2008) Mannose inhibits hyaluronan synthesis by down-regulation of the cellular pool of UDP-N-acetylhexosamines. *J Biol Chem* **283**, 7666-7673
55. Pouyssegur, J., Shiu, R. P., and Pastan, I. (1977) Induction of two transformation-sensitive membrane polypeptides in normal fibroblasts by a block in glycoprotein synthesis or glucose deprivation. *Cell* **11**, 941-947
56. Kumar, R., Yang, J., Larsen, R. D., and Stanley, P. (1990) Cloning and expression of N-acetylglucosaminyltransferase I, the medial Golgi transferase that initiates complex N-linked carbohydrate formation. *Proc Natl Acad Sci U S A* **87**, 9948-9952
57. Chang, V. T., Crispin, M., Aricescu, A. R., Harvey, D. J., Nettleship, J. E., Fennelly, J. A., Yu, C., Boles, K. S., Evans, E. J., Stuart, D. I., Dwek, R. A., Jones, E. Y., Owens, R. J., and Davis, S. J. (2007) Glycoprotein structural genomics: solving the glycosylation problem. *Structure* **15**, 267-273

58. Takahashi, S., Nakagawa, T., Banno, T., Watanabe, T., Murakami, K., and Nakayama, K. (1995) Localization of furin to the trans-Golgi network and recycling from the cell surface involves Ser and Tyr residues within the cytoplasmic domain. *J Biol Chem* **270**, 28397-28401
59. Tu, X., and Palczewski, K. (2012) Crystal structure of the globular domain of C1QTNF5: Implications for late-onset retinal macular degeneration. *J Struct Biol* **180**, 439-446
60. Ressl, S., Vu, B. K., Vivona, S., Martinelli, D. C., Sudhof, T. C., and Brunger, A. T. (2015) Structures of C1q-like proteins reveal unique features among the C1q/TNF superfamily. *Structure* **23**, 688-699
61. Helenius, A., and Aebi, M. (2004) Roles of N-linked glycans in the endoplasmic reticulum. *Annu Rev Biochem* **73**, 1019-1049
62. Eichler, R., Lenz, O., Garten, W., and Strecker, T. (2006) The role of single N-glycans in proteolytic processing and cell surface transport of the Lassa virus glycoprotein GP-C. *Virol J* **3**, 41
63. Kato, K., Jeanneau, C., Tarp, M. A., Benet-Pages, A., Lorenz-Depiereux, B., Bennett, E. P., Mandel, U., Strom, T. M., and Clausen, H. (2006) Polypeptide GalNAc-transferase T3 and familial tumoral calcinosis. Secretion of fibroblast growth factor 23 requires O-glycosylation. *J Biol Chem* **281**, 18370-18377
64. Schjoldager, K. T., Vester-Christensen, M. B., Goth, C. K., Petersen, T. N., Brunak, S., Bennett, E. P., Levery, S. B., and Clausen, H. (2011) A systematic study of site-specific GalNAc-type O-glycosylation modulating proprotein convertase processing. *J Biol Chem* **286**, 40122-40132
65. Schjoldager, K. T., Vester-Christensen, M. B., Bennett, E. P., Levery, S. B., Schwientek, T., Yin, W., Blixt, O., and Clausen, H. (2010) O-glycosylation modulates proprotein convertase activation of angiopoietin-like protein 3: possible role of polypeptide GalNAc-transferase-2 in regulation of concentrations of plasma lipids. *J Biol Chem* **285**, 36293-36303
66. Zhang, L., Syed, Z. A., van Dijk Hard, I., Lim, J. M., Wells, L., and Ten Hagen, K. G. (2014) O-glycosylation regulates polarized secretion by modulating Tango1 stability. *Proc Natl Acad Sci U S A* **111**, 7296-7301
67. Tagliabracci, V. S., Engel, J. L., Wiley, S. E., Xiao, J., Gonzalez, D. J., Nidumanda Appaiah, H., Koller, A., Nizet, V., White, K. E., and Dixon, J. E. (2014) Dynamic regulation of FGF23 by Fam20C phosphorylation, GalNAc-T3 glycosylation, and furin proteolysis. *Proc Natl Acad Sci U S A* **111**, 5520-5525
68. Gavel, Y., and von Heijne, G. (1990) Sequence differences between glycosylated and non-glycosylated Asn-X-Thr/Ser acceptor sites: implications for protein engineering. *Protein Eng* **3**, 433-442
69. Seidah, N. G. (2011) What lies ahead for the proprotein convertases? *Ann N Y Acad Sci* **1220**, 149-161
70. Ioffe, E., and Stanley, P. (1994) Mice lacking N-acetylglucosaminyltransferase I activity die at mid-gestation, revealing an essential role for complex or hybrid N-linked carbohydrates. *Proc Natl Acad Sci U S A* **91**, 728-732
71. Metzler, M., Gertz, A., Sarkar, M., Schachter, H., Schrader, J. W., and Marth, J. D. (1994) Complex asparagine-linked oligosaccharides are required for morphogenic events during post-implantation development. *EMBO J* **13**, 2056-2065
72. Hauri, H. P., Kappeler, F., Andersson, H., and Appenzeller, C. (2000) ERGIC-53 and traffic in the secretory pathway. *J Cell Sci* **113 (Pt 4)**, 587-596
73. Ruggiano, A., Foresti, O., and Carvalho, P. (2014) Quality control: ER-associated degradation: protein quality control and beyond. *J Cell Biol* **204**, 869-879

CHAPTER 3:

Protein modifications critical for myonectin/erythroferrone secretion and oligomer assembly*

*Text and figures in this chapter were published in *Biochemistry* in 2020:

Protein modifications critical for myonectin/erythroferrone secretion and oligomer assembly. Ashley N. Stewart, Hannah C. Little, David J. Clark, Hui Zhang, and G. William Wong, *Biochemistry* 2020

Ashley Stewart generated data for all figures with the exception of Figure 1 (GWW), Figure 3A,B (DJC and HZ), Figure 7A (GWW) and Figure 7B (DJC and HZ).

Abstract

Myonectin/erythroferrone (also known as CTRP15) is a secreted hormone with metabolic function and a role in stress erythropoiesis. Despite its importance in physiologic processes, biochemical characterization of the protein is lacking. Here, we show that multiple protein modifications are critical for myonectin secretion and multimerization. Abolishing *N*-linked glycosylation by tunicamycin, glucosamine supplementation, or glutamine substitutions of all four potential Asn glycosylation sites blocked myonectin secretion. Mass spectrometry confirmed that Asn-229 and Asn-281 were glycosylated, and substituting both Asn sites with Gln prevented myonectin secretion. Although Asn-319 is not identified as glycosylated, Gln substitution caused protein misfolding and retention in the endoplasmic reticulum. Of the four conserved cysteines, Cys-273 and Cys-278 were required for proper protein folding; Ala substitution of either site inhibited protein secretion. In contrast, Ala substitutions of Cys-142, Cys-194, or both markedly enhanced protein secretion, suggesting endoplasmic reticulum retention that facilitates myonectin oligomer assembly. Secreted myonectin consists of trimers, hexamers, and high molecular weight (HMW) oligomers. Formation of higher-order structures via inter-molecular disulfide bonds depended on Cys-142 and Cys-194, whereas the C142A mutant formed almost exclusively trimers and the C194 mutant was impaired in HMW oligomer formation. Most Pro residues within the short collagen domain of myonectin were also hydroxylated, a modification that stabilized the collagen triple helix. Inhibiting Pro hydroxylation or deleting the collagen domain markedly

reduced protein secretion. Together, our results reveal key determinants important for myonectin folding, secretion, and multimeric assembly and provide a basis for future structure/function studies.

Introduction

Beyond its necessity for locomotion, skeletal muscle regulates whole-body metabolism through postprandial glucose uptake (1). Skeletal muscle secretes many proteins, referred to as myokines, which mediate endocrine crosstalk between muscle and other tissue compartments to facilitate integrative control of energy homeostasis (2-4). Our efforts to discover novel endocrine factors that regulate inter-organ communications led to the identification and characterization of myonectin (CTRP15), a myokine produced by skeletal muscle in the basal state (5,6) and further induced by exercise (5,7).

Myonectin belongs to the larger C1q/TNF-related protein (CTRPs) family, members of which share a common C-terminal globular C1q domain (5,8-14). Gain- and loss-of-function studies *in vivo* demonstrate an important role for myonectin in modulating local (liver and adipose tissue) and systemic lipid metabolism (5,15), as well as conferring a protective function in the heart in the context of ischemia reperfusion injury (7). Independent of its metabolic and cardiovascular function, myonectin/erythroferrone plays important roles in stress erythropoiesis (16-21). In response to severe blood loss or anemia, erythroferrone

expression is markedly induced in bone marrow and spleen by erythropoietin; elevated plasma erythroferrone then mobilizes iron stores in the liver needed for erythropoiesis by suppressing the expression of hepcidin. Dysregulation of the erythroferrone-hepcidin axis contributes to iron overload in a mouse model of β-thalassemia (22,23) and in humans with myelodysplastic syndrome (24,25). Although dispensable for embryogenesis, erythroferrone may also play a role in development in a species-specific manner; knockdown of eryrthroferrone in *Xenopus* disrupts proper vascular network formation and primitive blood circulation (26).

Like all C1q family members (14,27-30), myonectin forms trimers as its basic structural unit; individual trimers are further assembled into higher-order structures such as hexamers and high molecular weight (HMW) oligomers (e.g., 12-18 mer) (5). In the case of adiponectin and CTRP12, different oligomeric forms have distinct biological activities and signaling properties (31-34). While the physiological functions of myonectin/erythroferrone are newly emerging and actively pursued, basic biochemical characterization of the protein is lacking, and the factors that influence myonectin secretion and its higher-order structural assembly are unknown. We aimed to uncover critical determinants—focusing on protein modifications—that regulate myonectin folding, secretion, and multimerization.

Our findings revealed key determinants and protein modifications important for myonectin folding, secretion, and multimeric assembly. This knowledge will inform future structure/function studies assessing naturally occurring polymorphisms that potentially alter protein modifications of myonectin/erythroferrone and their impact on secretion (and hence circulating level), multimerization, and biological activity.

Materials and methods

Materials

Tris(2-carboxyethyl)phosphine (TCEP) was obtained from Thermo Scientific (Rockford, IL). Mouse monoclonal anti-FLAG M2 antibody was purchased from Sigma-Aldrich (St. Louis, MO). Glucosamine, Iodoacetamide, and tunicamycin were obtained from Sigma-Aldrich. Trypsin and chymotrypsin were purchased from Promega (Madison, WI), hydrazine resin was from Bio-Rad (Hercules, CA), and peptide *N*-glycosidase F (PNGase F) and endoglycosidase H (Endo H) were from New England Biolabs (Ipswich, MA). The selective collagen prolyl 4-hydroxylase (CP4H) inhibitor [6-(5-Ethoxycarbonyl-thiazol-2-yl)-nicotinic acid ethyl ester; also known as diethyl-pythiDC] was obtained from Aobious (Gloucester, MA).

cDNA constructs

All C-terminal FLAG epitope-tagged mouse myonectin/erythroferrone/CTRP15 (NP_775571) single, double, and quadruple mutant constructs (N229Q, N281Q, N292Q, N319Q, S321A, N229Q/N281Q, C142A, C194A, C273A, C278A, C142A/C194A) were generated by either site-directed mutagenesis using a QuikChange kit (Stratagene, San Diego, CA) or by GenScript (Piscataway, NJ). The quadruple Asn mutant (N229Q/N281Q/N292Q/N319Q) is referred to as 4Q mutant throughout the text. The deletion mutant used in this study includes ΔCollagen (collagen domain deleted; amino acid 97-114). Each cDNA insert was cloned into the expression vector pCDNA3.1 (+) (Invitrogen, Carlsbad, CA). All constructs were verified by DNA sequencing.

Determination of signal peptidase cleavage site

Recombinant mouse wild-type myonectin was produced in mammalian HEK 293 cells and purified as described previously (5). Ten to twenty micrograms of purified protein were separated by SDS-PAGE, transferred to polyvinylidene fluoride (PVDF) membrane, and subjected to N-terminal amino acid sequencing at the synthesis and sequencing facility at Johns Hopkins University.

Protein digestion and *N*-linked glycopeptide enrichment

Urea was added to 25 μg of purified recombinant mouse myonectin (in 25 mM HEPES, 135 mM NaCl, pH 8) to a final concentration of 8 M to aid in protein digestion by proteases. Myonectin protein was reduced with 10 mM TECP, and

then alkylated with 15 mM iodoacetamide. 50 mM triethylammonium bicarbonate was added to reduce urea concentration to 1 M. Myonectin sample was subjected to trypsin (1:25 enzyme-protein ratio), followed by chymotrypsin (1:25 enzyme-protein ratio) digest at 37°C overnight. A solid-phase extraction method of *N*-linked glycoprotein (SPEG) was used to enrich glycosylated peptide as previously described (35,36). Peptides were first subjected to C18 stage tip clean-up (37), then oxidized with 10 mM sodium periodate at room temperature for 1 h. Peptides were desalted using C18 stage tip before conjugation to hydrazide resin. The overnight coupling reaction was carried out in 80% acetonitrile, 0.1% trifluoroacetic acid, and 1% aniline. Non-glycosylated peptides were removed by washing the resin three times with 1 mL of 50% acetonitrile, 1.5 M NaCl, HPLC-H_2O, and 25 mM triethylammonium bicarbonate. Overnight incubation with 3 µL of PNGase F in 25 mM triethylammonium bicarbonate was carried out to release the *N*-linked glycosite-containing peptides from the resin . Released glycosite-containing peptides were collected after centrifugation at 3,000 x g. The resin was then rinsed with 50% acetonitrile twice and the washes were pooled. The peptide solution was desalted, dried, and reconstituted in 0.1% formic acid and subjected to mass spectrometry (MS) analysis.

LC-MS/MS analysis and protein identification

ESI-LC-MS/MS was used to analyze the peptides as described (38). Approximately ~1 µg of the *N*-linked glycosite-containing peptides were separated using a Dionex Ultimate 3000 RSLC nano system (Thermo Scientific, Waltham,

MA) with a 75-μm x 15-cm Acclaim PepMap100 separating column (Thermo Scientific) protected by a 2-cm guard column (Thermo Scientific). The mobile phase consisted of 0.1% formic acid in water (A) and 0.1% formic acid/95% acetonitrile (B). Flow rate was set at 300 nL/min. The following gradient profile was used: 4-35% B for 70 min, 35-95% B for 5 min, 95% B for 10 min, and equilibrated in 4% B for 15 min. An Orbitrap Velos Pro mass spectrometer (Thermo Scientific) was used in MS analyses. Spray voltage was set at 2.2 kV. Orbitrap spectra (AGC $1x10^6$) were collected from 400-1800 m/z at a resolution of 60 K followed by data-dependent HCD MS/MS (at a resolution of 7500, collision energy 35%, activation time 0.1 ms) of the ten most abundant ions using an isolation width of 2.0 Da. Unassigned and singly charged ions were rejected by Charge state screening. A dynamic exclusion time of 35 sec was used to discriminate against previously selected ions. Peptides were identified using Proteome Discoverer software (Thermo Scientific, ver 1.3). Spectra were searched against the CTRP15/myonectin/erythroferrone protein sequence [UniProtKB – Q6PGN1, ERFE_MOUSE]. The precursor mass tolerance was set at 20 ppm and the MS/MS tolerance at 0.06 Da. Parameters of the search included: variable modifications such as methionine oxidation (+15.99492), asparagine deamidation (+0.984016), and proline hydroxylation (+15.99492); fixed modification such as cysteine carbamidomethylation (+57.02510); digestion enzymes such as trypsin and chymotrypsin, and a maximum of two missed cleavages were allowed.

Cell culture and transfection

HEK 293A cells (ATCC) were cultured in DMEM (Invitrogen) containing 10% fetal bovine serum (FBS), 4 mM L-glutamine, 100 units/mL penicillin, and 100 µg/mL streptomycin. Transfections were carried out using Lipofectamine (Invitrogen) according to the manufacturer's instructions. Twenty-four h post transfection, medium was replaced with serum-free Opti-MEM (Invitrogen). Both cell lysates and media from transfected cells were collected 24 h later. Cell lysates were prepared by solubilizing cells in whole cell extract buffer (20 mM Tris-HCL pH 7.5, 150 mM NaCl, 1 mM Na_2EDTA, 0.5% NP-40, and 10% glycerol) containing SIGMAFAST™ protease inhibitor cocktail (Sigma) and phosSTOP phosphatase inhibitor cocktail (Roche, Basel Swizerland). For the treatment groups, tunicamycin (0.5 µg/mL) or glucosamine (5 mM) was added to the culture medium 2 h before transfection. The dose of glucosamine used (5 mM) was known to disrupt *N*-glycosylation (39-41). For experiments involving the selective CP4H inhibitor, cells were cultured in media containing 50 µM of diethyl-pythiDC or vehicle control (DMSO; equal volume) for 1 h before transfection and the inhibitor was added to fresh media the following day. 24 h after transfection, medium was replaced with serum-free Opti-MEM (Invitrogen) containing tunicamycin, glucosamine, diethyl-pythiDC, or vehicle controls. Twenty four hour later, cell lysates and media were collected.

Immunoblot analysis

For immunoblot analyses, cell lysates were suspended in loading buffer containing 50 mM Tris, 2% SDS, 1% β-ME, 6% glycerol, and 0.01% bromophenol blue. The protein samples were denatured at 94°C for 15 min. Proteins were separated in 10% or 8-16% pre-cast mini-PROTEAN TGX gel (Bio-Rad), and transferred onto nitrocellulose or PVDF membrane (Bio-Rad). Membranes were blocked with 5% non-fat milk for 1 h, followed by incubation with mouse anti-FLAG M2 (1:1000) overnight. Immunoblots were washed three times (5 min each) in PBS containing 0.1% Tween-20, followed by incubation with horseradish peroxidase-conjugated secondary antibody (Amersham Biosciences, Little Chalfont, United Kingdom) at 1:2,000 for 1 h. Blots were washed 3 times (5 min each) in PBS containing 0.1% Tween 20, developed in ECL reagent (Millipore, Burlington, MA) for 5-10 min and visualized with MultiImage III FluorChem ® Q (Alpha Innotech, San Leandro, CA). Quantification of signal intensity was performed using Image J software (42).

Blue native gel electrophoresis

Blue native PAGE was carried out based on the Invitrogen NativePAGE Novex Bis-Tris gel system protocol. Briefly, samples were prepared by addition of 6.25 µL of NativePAGE sample buffer (Invitrogen; BN2003) to 18.75 uL of conditioned medium of transfected HEK 293 cells. Proteins were separated on a 3-12% 1.0 mm thick precast Bis-Tris gel (Invitrogen; BN1001) using the XCell II blot module. After 25 µL of prepared samples were loaded into wells, light blue cathode running buffer containing 0.002% Coomassie G-250 (Invitrogen; BN2004) and 1x anode

running buffer (Invitrogen; BN2001) were poured into the inner and outer chambers, respectively. The gel was run at a constant 150 volts, 15 amps, and 4°C for 150 min.

Before immunoblotting, PVDF membrane (BioRad; 1620177) was incubated in 100% methanol for 30 sec, then rinsed 2 min in distilled water and incubated in 1x NuPAGE transfer buffer (Invitrogen; NP00061) for 10 min. Following the run, gel was first incubated in transfer buffer for 2 min, then immediately transferred for 90 min at 100 volts and 4°C onto the prepared PVDF membrane using the BioRad Mini Trans-Blot® electrophoretic transfer cell. A stir bar was added to the cell and set to 350 rpm for the duration of the transfer to help maintain even buffer temperature and ion distribution.

Following transfer, the membrane was incubated in 8% acetic acid for 15 min, briefly rinsed with distilled water, then incubated in 100% methanol for 2 min. After a brief distilled water wash, the membrane was blocked with 5% nonfat milk for 1 h and probed with mouse anti-FLAG M2 antibody (Cell Signaling, Danvers, MA; 8146S) at 1:500 overnight. Immunoblots were washed three times (5 min each) in PBS containing 0.1% Tween 20 and incubated with horseradish peroxidase-conjugated secondary antibody (Cell Signaling; 7076S; 1:1000) for 1 h. Blots were washed three times (5 min each) in PBS containing 0.1% Tween 20, developed in ECL reagent (MilliporeSigma, Burlington, MA; GERPN2235) for 8 min, and visualized with MultiImage III FluorChem Q (Alpha Innotech).

Statistical analysis

Two-tailed Student's *t*-tests were used in all comparison. Values were considered significant at $P < 0.05$. All data are presented as mean ± standard error of the mean (SEM).

Results

N-linked glycosylation is required for myonectin secretion

As a secreted protein, myonectin/erythroferrone contains a hydrophobic signal peptide at the N-terminus. Although the SignalIP program(43) predicted that the signal peptide would be cleaved between Gly-26 and Val-27, N-terminal sequencing of purified mouse myonectin revealed "ESAE" to be the first four amino acids of the mature secreted protein, suggesting that the cleavage site is between Pro-28 and Glu-29 (**Fig. 1**). Although uncommon, proline at the P-1 position of the cleavage site was documented for other mammalian secretory and plasma membrane proteins (44-49).

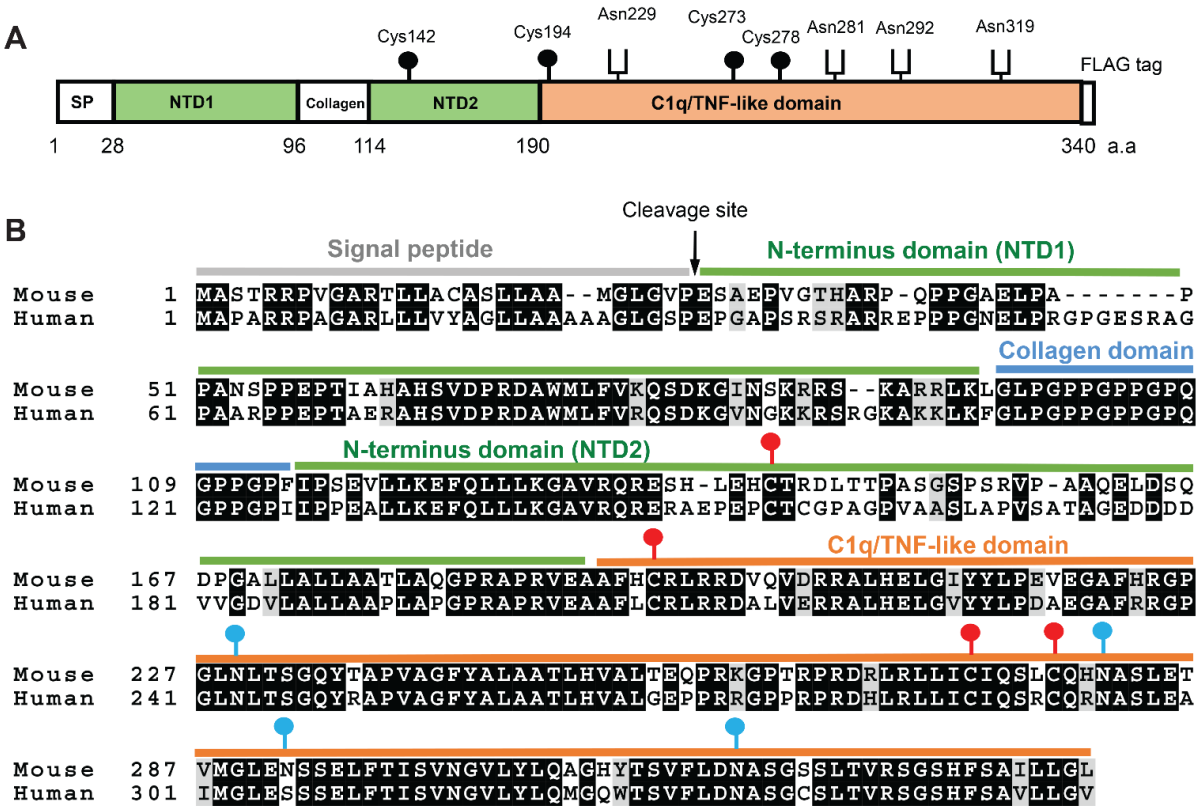

Figure 1. Conservation of protein modification sites between mouse and human myonectin. **A**, Domain structure of mouse myonectin. The four potential *N*-linked glycosylation sites (Asn-229, Asn-281, Asn-292, and Asn-319) that conform to the N-X-S/T motif are labeled. The positions of the four cysteine residues (Cys-142, Cys-194, Cys-273, and Cys-278) are also labeled. The presence of a FLAG epitope tag (DYKDDDK) located in the C-terminus of the protein is also indicated. **B**, Multiple sequence alignment of mouse (NP_775571) and human (NP_001278761) myonectin. Alignment was peformed using ClustalW program (50). The signal peptide, signal peptidase cleavage site, N-terminal domain 1 (NTD1), collagen domain, NTD2, and C1q/TNF-like domain are highlighted, as are all the conserved Cys residues and potential Asn glycosylation sites.

Mouse myonectin/erythroferrone contains four potential *N*-linked glycosylation sites (Asn-229, Asn-281, Asn-292, and Asn-319) that conform to the consensus sequon, N-X-S/T (where X is any amino acid except proline; **Fig. 1A**). Three of these sites (Asn-229, Asn-281, Asn-319) are conserved in human myonectin (**Fig. 1B**). When subjected to peptide:N-glycosidase F (PNGase F) digest, the apparent molecular weight of myonectin shifted on immunoblot, indicating that myonectin contains *N*-linked glycans (**Fig. 2A**), as we had previously shown (5). To determine whether *N*-linked glycosylation is required for proper myonectin folding and secretion, we used tunicamycin to completely block *N*-glycosylation (51,52). In heterologous HEK 293A cells expressing mouse myonectin, blocking *N*-linked glycosylation abolished protein secretion (**Fig. 2B**). UDP-*N*-acetylglucosamine (UDP-GlcNAc)—derived from the hexosamine biosynthesis pathway—is an essential sugar-nucleotide substrate for protein glycosylation. Excess production of UDP-GlcNAc by glucosamine supplementation can also disrupt *N*-glycosylation of proteins by interfering with the biosynthesis of dolichol-linked oligosaccharides (39). When we used 5 mM of glucosamine, a dose that reduces *N*-linked glycosylated proteins (39,53), we observed a block in myonectin secretion (**Fig. 2C**). In accordance with the results obtained with pharmacologic inhibition of *N*-linked glycosylation, the 4Q mutant that lacks all four potential *N*-linked glycosylation sites was also not secreted (**Fig. 2D**). These results indicate that protein glycosylation is required for proper myonectin folding and secretion from cells.

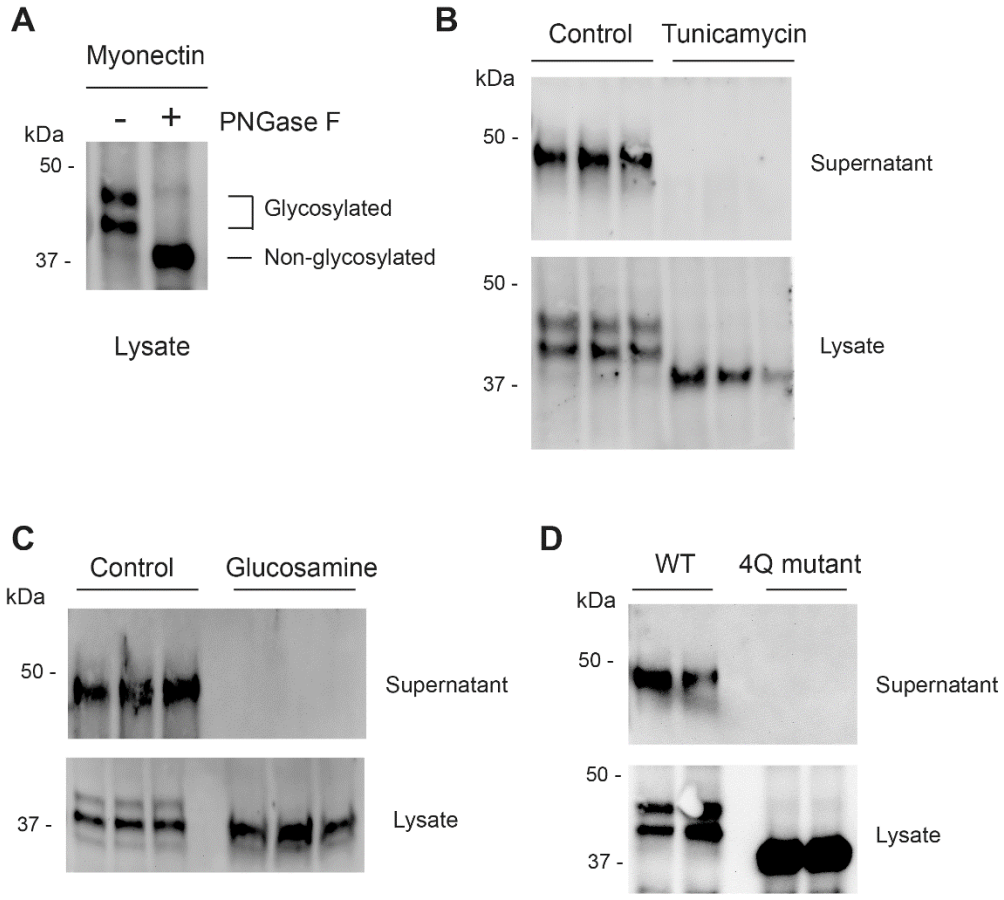

Figure 2. *N*-linked glycosylation is required for myonectin secretion. **A**, Peptide N:Glycosidase F (PNGase F) digest indicating that myonectin protein contains *N*-linked glycans. **B**, Inhibiting *N*-linked glycosylation by tunicamycin abolished myonectin secretion. **C**, Glucosamine (5 mM) supplementation, known to inhibit *N*-linked glycosylation, also blocked myonectin secretion. **D**, Substitution of all four potential Asn glycosylation residues (Asn-229, Asn-281, Asn-292, and Asn-319) with Gln (the 4Q mutant) abolished protein secretion. Representative immunoblots probed with an anti-FLAG antibody (recognizing the FLAG epitope-tagged myonectin) are shown. All the transfection and immunoblot experiments were repeated at least three times.

Myonectin secretion is dependent on glycosylation at Asn-229 or Asn-281

To determine which of the four potential *N*-linked glycosylation sites contains glycans, we subjected purified recombinant mouse myonectin made in mammalian HEK 293 cells to mass spectrometry analysis. As indicated by mass spectra, Asn-229 and Asn-281 were glycosylated (**Fig. 3A-B**). Replacing Asn-229 with Gln resulted in a shift of molecular weight of myonectin on immunoblot, confirming that Asn-229 is indeed glycosylated (**Fig. 3C**). When subjected to PNGase F digest, the apparent molecular weight of N229Q mutant further shifted on immunoblot, suggesting the presence of additional *N*-linked glycans (**Fig. 3D**). Substituting Asn-281 with Gln also resulted in a shift of molecular weight of myonectin on immunoblot, confirming that Asn-281 is also glycosylated (**Fig. 3E**). Since both Asn-229 and Asn-281 are glycosylated, the apparent molecular weight of N281Q could be further reduced by PNGase F treatment (**Fig. 3F**). Replacing both Asn-229 and Asn-281 with Gln in the double mutant completely abolished protein secretion (**Fig. 3G**). Treatment with PNGase F did not result in any futher shift in the apparent molecular weight of the double mutant (**Fig. 3H**), suggesting that these two sites are the only ones with detected glycosylation. The double mutant (N229Q/N281Q) protein that was retained inside the cell was presumably misfolded and formed higher molecular weight protein aggregates (**Fig. 3I**). These results indicate that glycosylation of either Asn-229 or Asn-281 is necessary for myonectin secretion from cells.

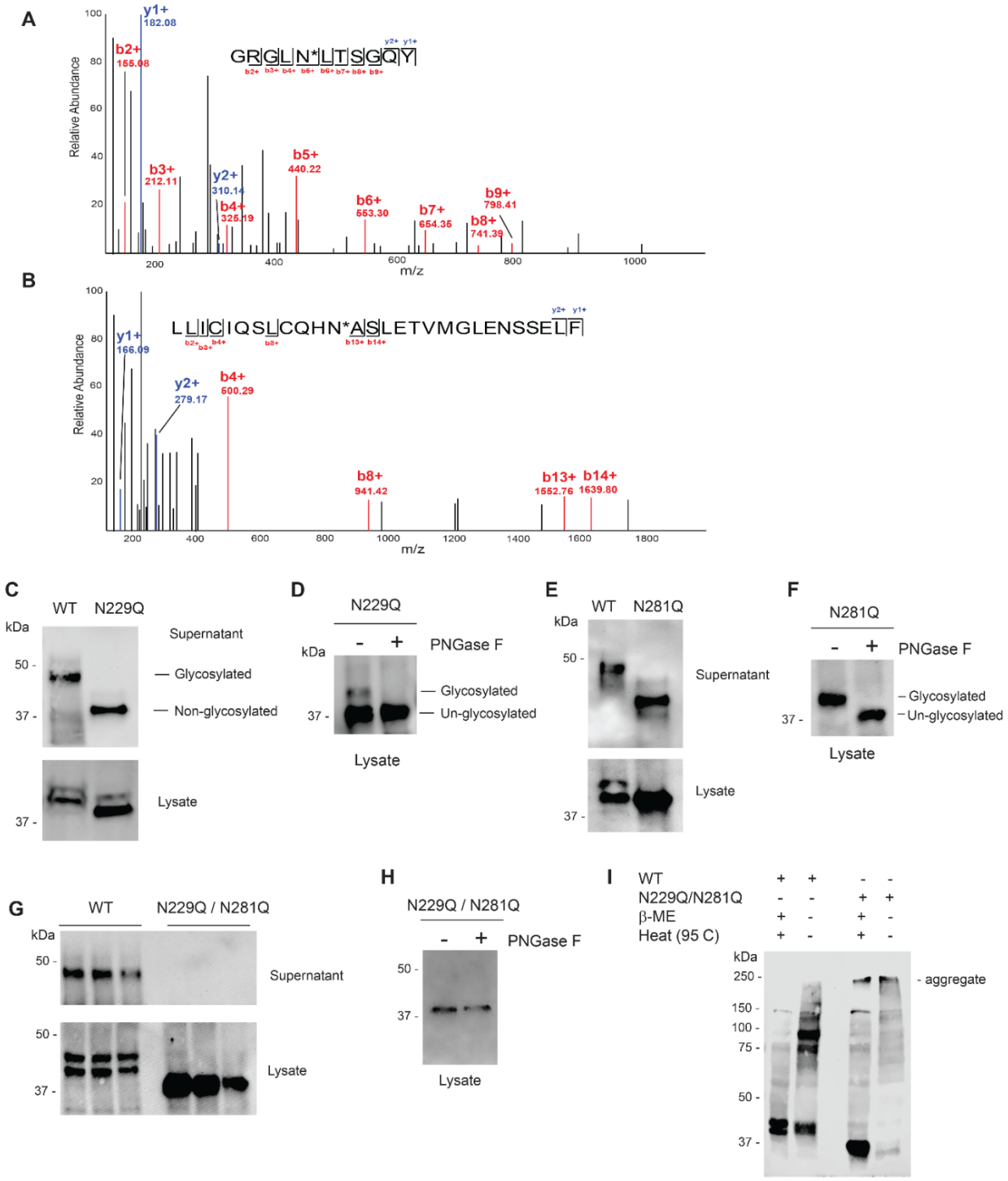

Figure 3. Mass spectrometry and mutational analysis of *N*-glycosylation in myonectin. **A-B**, MS/MS spectrum of the two glycopeptides derived from purified myonectin (made in mammalian HEK 293 cells) identified using Proteome Discoverer. Higher-energy collisional dissociation (HCD) generated b- (red) and

y- (blue) peptide fragments that allowed for mapping the glycosylation site as indicated by asterisk (*). Mass spectra indicating that Asn-229 and Asn-281 are glycosylated. **C**, Immunoblot analysis of cell lysate and supernatant of transfected HEK 293 cells expressing wild-type (WT) myonectin or the single N229Q mutant. **D**, Peptide N:Glycosidase F (PNGase F) digest of N229Q mutant indicating the presence of additional *N*-linked glycans. **E**, Immunoblot analysis of wild-type (WT) myonectin or the N281Q mutant. **F**, PNGase F digest of N281Q mutant indicating the presence of additional *N*-linked glycans. **G**, Substitution of both Asn-229 and Asn-281 with Gln in the double mutant abolished myonectin protein secretion. **H**, PNGase F digest of the double mutant (N229Q/N281Q) indicating that these two sites are the only ones detected as glycosylated. **I**, Formation of higher molecular weight protein aggregate of the N229Q/N281Q double mutant in transfected cells. Cell lysates were treated with (+) or without (-) heat (95°C) and reducing agent β-ME (β-mercaptoethanol) prior to Western blotting. Representative immunoblots probed with an anti-FLAG antibody (recognizing the FLAG epitope-tagged myonectin) are shown. All transfection and immunoblot experiments were repeated at least three independent times.

Asn-319 is required for proper protein folding

The C-terminal peptide fragments containing Asn-292 or Asn-319 were not detected by mass spectrometry. Therefore, we used site-directed mutagenesis to assess whether these sites contain *N*-linked glycans. Substitution of Asn-292 with Gln had no impact on protein secretion, nor did it alter the apparent molecular weight of the protein on immunoblot (**Fig. 4A**), indicating that Asn-292 is not detected as glycosylated. In contrast, replacing Asn-319 with Gln blocked protein secretion, but it did not shift the apparent molecular weight of the protein on immunoblot (**Fig. 4B**), suggesting that Asn-319 is not detected as a glycosylation site but is required for proper protein folding. To assess whether the misfolded N319Q mutant is retained in the endoplasmic reticulum (ER) because it failed ER quality control, we subjected the cell lysate to endoglycosidase H (Endo H) digestion. Sensitivity to Endo H digestion (due to the presence of high mannose-

type glycans) indicates that N319Q resides in the ER and has not transited to the Golgi (54). Endo H digest followed by immunoblot analysis confirmed that the misfolded N319Q mutant was retained in the ER (**Fig. 4C)**. To ensure that Asn-319 affects myonectin folding in the ER via a non-glycosylated mechanism, we substituted Ser-321 (within the N^{319}-X-S^{321} glycosylation sequon) with Ala. N-X-S/T is the critical recognition sequon for *N*-glycosylation, and substituting Ser or Thr within this sequon will abolish *N*-linked glycosylation (55). Because Asn-319 was not glycosylated, substitution of Ser-321 with Ala should not affect protein folding and secretion. Indeed, the S321A mutant was robustly expressed and secreted from cells (**Fig. 4D**). These results indicate that neither Asn-292 nor Asn-319 is glycosylated, but that Asn-319 (conserved in mouse and human) is critical for proper protein folding within the ER.

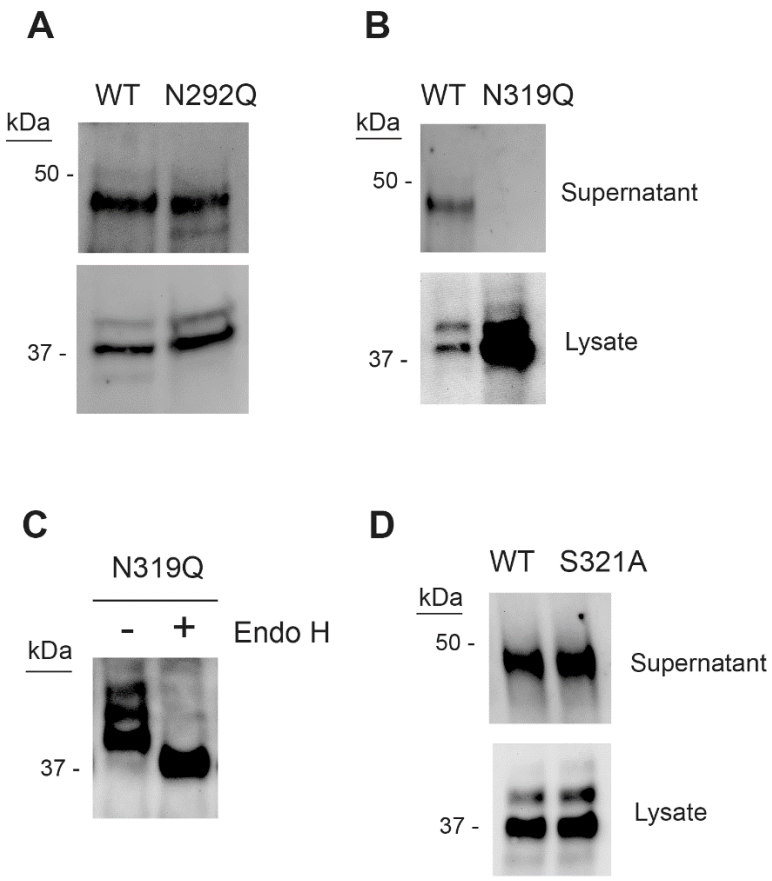

Figure 4. Asn-292 and Asn-319 are not detected as glycosylated sites but their substitution impacts protein folding and secretion. **A**, Immunoblot analysis of cell lysate and supernatant of transfected HEK 293 cells expressing wild-type (WT) myonectin or the N292Q mutant. **B**, Substitution of Asn-319 with Gln blocks myonectin secretion. **C**, Sensitivity of N319Q mutant to endoglycosidase H (Endo H) digestion indicates that the mutant protein remains in the endoplasmic reticulum, presumably due to protein misfolding. **D**, Immunoblot analysis of WT myonectin or the S321A mutant. Representative immunoblots probed with an anti-FLAG antibody (recognizing the FLAG epitope-tagged myonectin) are shown. All transfection and immunoblot experiments were repeated at least three independent times.

Conserved cysteine residues are important for protein folding and secretion

Myonectin possesses four cysteine residues (Cys-142, Cys-194, Cys-273, Cys-278) conserved between mouse and human (**Fig. 1**). Replacing either Cys-273 or Cys-278 located in the C-terminal globular domain prevented protein secretion (**Fig. 5A**). These mutants were sensitive to Endo H digest (**Fig. 5B**), indicating that they were retained in the ER, presumably due to protein mis-folding. In striking contrast, substituting Cys-142, located in the N-terminal domain, with Ala significantly enhanced myonectin secretion (**Fig. 5C**). Replacing Cys-194 with Ala also significantly increased protein secretion (**Fig. 5D**). When both Cys-142 and Cys-194 were substituted with Ala in the double mutant, we did not observe further enhancement of protein secretion (**Fig. 5E**). These results indicate the important role of individual Cys residues in dictating proper protein folding and secretion.

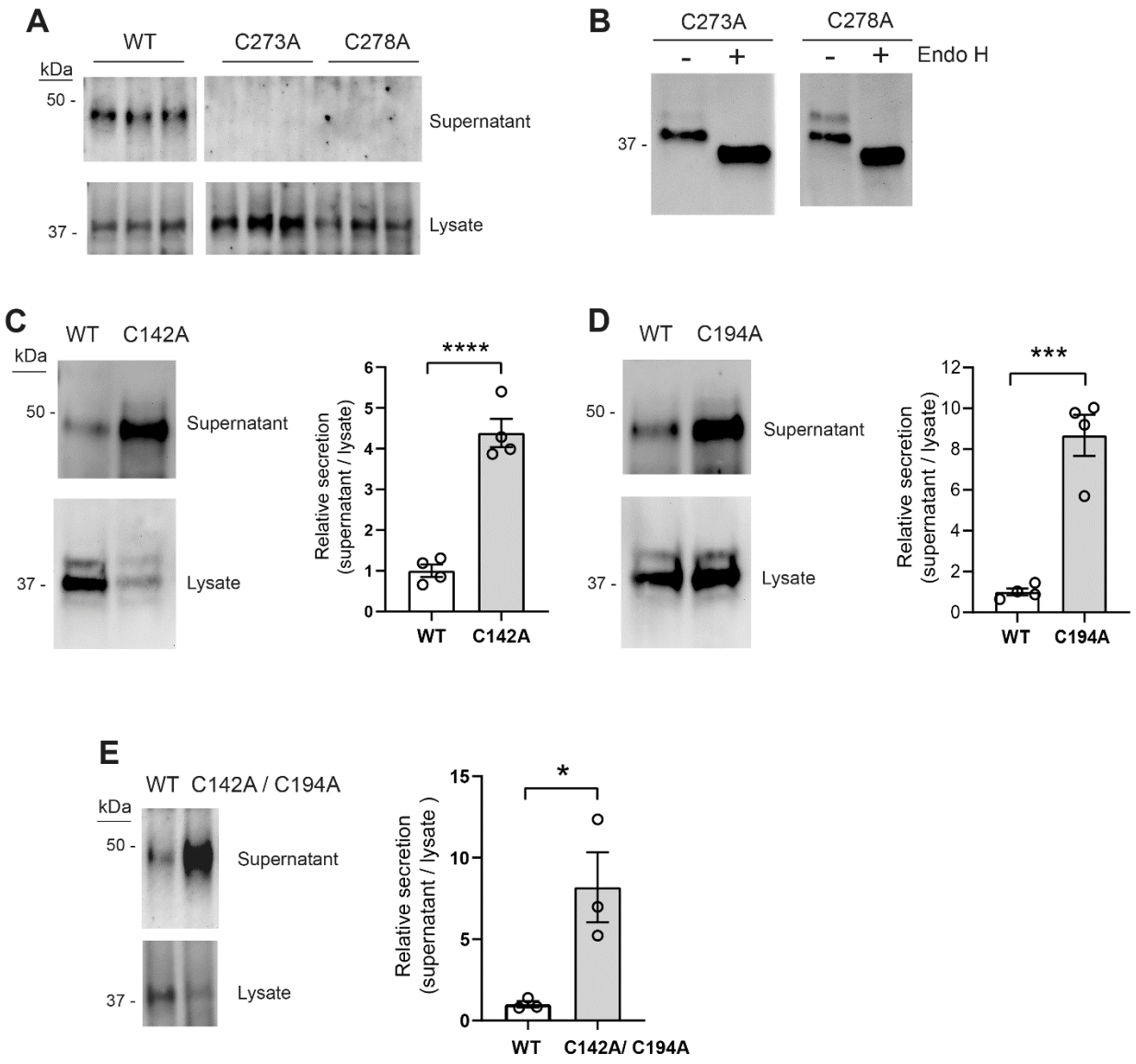

Figure 5. Impact of conserved cysteine residues on myonectin secretion. **A**, Immunoblot analysis of cell lysates and supernatant of transfected HEK 293 cells expressing wild-type (WT) myonectin or the C273A or C278A mutant. **B**, Sensitivity of C273A and C278A mutants to endoglycosidase H (Endo H) digest indicates that the mutant proteins remain in the endoplasmic reticulum, presumably due to protein misfolding. **C**, Substitution of Cys-142 with Ala enhances myonectin secretion. The extent of protein secretion is quantified as the amount of secreted myonectin found in the supernatant relative to intracellular myonectin based on four independent experiments. **D**, Substitution of Cys-194 with Ala enhances myonectin secretion. Quantification of the relative protein secretion normalized to intracellular myonectin is based on four independent experiments. **E**, Substitution of both Cys-142 and Cys-194 with Ala in the double mutant enhances myonectin secretion. Quantification of the relative

protein secretion normalized to intracellular myonectin is based on three independent experiments. All data shown are mean ± S.E.M.; *P<0.05, ***P<0.001, ****P<0.0001.

Cys-142 and Cys-194 are required for the assembly of hexamer and HMW oligomer

All secreted proteins containing the globular C1q domain form trimers as their basic structural unit (14,27-30); adjacent trimers can be further assembled into hexamers and HMW oligomers (with 12-18 units) (9,56-58). Assembly of higher-order structures greater than a trimer involves inter-molecular disulfide bonds mediated by one or more of the conserved Cys residues located in the N-terminus (9,32,34). We used blue native gel electrophoresis to assess if Cys-142 or Cys-194 is required for assembly of high-order structures. Native immunoblot indicated that wild-type (WT) myonectin forms trimers, hexamers, and HMW oligomers (**Fig. 6A**), with the approximate distribution of 52% trimer, 8% hexamer, and 40% HMW oligomer (**Fig. 6B**). Substituting Cys-142 with Ala resulted in the near-exclusive formation of trimers (**Fig. 6A-B;** 93% trimer, 0.2% hexamer, 4% HMW oligomer). In contrast, replacing Cys-194 with Ala had no impact on the assembly of trimers and hexamers, but resulted in a significant reduction (~34%) in the formation of HMW oligomers (**Fig. 6A-B**). These results indicate that both Cys-142 and Cys-194 mediate inter-molecular disulfide bonds required for the formation of higher-order hexamers and/or HMW oligomers.

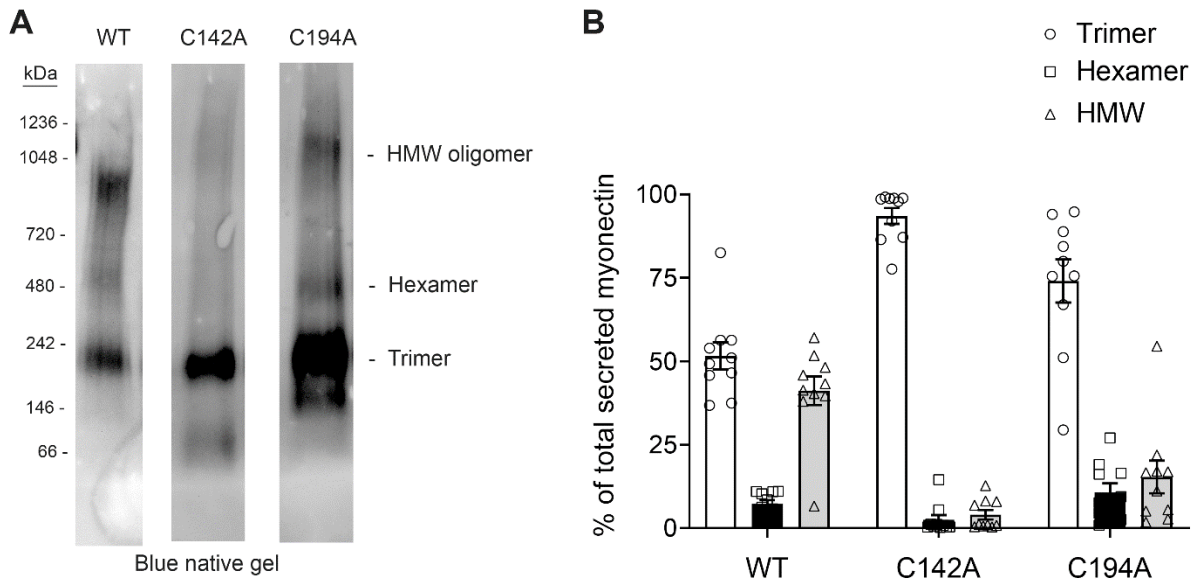

Figure 6. Formation of hexamer and higher-order oligomeric complexes depends on Cys-142. **A**, Representative blue native gel immunoblot of wild-type (WT) myonectin and C142A and C194A mutants. **B**, Quantification of the proportion (as % of total secreted myonectin) of trimers, hexamers, and high molecular weight (HMW) oligomers based on ten independent experiments from four separate transfections.

Protein modification of collagen domain

Both human and mouse myonectin/erythroferrone possess a short collagen-like domain located between the N-terminal domain 1 (NTD1) and NTD2 (**Fig. 7A**). This short collagen domain consists of six Gly-X-Y repeats (where X and Y are frequently proline or lysine), the same repeating unit found in all collagen (59). Proline hydroxylation and lysine glycosylation are important for the stability of the triple helical structure of the collagen domain (59-61). Mouse myonectin/erythroferrone contains nine proline residues that can be hydroxylated (Pro-99, Pro-101, Pro-102, Pro-104, Pro-105, Pro-107, Pro-110, Pro-111, and Pro-113) (**Fig. 7A**); all nine of the proline residues are conserved in human myonectin

(NP_001278761). Using mass spectrometry, we provided direct evidence that the first six proline residues (Pro-99, Pro-101, Pro-102, Pro-104, Pro-105, and Pro-107) are hydroxylated (**Fig. 7B**). The number of peptide-spectrum matches (PSM) for each of the six hydroxyl-proline was 42, 115, 77, 63, 54, and 7, respectively. In contrast, there were only 5, 1, 1, and 1 PSM that corresponded to hydroxylated Pro-110, Pro-111, Pro-113, and Pro-116, respectively. Although suggestive, the low PSM counts preclude definitive evidence for proline hydroxylation at these sites. These results indicate that most of the conserved proline residues within the Gly-X-Y repeats are hydroxylated.

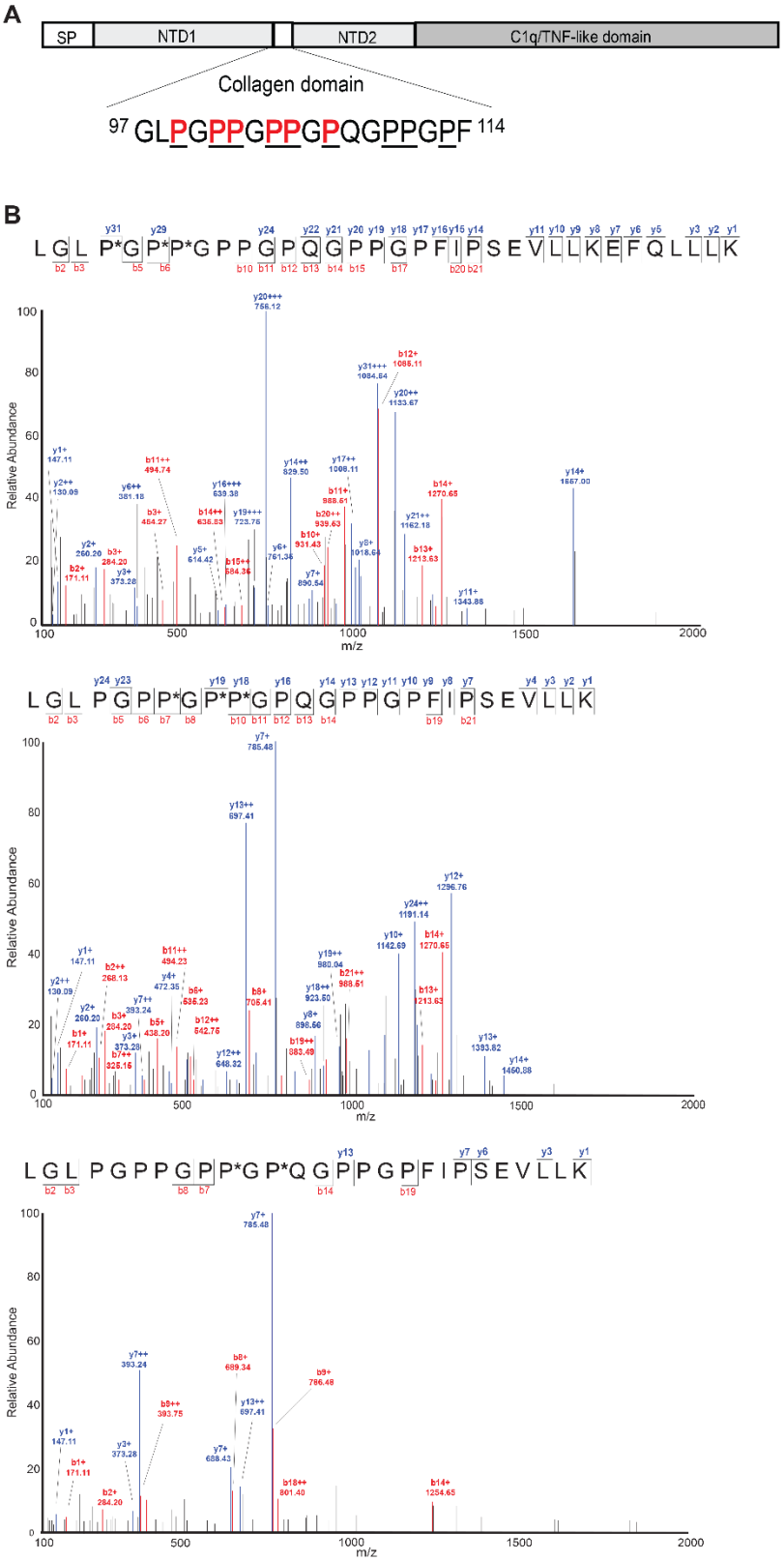
A
SP
NTD1
NTD2
C1q/TNF-like domain
Collagen domain
97 GLPGPPGPPGPQGPPGPF 114
B
LGL P*GP*P*GPPGPQGPPGPFIPSEVLLKEFQLLLK
Relative Abundance
m/z
LGL PGPP*GP*P*GPQGPPGPFIPSEVLLK
LGL PGPPGPP*GP*QGPPGPFIPSEVLLK

Figure 7. Proline hydroxylation within the collagen domain of myonectin. **A**, Schematic showing the proline residues found in the six Gly-X-Y repeats of the collagen-like domain of mouse myonectin. All nine proline residues are conserved in human myonectin. Hydroxylated prolines as determined by mass spectrometry analysis are highlighted in red. **B**, MS/MS spectrum of the three peptides derived from myonectin identified using Proteome Discoverer. Higher-energy collisional dissociation generated b- (red) and y- (blue) peptide fragments that allow for the mapping of proline hydroxylation sites are indicated by asterisk(*). Mass spectra indicate that Pro-99, Pro-101, Pro-102, Pro-104, Pro-105, and Pro-107 are hydroxylated.

Inhibiting proline hydroxylation or deleting the collagen domain substantially impairs myonectin secretion

We next addressed whether hydroxylation of the proline residues within the collagen domain of myonectin affects its expression and secretion. Collagen prolyl 4-hydroxylase (CP4H) catalyzes the hydroxylation of proline within the collagen domain (62) and diethyl-pythiDC is a selective inhibitor of CP4H (63). Inhibiting CP4H with diethyl-pythiDC (50 μM) significantly reduced myonectin secretion from transfected cells (**Fig. 8A-B**). The G-X-Y repeats in the collagen domain promote the formation of triple helical structure (64,65). To determine the consequence of removing the short collagen domain (containing at least nine hydroxyprolines; **Fig. 7A**), we generated a mutant protein lacking the collagen domain (six Gly-X-Y repeats). Relative to wild-type myonectin, the secretion of mutant protein lacking the collagen domain was also significantly (~85%) reduced (**Fig. 8C-D**). These results suggest contribution of the collagen domain and its hydroxyprolines to the assembly and/or stability of the basic trimeric structural unit of myonectin during biosynthesis before secretion.

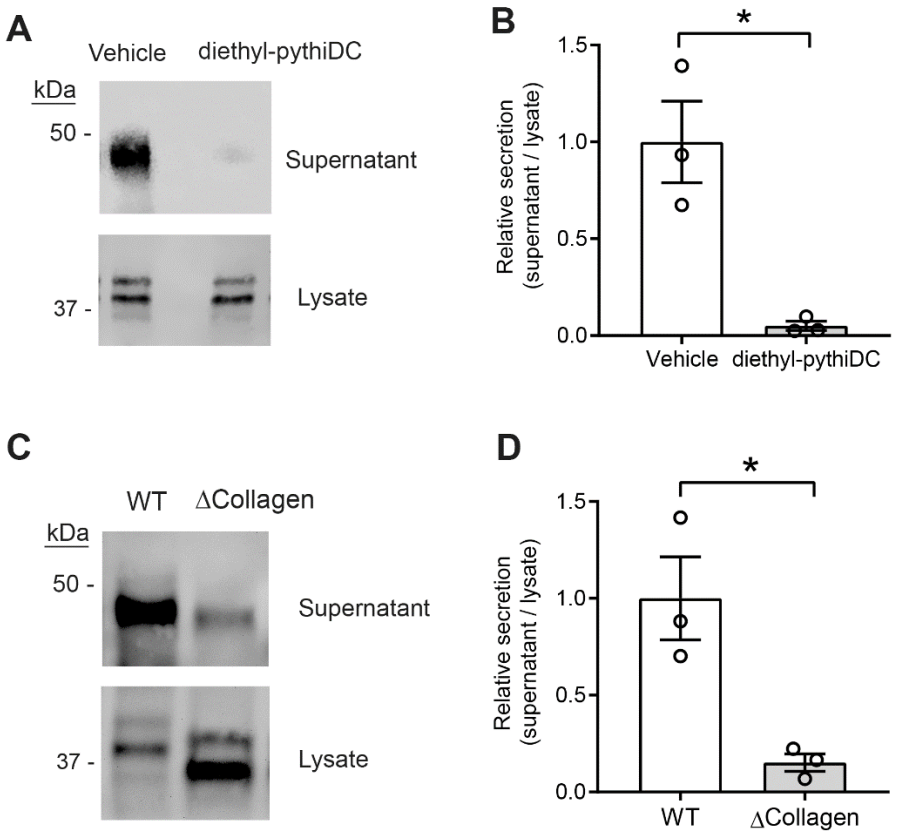

Figure 8. Inhibiting proline hydroxylation or deleting the collagen domain markedly reduces myonectin secretion. **A**, Immunoblot analysis of cell lysate and supernatant of transfected HEK 293 cells expressing wild-type (WT) myonectin treated with vehicle control (DMSO) or 50 μM diethyl-pythiDC (selective inhibitor of CP4H). **B**, Quantification of relative protein secretion from three independent experiment as shown in A. **C**, Immunoblot analysis of cell lysate and supernatant of transfected HEK 293 cells expressing wild-type (WT) myonectin or the collagen-deleted mutant (ΔCollagen). **D**, Quantification of relative protein secretion of WT and ΔCollagen mutant based on three independent experiments. All data shown are mean ± S.E.M.; **P*<0.05.

Discussion

The findings presented here describe protein modifications critical for myonectin folding, secretion, and high-order structure formation. *N*-linked glycosylation was required for myonectin secretion and Cys-mediated intermolecular disulfide bond formation was necessary for the assembly of hexameric and HMW oligomeric forms of the protein. The short collagen domain, with its hydroxylated prolines, was needed for efficient myonectin secretion.

Many secretory proteins are glycosylated as they transit through the secretory pathways during biosynthesis. One critical function of *N*-linked glycosylation is to assist in protein folding in the ER (66,67). This function is part of an important protein quality control system where dedicated ER-localized lectin chaperones (e.g., calnexin and calreticulin) bind to specific *N*-linked glycan structures on glycoproteins (68). Multiple rounds of capture and release by the lectin chaperones occur until the glycoprotein is correctly folded into its native conformation, then it is released from the ER and transported to the Golgi (68,69). Proteins that are misfolded will be retained in the ER and be degraded via the ERAD or other pathways (70). Likewise, *N*-linked glycosylation of myonectin is also critical for its proper folding and eventual secretion from cells. We found that either Asn-229 or Asn-281, when glycosylated, was sufficient for protein secretion; however, when glycosylation was completely abolished in the N229Q/N281Q double mutant, the protein failed to be secreted, presumably due to protein misfolding. These results were corroborated by pharmacologic inhibition of *N*-linked glycosylation with

tunicamycin or high dose of glucosamine. In accordance with their importance in protein folding and secretion, both Asn-229 and Asn-281 are conserved in mouse and human myonectin.

Myonectin exists in different multimeric forms (5). Here, we showed that mature secreted myonectin forms trimers, hexamers, and HMW oligomers. All biochemically characterized C1q family members form trimers as their basic structural unit, a feature confirmed by crystal structures(28-30,71,72). Trimer formation is driven by the C-terminal globular C1q domain with its highly conserved hydrophobic residues located at the interface of each monomer. Higher-order structures greater than a trimer, however, are formed by linking multiple trimeric units via inter-molecular disulfide bonds (9,32,34). For this reason, we systematically mutated each of the four conserved Cys residues in myonectin to determine which is critical for the assembly of higher-order structures. Two of the Cys residues (Cys-273 and Cys-278) were critical for proper protein folding and secretion; substitution of either Cys with Ala resulted in protein misfolding and retention in the ER. The C1q domain located in the C-terminus of the protein forms a compact globular structure (28-30,71,72) and, given the location of Cys-273 and Cys-278 within the globular C1q domain, it is not surprising that substitution of either conserved Cys residue led to protein misfolding and retention in the ER. Because the globular domain of myonectin shares less than 30% amino acid identity with other related C1q family members, the existing crystal structures could

not be used to accurately model how mutation of Cys-273 or Cys-278 interferes with myonectin globular domain folding.

In contrast, Cys-142 and Cys-194 play important roles in myonectin oligomerization. Substituting Cys-142 with Ala led to the near exclusive formation of trimers, indicating the critical importance of the N-terminal Cys in mediating inter-molecular disulfide bonds necessary for the assembly of trimers into hexamers and HMW oligomers. However, substituting Cys-194 with Ala significantly impaired, but did not abolish, the formation of HMW oligomers. This result suggests that Cys-194 (located near the junction between NTD2 and the globular C1q domain) facilitates HMW oligomer formation, but is not required. Thus, of the two Cys residues, only the N-terminal Cys-142 in myonectin is essential for the formation of higher-order hexamers and HMW oligomers. The conserved N-terminal Cys residue also appears to be a general feature shared by other C1q family members studied to date (9,32,34).

Not only do Cys-142 and Cys-194 facilitate multimeric assembly of myonectin complexes via inter-molecular disulfide bond formation, their substitutions with Ala also strikingly enhanced protein secretion. The role of N-terminal Cys residues in regulating the rate of protein secretion was demonstrated for adiponectin and CTRP11, two related members of the C1q family (13,73). Our data suggest that myonectin may be transiently retained in the ER during its biosynthesis via a thiol-mediated retention mechanism, whereby Cys-142 or Cys-

194 forms reversible disulfide bonds with ER resident oxidoreductases to facilitate the assembly of higher-order multimeric complexes (hexamers and HMW oligomers) before protein secretion. Replacing either Cys residue with Ala may shorten the transit time in the ER and lead to higher secretion of the basic trimeric complexes of myonectin. The thiol-mediated ER retention mechanism was first discovered in the course of understanding polymeric immunoglobulin (IgM) assembly and secretion in plasma cells (74,75). Cys-575 of the μ chain is responsible for ER retention (75) by forming disulfide bonds with resident ER oxidoreductases (76) and the secretory rate of additional proteins (IgA and Ig λ light chain) from different cells was also found to be similarly regulated (77,78). Of particular relevance to the present study is the assembly and secretion of adiponectin (a C1q family member) hexameric and HMW oligomeric complexes. A substantial pool of properly folded adiponectin is retained in the ER through the thiol-mediated ER retention mechanism involving its N-terminal Cys-39 forming a transient disulfide bond with the ER oxidoreductase, ERp44 (73). Abrogating this interaction led to enhanced secretion of adiponectin trimers. Another ER chaperone, Ero1-Lα, facilitates the release of adiponectin from ERp44 (73). The levels of these two chaperones, under different cellular and metabolic states, dictates the proportion of adiponectin trimers, hexamers, and HMW oligomers secreted from adipocytes (73). Additionally, oxidoreductase-like protein (DsbA-L) may also play a role in the multimerization of adiponectin (79). Based on our current data and previous studies, we speculate that myonectin likely employs a similar thiol-mediated retention mechanism to regulate the assembly and

secretion of different multimeric complexes, possibly in response to changes in cellular states. The significance and relevance of different oligomeric complexes of adiponectin relates to their biological activity and signaling specificity (32-34), differential association with disease states (80,81), and location (82). Given that myonectin is produced by skeletal muscle under basal conditions (5) and can be induced in different tissues and cell types in response to physiologic perturbations (7,16,17,20-22,83), future studies are warranted to determine whether different oligomeric complexes of myonectin/erythroferrone are differentially secreted by distinct cell types under different conditions. Future studies are also needed to assess whether there are differences in biological activity among different complexes of myonectin, and whether distinct complexes are associated with disease states (84).

In addition to glycosylation and Cys-mediated multimerization, proline residues within the short collagen domain were hydroxylated. The protein modification of proline was initially found in collagens (85) and subsequently also identified in other proteins containing the collagen domain (8,86,87). Proline hydroxylation by CP4H stabilizes the collagen triple helix (85,88,89), and does so by forming hydrogen bonds with water molecules surrounding the triple helix (64,90). Inhibiting proline hydroxylation markedly reduced myonectin secretion in our study. It appears that proline hydroxylation is required for efficient secretion of proteins containing a collagen domain, and this was observed in complement C1q where inhibition of proline hydroxylation also greatly reduced protein

secretion from cells (91). Our data showed that myonectin lacking the short (six Gly-X-Y repeats) collagen domain is substantially impaired in its secretion. Because the basic structural unit of myonectin is a trimer, we speculate that the collagen triple helix and its hydroxyprolines likely confer stability to the N-terminal extended stalk-like structure preceding the C-terminal globular trimers. An example is the globular C1q domain of collagen X initiating trimerization and trimeric complex stabilization by the collagen triple helix (92,93).

In summary, this study provided biochemical insights into key determinants and protein modifications important for myonectin folding, secretion, and multimeric assembly. One caveat of the study, however, is that myonectin secretion and assembly was evaluated in human embryonic kidney (HEK) cells and it is possible that the patterns of protein modification could be distinct in skeletal muscle and that further studies will be needed to investigate this possibility. Nonetheless, the knowledge obtained here will catalyze future structure/function studies assessing naturally occurring polymorphisms that alter protein modifications of myonectin/erythroferrone and their impact on secretion (and hence circulating level), multimerization, and biological activity. These changes may influence myonectin's function in the context of pathophysiology.

References

1. Wasserman, D. H., Kang, L., Ayala, J. E., Fueger, P. T., and Lee-Young, R. S. (2011) The physiological regulation of glucose flux into muscle in vivo. *J Exp Biol* **214**, 254-262
2. Pedersen, B. K. (2013) Muscle as a secretory organ. *Compr Physiol* **3**, 1337-1362
3. Pedersen, B. K., and Febbraio, M. A. (2012) Muscles, exercise and obesity: skeletal muscle as a secretory organ. *Nat Rev Endocrinol* **8**, 457-465
4. Eckel, J. (2019) Myokines in metabolic homeostasis and diabetes. *Diabetologia* **62**, 1523-1528
5. Seldin, M. M., Peterson, J. M., Byerly, M. S., Wei, Z., and Wong, G. W. (2012) Myonectin (CTRP15), a novel myokine that links skeletal muscle to systemic lipid homeostasis. *J Biol Chem* **287**, 11968-11980
6. Seldin, M. M., Lei, X., Tan, S. Y., Stanson, K. P., Wei, Z., and Wong, G. W. (2013) Skeletal muscle-derived myonectin activates the mTOR pathway to suppress autophagy in liver. *J Biol Chem* **289**, 36073-36082
7. Otaka, N., Shibata, R., Ohashi, K., Uemura, Y., Kambara, T., Enomoto, T., Ogawa, H., Ito, M., Kawanishi, H., Maruyama, S., Joki, Y., Fujikawa, Y., Narita, S., Unno, K., Kawamoto, Y., Murate, T., Murohara, T., and Ouchi, N. (2018) Myonectin Is an Exercise-Induced Myokine That Protects the Heart From Ischemia-Reperfusion Injury. *Circ Res* **123**, 1326-1338
8. Wong, G. W., Krawczyk, S. A., Kitidis-Mitrokostas, C., Ge, G., Spooner, E., Hug, C., Gimeno, R., and Lodish, H. F. (2009) Identification and characterization of CTRP9, a novel secreted glycoprotein, from adipose tissue that reduces serum glucose in mice and forms heterotrimers with adiponectin. *FASEB J* **23**, 241-258
9. Wong, G. W., Krawczyk, S. A., Kitidis-Mitrokostas, C., Revett, T., Gimeno, R., and Lodish, H. F. (2008) Molecular, biochemical and functional characterizations of C1q/TNF family members: adipose-tissue-selective expression patterns, regulation by PPAR-gamma agonist, cysteine-mediated oligomerizations, combinatorial associations and metabolic functions. *Biochem J* **416**, 161-177
10. Wong, G. W., Wang, J., Hug, C., Tsao, T. S., and Lodish, H. F. (2004) A family of Acrp30/adiponectin structural and functional paralogs. *Proc Natl Acad Sci U S A* **101**, 10302-10307
11. Wei, Z., Peterson, J. M., Lei, X., Cebotaru, L., Wolfgang, M. J., Baldeviano, G. C., and Wong, G. W. (2012) C1q/TNF-related protein-12 (CTRP12), a novel adipokine that improves insulin sensitivity and glycemic control in mouse models of obesity and diabetes. *J Biol Chem* **287**, 10301-10315
12. Wei, Z., Peterson, J. M., and Wong, G. W. (2011) Metabolic regulation by C1q/TNF-related protein-13 (CTRP13): activation of AMP-activated protein kinase and suppression of fatty acid-induced JNK signaling. *J Biol Chem* **286**, 15652-15665
13. Wei, Z., Seldin, M. M., Natarajan, N., Djemal, D. C., Peterson, J. M., and Wong, G. W. (2013) C1q/Tumor Necrosis Factor-related Protein 11 (CTRP11), a Novel Adipose Stroma-derived Regulator of Adipogenesis. *J Biol Chem* **288**, 10214-10229
14. Kishore, U., Gaboriaud, C., Waters, P., Shrive, A. K., Greenhough, T. J., Reid, K. B., Sim, R. B., and Arlaud, G. J. (2004) C1q and tumor necrosis factor superfamily: modularity and versatility. *Trends Immunol* **25**, 551-561

15. Little, H. C., Rodriguez, S., Lei, X., Tan, S. Y., Stewart, A. N., Sahagun, A., Sarver, D. C., and Wong, G. W. (2019) Myonectin deletion promotes adipose fat storage and reduces liver steatosis. *FASEB J* **33**, 8666-8687
16. Kautz, L., Jung, G., Nemeth, E., and Ganz, T. (2014) Erythroferrone contributes to recovery from anemia of inflammation. *Blood* **124**, 2569-2574
17. Kautz, L., Jung, G., Valore, E. V., Rivella, S., Nemeth, E., and Ganz, T. (2014) Identification of erythroferrone as an erythroid regulator of iron metabolism. *Nat Genet* **46**, 678-684
18. Arezes, J., Foy, N., McHugh, K., Sawant, A., Quinkert, D., Terraube, V., Brinth, A., Tam, M., LaVallie, E. R., Taylor, S., Armitage, A. E., Pasricha, S. R., Cunningham, O., Lambert, M., Draper, S. J., Jasuja, R., and Drakesmith, H. (2018) Erythroferrone inhibits the induction of hepcidin by BMP6. *Blood* **132**, 1473-1477
19. Aschemeyer, S., Gabayan, V., Ganz, T., Nemeth, E., and Kautz, L. (2017) Erythroferrone and matriptase-2 independently regulate hepcidin expression. *Am J Hematol* **92**, E61-E63
20. Latour, C., Wlodarczyk, M. F., Jung, G., Gineste, A., Blanchard, N., Ganz, T., Roth, M. P., Coppin, H., and Kautz, L. (2017) Erythroferrone contributes to hepcidin repression in a mouse model of malarial anemia. *Haematologica* **102**, 60-68
21. Jiang, X., Gao, M., Chen, Y., Liu, J., Qi, S., Ma, J., Zhang, Z., and Xu, Y. (2016) EPO-dependent induction of erythroferrone drives hepcidin suppression and systematic iron absorption under phenylhydrazine-induced hemolytic anemia. *Blood Cells Mol Dis* **58**, 45-51
22. Kautz, L., Jung, G., Du, X., Gabayan, V., Chapman, J., Nasoff, M., Nemeth, E., and Ganz, T. (2015) Erythroferrone contributes to hepcidin suppression and iron overload in a mouse model of beta-thalassemia. *Blood* **126**, 2031-2037
23. Arezes, J., Foy, N., McHugh, K., Quinkert, D., Benard, S., Sawant, A., Frost, J. N., Armitage, A. E., Pasricha, S. R., Lim, P. J., Tam, M. S., Lavallie, E., Pittman, D. D., Cunningham, O., Lambert, M., Murphy, J. E., Draper, S. J., Jasuja, R., and Drakesmith, H. (2020) Antibodies against the erythroferrone N-terminal domain prevent hepcidin suppression and ameliorate murine thalassemia. *Blood* **135**, 547-557
24. Bondu, S., Alary, A. S., Lefevre, C., Houy, A., Jung, G., Lefebvre, T., Rombaut, D., Boussaid, I., Bousta, A., Guillonneau, F., Perrier, P., Alsafadi, S., Wassef, M., Margueron, R., Rousseau, A., Droin, N., Cagnard, N., Kaltenbach, S., Winter, S., Kubasch, A. S., Bouscary, D., Santini, V., Toma, A., Hunault, M., Stamatoullas, A., Gyan, E., Cluzeau, T., Platzbecker, U., Ades, L., Puy, H., Stern, M. H., Karim, Z., Mayeux, P., Nemeth, E., Park, S., Ganz, T., Kautz, L., Kosmider, O., and Fontenay, M. (2019) A variant erythroferrone disrupts iron homeostasis in SF3B1-mutated myelodysplastic syndrome. *Sci Transl Med* **11**, 1-14
25. Miura, S., Kobune, M., Horiguchi, H., Kikuchi, S., Iyama, S., Murase, K., Goto, A., Ikeda, H., Takada, K., Miyanishi, K., and Kato, J. (2019) EPO-R+ myelodysplastic cells with ring sideroblasts produce high erythroferrone levels to reduce hepcidin expression in hepatic cells. *Blood Cells Mol Dis* **78**, 1-8
26. Melchert, J., Henningfeld, K. A., Richts, S., Lingner, T., Jonigk, D., and Pieler, T. (2020) The secreted BMP antagonist ERFE is required for the development of a functional circulatory system in Xenopus. *Dev Biol* **459**, 138-148
27. Ghai, R., Waters, P., Roumenina, L. T., Gadjeva, M., Kojouharova, M. S., Reid, K. B., Sim, R. B., and Kishore, U. (2007) C1q and its growing family. *Immunobiology* **212**, 253-266

28. Gaboriaud, C., Juanhuix, J., Gruez, A., Lacroix, M., Darnault, C., Pignol, D., Verger, D., Fontecilla-Camps, J. C., and Arlaud, G. J. (2003) The crystal structure of the globular head of complement protein C1q provides a basis for its versatile recognition properties. *J Biol Chem* **278**, 46974-46982
29. Ressl, S., Vu, B. K., Vivona, S., Martinelli, D. C., Sudhof, T. C., and Brunger, A. T. (2015) Structures of C1q-like proteins reveal unique features among the C1q/TNF superfamily. *Structure* **23**, 688-699
30. Shapiro, L., and Scherer, P. E. (1998) The crystal structure of a complement-1q family protein suggests an evolutionary link to tumor necrosis factor. *Curr Biol* **8**, 335-338
31. Wei, Z., Lei, X., Seldin, M. M., and Wong, G. W. (2012) Endopeptidase cleavage generates a functionally distinct isoform of C1q/tumor necrosis factor-related protein-12 (CTRP12) with an altered oligomeric state and signaling specificity. *J Biol Chem* **287**, 35804-35814
32. Pajvani, U. B., Du, X., Combs, T. P., Berg, A. H., Rajala, M. W., Schulthess, T., Engel, J., Brownlee, M., and Scherer, P. E. (2003) Structure-function studies of the adipocyte-secreted hormone Acrp30/adiponectin. Implications fpr metabolic regulation and bioactivity. *J Biol Chem* **278**, 9073-9085
33. Tsao, T. S., Murrey, H. E., Hug, C., Lee, D. H., and Lodish, H. F. (2002) Oligomerization state-dependent activation of NF-kappa B signaling pathway by adipocyte complement-related protein of 30 kDa (Acrp30). *J Biol Chem* **277**, 29359-29362
34. Tsao, T. S., Tomas, E., Murrey, H. E., Hug, C., Lee, D. H., Ruderman, N. B., Heuser, J. E., and Lodish, H. F. (2003) Role of disulfide bonds in Acrp30/adiponectin structure and signaling specificity. Different oligomers activate different signal transduction pathways. *J Biol Chem* **278**, 50810-50817
35. Tian, Y., Zhou, Y., Elliott, S., Aebersold, R., and Zhang, H. (2007) Solid-phase extraction of N-linked glycopeptides. *Nat Protoc* **2**, 334-339
36. Zhang, H., Li, X. J., Martin, D. B., and Aebersold, R. (2003) Identification and quantification of N-linked glycoproteins using hydrazide chemistry, stable isotope labeling and mass spectrometry. *Nat Biotechnol* **21**, 660-666
37. Wisniewski, J. R., Zougman, A., and Mann, M. (2009) Combination of FASP and StageTip-based fractionation allows in-depth analysis of the hippocampal membrane proteome. *J Proteome Res* **8**, 5674-5678
38. Yang, W., Laeyendecker, O., Wendel, S. K., Zhang, B., Sun, S., Zhou, J. Y., Ao, M., Moore, R. D., Jackson, J. B., and Zhang, H. (2014) Glycoproteomic study reveals altered plasma proteins associated with HIV elite suppressors. *Theranostics* **4**, 1153-1163
39. Beriault, D. R., Dang, V. T., Zhong, L. H., Petlura, C. I., McAlpine, C. S., Shi, Y., and Werstuck, G. H. (2017) Glucosamine induces ER stress by disrupting lipid-linked oligosaccharide biosynthesis and N-linked protein glycosylation. *Am J Physiol Endocrinol Metab* **312**, E48-E57
40. Chen, C. L., Liang, C. M., Chen, Y. H., Tai, M. C., Lu, D. W., and Chen, J. T. (2012) Glucosamine modulates TNF-alpha-induced ICAM-1 expression and function through O-linked and N-linked glycosylation in human retinal pigment epithelial cells. *Invest Ophthalmol Vis Sci* **53**, 2281-2291
41. Chien, M. W., Lin, M. H., Huang, S. H., Fu, S. H., Hsu, C. Y., Yen, B. L., Chen, J. T., Chang, D. M., and Sytwu, H. K. (2015) Glucosamine Modulates T Cell Differentiation through Down-regulating N-Linked Glycosylation of CD25. *J Biol Chem* **290**, 29329-29344

42. Schneider, C. A., Rasband, W. S., and Eliceiri, K. W. (2012) NIH Image to ImageJ: 25 years of image analysis. *Nat Methods* **9**, 671-675
43. Almagro Armenteros, J. J., Tsirigos, K. D., Sonderby, C. K., Petersen, T. N., Winther, O., Brunak, S., von Heijne, G., and Nielsen, H. (2019) SignalP 5.0 improves signal peptide predictions using deep neural networks. *Nat Biotechnol* **37**, 420-423
44. van den Elsen, P., Shepley, B. A., Cho, M., and Terhorst, C. (1985) Isolation and characterization of a cDNA clone encoding the murine homologue of the human 20K T3/T-cell receptor glycoprotein. *Nature* **314**, 542-544
45. Linzer, D. I., and Talamantes, F. (1985) Nucleotide sequence of mouse prolactin and growth hormone mRNAs and expression of these mRNAs during pregnancy. *J Biol Chem* **260**, 9574-9579
46. Littman, D. R., Thomas, Y., Maddon, P. J., Chess, L., and Axel, R. (1985) The isolation and sequence of the gene encoding T8: a molecule defining functional classes of T lymphocytes. *Cell* **40**, 237-246
47. van den Elsen, P., Georgopoulos, K., Shepley, B. A., Orkin, S., and Terhorst, C. (1986) Exon/intron organization of the genes coding for the delta chains of the human and murine T-cell receptor/T3 complex. *Proc Natl Acad Sci U S A* **83**, 2944-2948
48. Lopez, J. A., Chung, D. W., Fujikawa, K., Hagen, F. S., Papayannopoulou, T., and Roth, G. J. (1987) Cloning of the alpha chain of human platelet glycoprotein Ib: a transmembrane protein with homology to leucine-rich alpha 2-glycoprotein. *Proc Natl Acad Sci U S A* **84**, 5615-5619
49. McLean, J. W., Tomlinson, J. E., Kuang, W. J., Eaton, D. L., Chen, E. Y., Fless, G. M., Scanu, A. M., and Lawn, R. M. (1987) cDNA sequence of human apolipoprotein(a) is homologous to plasminogen. *Nature* **330**, 132-137
50. Larkin, M. A., Blackshields, G., Brown, N. P., Chenna, R., McGettigan, P. A., McWilliam, H., Valentin, F., Wallace, I. M., Wilm, A., Lopez, R., Thompson, J. D., Gibson, T. J., and Higgins, D. G. (2007) Clustal W and Clustal X version 2.0. *Bioinformatics* **23**, 2947-2948
51. Elbein, A. D. (1987) Inhibitors of the biosynthesis and processing of N-linked oligosaccharide chains. *Annu Rev Biochem* **56**, 497-534
52. Tkacz, J. S., and Lampen, O. (1975) Tunicamycin inhibition of polyisoprenyl N-acetylglucosaminyl pyrophosphate formation in calf-liver microsomes. *Biochem Biophys Res Commun* **65**, 248-257
53. Stewart, A. N., Tan, S. Y., Clark, D. J., Zhang, H., and Wong, G. W. (2019) N-Linked Glycosylation-Dependent and -Independent Mechanisms Regulating CTRP12 Cleavage, Secretion, and Stability. *Biochemistry* **58**, 727-741
54. Kornfeld, R., and Kornfeld, S. (1985) Assembly of asparagine-linked oligosaccharides. *Annu Rev Biochem* **54**, 631-664
55. Hart, G. W., Brew, K., Grant, G. A., Bradshaw, R. A., and Lennarz, W. J. (1979) Primary structural requirements for the enzymatic formation of the N-glycosidic bond in glycoproteins. Studies with natural and synthetic peptides. *J Biol Chem* **254**, 9747-9753
56. Suzuki, S., Wilson-Kubalek, E. M., Wert, D., Tsao, T. S., and Lee, D. H. (2007) The oligomeric structure of high molecular weight adiponectin. *FEBS Lett* **581**, 809-814
57. Radjainia, M., Wang, Y., and Mitra, A. K. (2008) Structural polymorphism of oligomeric adiponectin visualized by electron microscopy. *J Mol Biol* **381**, 419-430

58. Briggs, D. B., Jones, C. M., Mashalidis, E. H., Nunez, M., Hausrath, A. C., Wysocki, V. H., and Tsao, T. S. (2009) Disulfide-dependent self-assembly of adiponectin octadecamers from trimers and presence of stable octadecameric adiponectin lacking disulfide bonds in vitro. *Biochemistry* **48**, 12345-12357
59. Vitagliano, L., Berisio, R., Mazzarella, L., and Zagari, A. (2001) Structural bases of collagen stabilization induced by proline hydroxylation. *Biopolymers* **58**, 459-464
60. Peake, P. W., Hughes, J. T., Shen, Y., and Charlesworth, J. A. (2007) Glycosylation of human adiponectin affects its conformation and stability. *J Mol Endocrinol* **39**, 45-52
61. Wang, Y., Lam, K. S., Yau, M. H., and Xu, A. (2008) Post-translational modifications of adiponectin: mechanisms and functional implications. *Biochem J* **409**, 623-633
62. Gorres, K. L., and Raines, R. T. (2010) Prolyl 4-hydroxylase. *Crit Rev Biochem Mol Biol* **45**, 106-124
63. Vasta, J. D., Andersen, K. A., Deck, K. M., Nizzi, C. P., Eisenstein, R. S., and Raines, R. T. (2016) Selective Inhibition of Collagen Prolyl 4-Hydroxylase in Human Cells. *ACS Chem Biol* **11**, 193-199
64. Bella, J., Eaton, M., Brodsky, B., and Berman, H. M. (1994) Crystal and molecular structure of a collagen-like peptide at 1.9 A resolution. *Science* **266**, 75-81
65. Ramshaw, J. A., Shah, N. K., and Brodsky, B. (1998) Gly-X-Y tripeptide frequencies in collagen: a context for host-guest triple-helical peptides. *J Struct Biol* **122**, 86-91
66. Helenius, A., and Aebi, M. (2001) Intracellular functions of N-linked glycans. *Science* **291**, 2364-2369
67. Helenius, A., and Aebi, M. (2004) Roles of N-linked glycans in the endoplasmic reticulum. *Annu Rev Biochem* **73**, 1019-1049
68. Xu, C., and Ng, D. T. (2015) Glycosylation-directed quality control of protein folding. *Nat Rev Mol Cell Biol* **16**, 742-752
69. Hauri, H. P., Kappeler, F., Andersson, H., and Appenzeller, C. (2000) ERGIC-53 and traffic in the secretory pathway. *J Cell Sci* **113 (Pt 4)**, 587-596
70. Ruggiano, A., Foresti, O., and Carvalho, P. (2014) Quality control: ER-associated degradation: protein quality control and beyond. *J Cell Biol* **204**, 869-879
71. Tu, X., and Palczewski, K. (2012) Crystal structure of the globular domain of C1QTNF5: Implications for late-onset retinal macular degeneration. *J Struct Biol* **180**, 439-446
72. Kvansakul, M., Bogin, O., Hohenester, E., and Yayon, A. (2003) Crystal structure of the collagen alpha1(VIII) NC1 trimer. *Matrix Biol* **22**, 145-152
73. Wang, Z. V., Schraw, T. D., Kim, J. Y., Khan, T., Rajala, M. W., Follenzi, A., and Scherer, P. E. (2007) Secretion of the adipocyte-specific secretory protein adiponectin critically depends on thiol-mediated protein retention. *Mol Cell Biol* **27**, 3716-3731
74. Alberini, C. M., Bet, P., Milstein, C., and Sitia, R. (1990) Secretion of immunoglobulin M assembly intermediates in the presence of reducing agents. *Nature* **347**, 485-487
75. Sitia, R., Neuberger, M., Alberini, C., Bet, P., Fra, A., Valetti, C., Williams, G., and Milstein, C. (1990) Developmental regulation of IgM secretion: the role of the carboxy-terminal cysteine. *Cell* **60**, 781-790
76. Anelli, T., Alessio, M., Bachi, A., Bergamelli, L., Bertoli, G., Camerini, S., Mezghrani, A., Ruffato, E., Simmen, T., and Sitia, R. (2003) Thiol-mediated

protein retention in the endoplasmic reticulum: the role of ERp44. *EMBO J* **22**, 5015-5022
77. Guenzi, S., Fra, A. M., Sparvoli, A., Bet, P., Rocco, M., and Sitia, R. (1994) The efficiency of cysteine-mediated intracellular retention determines the differential fate of secretory IgA and IgM in B and plasma cells. *Eur J Immunol* **24**, 2477-2482
78. Reddy, P., Sparvoli, A., Fagioli, C., Fassina, G., and Sitia, R. (1996) Formation of reversible disulfide bonds with the protein matrix of the endoplasmic reticulum correlates with the retention of unassembled Ig light chains. *EMBO J* **15**, 2077-2085
79. Liu, M., Zhou, L., Xu, A., Lam, K. S., Wetzel, M. D., Xiang, R., Zhang, J., Xin, X., Dong, L. Q., and Liu, F. (2008) A disulfide-bond A oxidoreductase-like protein (DsbA-L) regulates adiponectin multimerization. *Proc Natl Acad Sci U S A* **105**, 18302-18307
80. Pajvani, U. B., Hawkins, M., Combs, T. P., Rajala, M. W., Doebber, T., Berger, J. P., Wagner, J. A., Wu, M., Knopps, A., Xiang, A. H., Utzschneider, K. M., Kahn, S. E., Olefsky, J. M., Buchanan, T. A., and Scherer, P. E. (2004) Complex distribution, not absolute amount of adiponectin, correlates with thiazolidinedione-mediated improvement in insulin sensitivity. *J Biol Chem* **279**, 12152-12162
81. Basu, R., Pajvani, U. B., Rizza, R. A., and Scherer, P. E. (2007) Selective downregulation of the high molecular weight form of adiponectin in hyperinsulinemia and in type 2 diabetes: differential regulation from nondiabetic subjects. *Diabetes* **56**, 2174-2177
82. Kusminski, C. M., McTernan, P. G., Schraw, T., Kos, K., O'Hare, J. P., Ahima, R., Kumar, S., and Scherer, P. E. (2007) Adiponectin complexes in human cerebrospinal fluid: distinct complex distribution from serum. *Diabetologia* **50**, 634-642
83. Robach, P., Gammella, E., Recalcati, S., Girelli, D., Castagna, A., Roustit, M., Lundby, C., Lundby, A. K., Bouzat, P., Verges, S., Sechaud, G., Banco, P., Uhr, M., Cornu, C., Sallet, P., and Cairo, G. (2020) Induction of erythroferrone in healthy humans by micro-dose recombinant erythropoietin or high-altitude exposure. *Haematologica* **Epub** haematol.2019.233874
84. Appleby, S., Chew-Harris, J., Troughton, R. W., Richards, A. M., and Pemberton, C. J. (2020) Analytical and biological assessment of circulating human erythroferrone. *Clin Biochem* **79**, 41-47
85. Berg, R. A., and Prockop, D. J. (1973) The thermal transition of a non-hydroxylated form of collagen. Evidence for a role for hydroxyproline in stabilizing the triple-helix of collagen. *Biochem Biophys Res Commun* **52**, 115-120
86. Deans, M. R., Peterson, J. M., and Wong, G. W. (2010) Mammalian Otolin: a multimeric glycoprotein specific to the inner ear that interacts with otoconial matrix protein Otoconin-90 and Cerebellin-1. *PLoS One* **5**, e12765
87. Wang, Y., Xu, A., Knight, C., Xu, L. Y., and Cooper, G. J. (2002) Hydroxylation and glycosylation of the four conserved lysine residues in the collagenous domain of adiponectin. Potential role in the modulation of its insulin-sensitizing activity. *J Biol Chem* **277**, 19521-19529
88. Holmgren, S. K., Taylor, K. M., Bretscher, L. E., and Raines, R. T. (1998) Code for collagen's stability deciphered. *Nature* **392**, 666-667
89. Shoulders, M. D., and Raines, R. T. (2009) Collagen structure and stability. *Annu Rev Biochem* **78**, 929-958

90. Bella, J., Brodsky, B., and Berman, H. M. (1995) Hydration structure of a collagen peptide. *Structure* **3**, 893-906
91. Tschank, G., Raghunath, M., Gunzler, V., and Hanauske-Abel, H. M. (1987) Pyridinedicarboxylates, the first mechanism-derived inhibitors for prolyl 4-hydroxylase, selectively suppress cellular hydroxyprolyl biosynthesis. Decrease in interstitial collagen and Clq secretion in cell culture. *Biochem J* **248**, 625-633
92. Bateman, J. F., Freddi, S., McNeil, R., Thompson, E., Hermanns, P., Savarirayan, R., and Lamande, S. R. (2004) Identification of four novel COL10A1 missense mutations in schmid metaphyseal chondrodysplasia: further evidence that collagen X NC1 mutations impair trimer assembly. *Hum Mutat* **23**, 396
93. Bogin, O., Kvansakul, M., Rom, E., Singer, J., Yayon, A., and Hohenester, E. (2002) Insight into Schmid metaphyseal chondrodysplasia from the crystal structure of the collagen X NC1 domain trimer. *Structure* **10**, 165-173

CHAPTER 4

PRADC1: A novel metabolic-responsive secretory protein that modulates physical activity and adiposity*

*Text and figures in this chapter were published in *FASEB* in 2019:

PRADC1: a novel metabolic-responsive secretory protein that modulates physical activity and adiposity. Susana Rodriguez[†], Ashley N. Stewart[†], Xia Lei, Xi Cao, Hannah C. Little, Vincent Fong, Dylan C. Sarver, and G. William Wong, *The FASEB Journal* 2019 33:12, 14748-14759
[†]Both authors contributed equally to this work.

Ashley Stewart generated data for the following figures and tables: Figure 2B, Table 1, Figure 3, Figure 4, Supplemental Figure S1, Supplemental Figure S2, and Supplemental Figure S3.

Abstract

Inter-organ communication mediated by secreted proteins plays a pivotal role in metabolic homeostasis, yet the function of many circulating secretory proteins remains unknown. Here, we describe the function of Protease Associated Domain Containing 1 (PRADC1), an enigmatic secretory protein widely expressed in humans and mice. In metabolically active tissues (liver, muscle, fat, heart, and kidney), we showed that *Pradc1* expression is significantly suppressed by fasting-and-refeeding and reduced in kidney and brown fat in the context of obesity. PRADC1 is dispensable for whole-body metabolism when mice are fed a low-fat diet. However, in obesity induced by high-fat feeding, PRADC1-deficient female mice have reduced weight gain and adiposity despite similar caloric intake. Decreased fat mass is attributed, in part, to increased metabolic rate, physical activity, and energy expenditure in these animals. Reduced adiposity in PRADC1-deficient mice, however, does not improve systemic glucose and lipid metabolism, insulin sensitivity, liver steatosis, or adipose inflammation. Thus, in PRADC1-deficient animals, decreased fat mass and enhanced physical activity are insufficient to confer a healthy metabolic phenotype in the context of an obesogenic diet. Our results shed light on the physiological function of PRADC1 and the complex regulation of metabolic health.

Introduction

Regulation of systemic metabolism and energy balance requires integrative mechanisms involving multiple tissues and organs. Secreted hormones mediate inter-organ communication necessary to maintain energy homeostasis. Although >3,000 human genes encode proteins with a signal peptide for secretion (1-3) and mass spectrometry can detect over three thousand proteins in plasma (3), the function of most of the secretory proteins in circulation remains poorly defined or unknown.

To uncover novel secreted metabolic regulators, we assessed the expression of candidate genes that encode for secretory proteins with unknown functions. We determined which of the candidate genes whose expression is responsive to metabolic and nutritional cues, suggestive of involvement in metabolic processes. Here, we focus our functional studies on one such gene, Protease Associated Domain Containing 1 (*Pradc1*), and show that it encodes a novel secreted regulator of energy metabolism.

PRADC1 (also known as PAP21) is a ~30 kDa *N*-glycosylated secretory protein with a protease associated domain (4). An ortholog encoding PRADC1 is found in *Drosophila*, worms (*C. elegans*), zebrafish, *Xenopus,* mice, and humans. While its evolutionary conservation across species (4) suggests a basic necessity for the gene, the biological function of PRADC1 remains elusive. We found that PRADC1 is widely expressed in both human and mouse tissues and its expression in metabolically active tissues is acutely regulated by fasting and refeeding while

being chronically altered in a diet-induced obese mouse model. Using a genetic loss-of-function mouse model, we demonstrated an important sex-dependent role for PRADC1 in modulating physical activity and adiposity in the context of obesity induced by high-fat feeding. Despite reduced body weight and adiposity, PRADC1-deficient female mice fed a high-fat diet did not exhibit an improved metabolic profile compared to wild-type littermates. Thus, PRADC1-deficient mice appear to have reduced adiposity and enhanced locomotor activity uncoupled from metabolic health. Our mouse model establishes the biological function of PRADC1, providing a physiological context to further understand its mechanisms of action.

Materials and Methods

Gene expression profiling

Gene expression profiling was performed using the TissueScan^{TM} (OriGene) human major tissue qPCR array (#HMRT303) and mouse tissues from wild-type C57BL/6J mice. Primers used in real-time PCR analysis were: human PRADC1 forward, 5'-CACGGCTTCCGTATCCATGAT-3' and reverse, 5'-GGTGAATCTGCTCATAC CTTGTG-3'; mouse *Pradc1* forward, 5'-TGAGTCCTGGGGATATTCGATAC-3' and reverse 5'-CAGCAGGG ACGAGGTGAATC-3'. For human *PRADC1*, all expression data were normalized to *GAPDH*. For mouse *Pradc1*, all expression data were normalized to *β-actin*.

Animals

Eight-week-old C57BL/6J male mice were obtained from The Jackson Laboratory (Bar Harbor, ME). Mouse tissues from different brain regions were collected from fasted and refed experiments. For the fasted group, food was removed for 16 h (beginning 10 h into the light cycle), and mice were euthanized 2 h into the light cycle. For the refed group, mice were fasted for 16 h and refed with chow pellets for 3 h before being euthanized. The *Pradc1* null mouse strain (*Pradc1*$^{tm1(KOMP)Vlcg}$) was generated by Regeneron Pharmaceuticals (Tarrytown, New York) (1). Live mice were generated from *Pradc1* (+/-) sperm obtained from the KOMP Repository (www.komp.org). Mouse *Pradc1* gene is located on chromosome 6; the gene consists of three exons and two introns and is 4,516 bp. To generate PRADC1-deficient mice, a total of 4,095 bp that comprise the entire coding region of the gene (from immediately downstream of the ATG start codon to part of the 3'UTR) were replaced with a targeting cassette containing a β-galactosidase reporter gene, *LacZ,* and a neomycin-resistant gene. Only the 5' and 3' UTRs of *Pradc1* gene remained after replacement with the cassette. This strategy ensured that knockout (KO) mice were completely devoid of PRADC1 protein. Genotyping primers for the *Pradc1* wild-type (WT) allele were: forward, 5'-TCTGGAGGTTCAGCAGGGAC-3' and reverse, 5'-CCTGGGAGGCAGAGCT AGATTC-3'. The size of the amplified WT PCR product was 388 bp. Primers for the knockout (KO) allele were: *LacZ*-forward, 5'-GGTAAACTGGCTCGGATTAGGG -3' and *LacZ*-reverse, 5'-TTGACTGTAGCGGCTGAT GTTG-3'. The size of the amplified KO PCR product

was 211 bp. *Pradc1* KO mice were generated on a C57BL/6N genetic background. All mice used in this study were generated by intercrossing *Pradc1* (+/-) mice to obtain KO and WT littermates, and at least two independent cohorts of mice were used per diet group. *Pradc1* KO (-/-) mice and WT (+/+) littermates were housed together in polycarbonate cages on a 12-h light-dark photocycle with *ad libitum* access to water and food, with no more than 5 adult mice per cage. Mice were fed a high-fat diet (HFD; 60% kcal derived from fat, Research Diets # D12492) or a matched control low-fat diet (LFD; 10% kcal derived from fat, Research Diets #D12450B). Diet was provided at the time of weaning (at 4 wk of age). At termination of the study, animals were fasted for 16 h, except for the HFD-fed *Pradc1* KO female mice, which were fasted for 2 h before euthanasia. Tissues were collected, snap-frozen in liquid nitrogen, and kept at −80°C until analysis. All animal protocols were submitted to and approved by the Institutional Animal Care and Use Committee of The Johns Hopkins University School of Medicine (protocol# MO16M431).

Serum collection and Analysis

Blood samples were collected by tail vein bleed and serum was isolated using Microvette CB 300 (Sarstedt, Newton, NC) per the manufacturer's instructions. Serum triglyceride (TG) and cholesterol (CH) levels were measured using an Infinity kit (Thermo Fisher Scientific, Middletown, VA) per the manufacturer's instructions. Serum non-esterified fatty acids (NEFA) were measured using a

NEFA-HR(2) kit (Wako Chemicals, Richmond, VA). Serum β-hydroxybutyrate (BHB) was measured using a LiquiColor assay (Stanbio).

ELISAs

Serum insulin and FGF21, adiponectin (EZMADP-60K), and leptin (EZML-82K) levels were measured using Millipore ELISA kits (MilliporeSigma, Burlington, MA). Serum corticosterone was obtained using the Mouse/Rat Corticosterone kit from ALPCO (ALPCO, Salem, NH). Serum T3, T4, and TSH levels were obtained using the MILLIPLEX MAP Rat Thyroid Hormone Magnetic Bead Panel (MilliporeSigma). For the multiplex assay, standard curves were generated for each hormone. Serum was diluted according to the manufacturer's instructions. Samples and standards were analyzed using a Luminex 200 instrument (Luminex, Austin, TX) and XPonent 3.1 software (MilliporeSigma).

Glucose and insulin tolerance test

For glucose tolerance tests, food was removed for 16 h (overnight) before mice were intraperitoneally (i.p.) injected with a dose of 1 g of glucose/kg body weight diluted in 0.9% sterile filtered saline. Blood glucose was measured at 0, 15, 30, 60, and 120 min after glucose injection using a glucometer (NovaMax Plus, Billerica, MA). For insulin tolerance tests, mice were fasted for 2 h before receiving an i.p. injection of insulin at a dose of 0.75 U/kg body weight (low-fat diet males and females, high-fat diet females) or 1.5 U/kg body weight (high-fat diet males). Blood

glucose was measured at 0, 15, 30, 60, and 90 min after insulin injection as described above.

Hepatic lipid extraction

Livers were harvested from the HFD-fed *Pradc1* KO female mice following a 2 h food removal. Tissues were collected, flash frozen in liquid nitrogen, and stored at -80°C. Between 50-100 mg of liver tissue was homogenized in 500 ul of ice-cold distilled water. A portion of the homogenate (200 µL) was collected for lipid extraction by mixing with 1 mL of 2:1 chloroform-methanol and centrifuged at 313 *g* for 5 min at 4°C. The chloroform phase was collected and dried under vacuum. Samples were reconstituted in a mixture of 3:1:1 tert-butanol-MeOH-Triton X-100 before TG and CH content was determined using Infinity kits as described above. Samples were normalized to mass content.

Adipose tissue lipolysis

Mice were fasted for 2 h before receiving an *i.p.* injection of the β_3-adrenergic receptor agonist, CL 316243 (Santa Cruz Biotechnology) at a dose of 1 mg/kg body weight. Blood glucose was measured with a glucometer before and 15 minutes post injection. Blood was collected by the tail-vein into Microvette CB 300 capillary tubes capillary tubes before and 15 minutes post injection. Serum was isolated and assayed for NEFA (Wako Diagnostics, Mountain View, CA) and glycerol (Sigma-Aldrich, St. Louis, MO) content following manufacturer's instructions.

Body Composition Analysis

Body composition analyses for fat and lean mass were performed on mice at 24 wk of age using Echo-MRI-100 (Echo Medical Systems, Waco, TX) at The Johns Hopkins University School of Medicine mouse phenotyping core facility.

Indirect calorimetry

HFD-fed WT and KO female mice at 24 wk of age were assessed daily for body weight changes, food intake (corrected for spillage), physical activity, and whole-body metabolic profiling in the Comprehensive Laboratory Animal Monitoring System (Columbus Instruments) as previously described (5). Data were collected for four days to confirm that mice were acclimated to the calorimetry chambers (indicated by stable body weights, food intake, and diurnal metabolic patterns), and data were analyzed from the fourth day.

Histology and analysis of crown-like structures (CLS) of adipose tissue

Gonadal (gWAT) and inguinal (iWAT) adipose tissue from WT and *Pradc1*-KO mice were fixed immediately in 10% formalin at 4°C following dissection. Fixed tissues were embedded in paraffin, sectioned, and stained with hematoxylin and eosin at the Histology Reference Laboratory at The Johns Hopkins University School of Medicine. Images were captured with an Axioplan upright microscope with an Axiocam color CCD camera (Carl Zeiss Microscopy). To quantify the crown-like structures (CLS), an RGB image (1378 μm × 1091.8 μm) with a set scale of 1000 pixels = 1060 μm was used. CLSs were identified as clusters of

macrophages that had infiltrated the adipose tissue and formed ring-like structures. The number of CLSs was manually counted in five random fields for each section. Nine mice in each group were sectioned and counted.

Adipocyte cell size analysis

Adipocyte size was measured using MRI Adipocyte Tools' macro in ImageJ software as previously described (6).

Blood and tissue collection

WT and *Pradc1*-KO mice were fasted for 2 h, anesthetized with isoflurane, and blood was collected through the retro-orbital plexus using capillary tubes (Fisher Scientific, Hampton, NH). Tissues were immediately harvested from euthanized mice and flash frozen in liquid nitrogen and stored at -80°C until further processing.

Quantitative real-time PCR analysis

Total RNA was isolated from tissues using TRIzol (Thermo Fisher Scientific, Waltham, MA) according to the manufacturer's instructions. Samples were treated with DNAseI (New England Biolabs, Ipswich, MA) to remove genomic DNA contamination and subjected to 3M (pH 5.2) sodium acetate (Quality Biological, Gaithersburg, MD) precipitation to purify RNA samples. In brief, sodium acetate was added at 1/10 the volume of the sample followed by the addition of 2.5 volumes of ice cold 100% ethanol and mixed thoroughly. Samples were incubated at -80°C overnight and then centrifuged at 12,000 x g for 20 minutes at 4°C and

the supernatant was decanted. The RNA pellets were washed twice using 1 mL of ice cold 75% ethanol and centrifuged at 12,000 x g at 4°C. A quick spin was performed to remove any traces of residual ethanol in the pellet using a very fine pipette tip. Purified RNA was reverse transcribed using the GoScript Reverse transcription system (Promega, Madison, WI). Quantitative real-time PCR analyses were performed on a CFX Connect system (Bio-Rad Laboratories, Hercules, CA) using iTaq Universal SYBR Green Supermix (Bio-Rad) per the manufacturer's directions. Data were normalized to *36B4* (adipose tissue), *18S rRNA* (skeletal muscle), and *β-actin* (liver) and expressed as relative mRNA levels using the **ΔΔ**Ct method (7). All the primers used were previously published (8-10).

Statistical analysis

Comparisons between two groups of data were performed using two-tailed Student's t-tests with 95% confidence intervals, and ANOVAs were used to make comparisons involving more than two groups. Graphpad Prism 7 software was used for statistical analyses and values were considered to be statistically significant at P <0.05. For all data, $*P < 0.05$, $**P < 0.01$, and $***P < 0.001$. All data are presented as mean ± SE.

Results

Expression of *Pradc1* transcript in metabolically active tissues is regulated by the nutritional state of the animal

Human and mouse PRADC1 protein are highly conserved (Fig. 1A), differing by only one amino acid in the mature protein (excluding the signal peptide). Both human and mouse *PRADC1* were widely expressed among a variety of tissues (Fig. 1B, C). Expression of *Pradc1* in metabolically active tissues (liver, muscle, adipose, and heart), as well as different brain regions (cortex and hypothalamus), was acutely regulated by the nutritional state. In the refed state (overnight fast followed by a 3 h food intake), we observed a striking suppression of *Pradc1* mRNA in different tissues and brain regions of normal wild-type chow-fed mice (Fig. 1D). In the context of obesity induced by a high-fat diet, the expression of *Pradc1* was also reduced in kidney and brown adipose tissue (BAT) relative to mice fed a control low-fat diet (Fig. 1E). These data suggest a potential metabolic function for PRADC1.

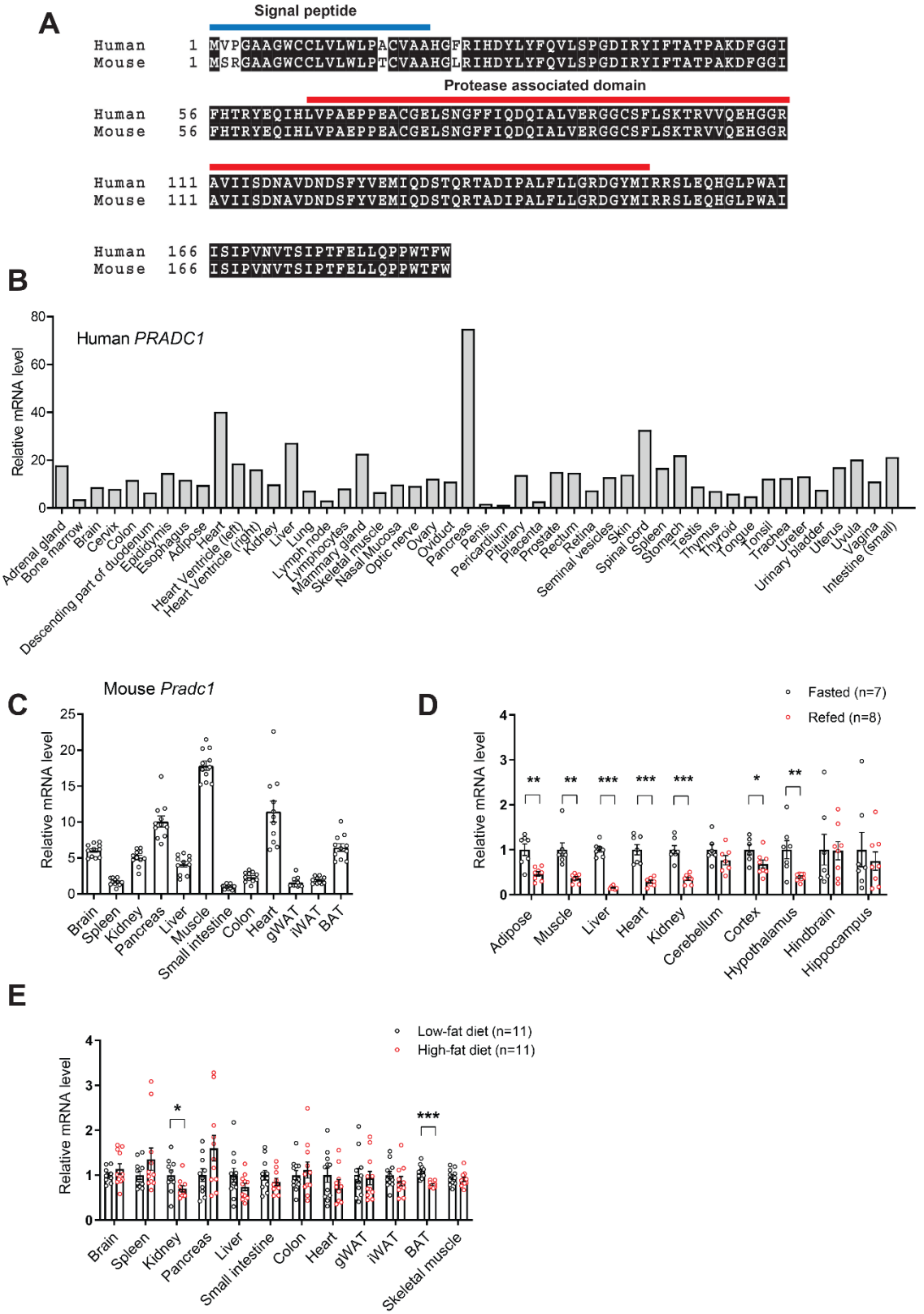
A
Signal peptide
Protease associated domain
Human 1 MVPGAAGWCCLVLWLPACVAAHGFRIHDYLYFQVLSPGDIRYIFTATPAKDFGGI
Mouse 1 MSRGAAGWCCLVLWLPTCVAAHGLRIHDYLYFQVLSPGDIRYIFTATPAKDFGGI
Human 56 FHTRYEQIHLVPAEPPEACGELSNGFFIQDQIALVERGGCSFLSKTRVVQEHGGR
Mouse 56 FHTRYEQIHLVPAEPPEACGELSNGFFIQDQIALVERGGCSFLSKTRVVQEHGGR
Human 111 AVIISDNAVDNDSFYVEMIQDSTQRTADIPALFLLGRDGYMIRRSLEQHGLPWAI
Mouse 111 AVIISDNAVDNDSFYVEMIQDSTQRTADIPALFLLGRDGYMIRRSLEQHGLPWAI
Human 166 ISIPVNVTSIPTFELLQPPWTFW
Mouse 166 ISIPVNVTSIPTFELLQPPWTFW
B
Human PRADC1
Relative mRNA level
Adrenal gland
Bone marrow
Brain
Cervix
Colon
Descending part of duodenum
Epididymis
Esophagus
Adipose
Heart
Heart Ventricle (left)
Heart Ventricle (right)
Kidney
Liver
Lung
Lymph node
Lymphocytes
Mammary gland
Skeletal muscle
Nasal Mucosa
Optic nerve
Ovary
Oviduct
Pancreas
Penis
Pericardium
Pituitary
Placenta
Prostate
Rectum
Retina
Seminal vesicles
Skin
Spinal cord
Spleen
Stomach
Testis
Thymus
Thyroid
Tongue
Tonsil
Trachea
Ureter
Urinary bladder
Uterus
Uvula
Vagina
Intestine (small)
C
Mouse Pradc1
Relative mRNA level
Brain
Spleen
Kidney
Pancreas
Liver
Muscle
Small intestine
Colon
Heart
gWAT
iWAT
BAT
D
Fasted (n=7)
Refed (n=8)
Relative mRNA level
Adipose
Muscle
Liver
Heart
Kidney
Cerebellum
Cortex
Hypothalamus
Hindbrain
Hippocampus
E
Low-fat diet (n=11)
High-fat diet (n=11)
Relative mRNA level
Brain
Spleen
Kidney
Pancreas
Liver
Small intestine
Colon
Heart
gWAT
iWAT
BAT
Skeletal muscle

Figure 1. Expression and regulation of *Pradc1* in various tissues under different physiological states. ***A***, Sequence alignment of full-length human (NP_115695) and mouse (NP_001156899) PRADC1 proteins. The predicted signal peptide and protease associated domain are indicated. ***B***, Expression of *PRADC1* in human tissue panel. ***C***, Expression of *Pradc1* in mouse tissues (n=11). ***D***, Real-time PCR analysis of the expression of *Pradc1* in different tissues and brain regions from mice subjected to an overnight fast (fasted group; n=7) or an overnight fast followed by 3 h of refeeding (refed group; n=8). ***E***, Real-time PCR analysis of the expression of *Pradc1* in different tissues from mice fed a control low-fat diet (n=11) or a high-fat diet (n=11). Expression levels were normalized to *β-actin*. BAT, brown adipose tissue; gWAT, gonadal white adipose tissue; iWAT, inguinal white adipose tissue. Data are expressed as mean ± SEM. **P* < 0.05, ***P* < 0.01, ****P*<0.001.

Loss-of-function mouse model for PRADC1

We employed a whole-body knockout mouse model to determine the requirement for PRADC1 in metabolic homeostasis. The gene targeting strategy involved the replacement of the entire protein-coding region of PRADC1 with the β-galactosidase (LacZ) and neomycin-resistance cassette (Fig. 2A). Our PCR analysis confirmed the genotype of the WT and KO mice (Fig. 2B). As expected, in the KO mice, *Pradc1* transcript was not detected in the adipose tissue, heart, muscle, or pancreas (Fig. 2C). *Pradc1* KO mice of both sexes were born at the expected Mendelian ratio and the animals appeared normal with no gross developmental abnormalities.

PRADC1 deficiency is dispensable for metabolic homeostasis under basal conditions

When fed a control low-fat diet (LFD), WT and *Pradc1* KO mice of either sex gained similar weight over time, had no differences in insulin sensitivity as measured by glucose and insulin tolerance tests, and exhibited no differences in fasting blood glucose or serum triglyceride, cholesterol, non-esterified free fatty acids, or β-hydroxybutyrate (Supplemental Fig. S1 and S2). Only LFD-fed *Pradc1* KO male mice showed increased fasting NEFA levels compared to WT mice (Supplemental Fig. S1G). These data indicate that PRADC1 is dispensable for glucose and lipid metabolism under the basal condition where mice were consuming a control LFD. We also observed no differences in organ weights and blood glucose levels between genotypes of either sex (Table 1).

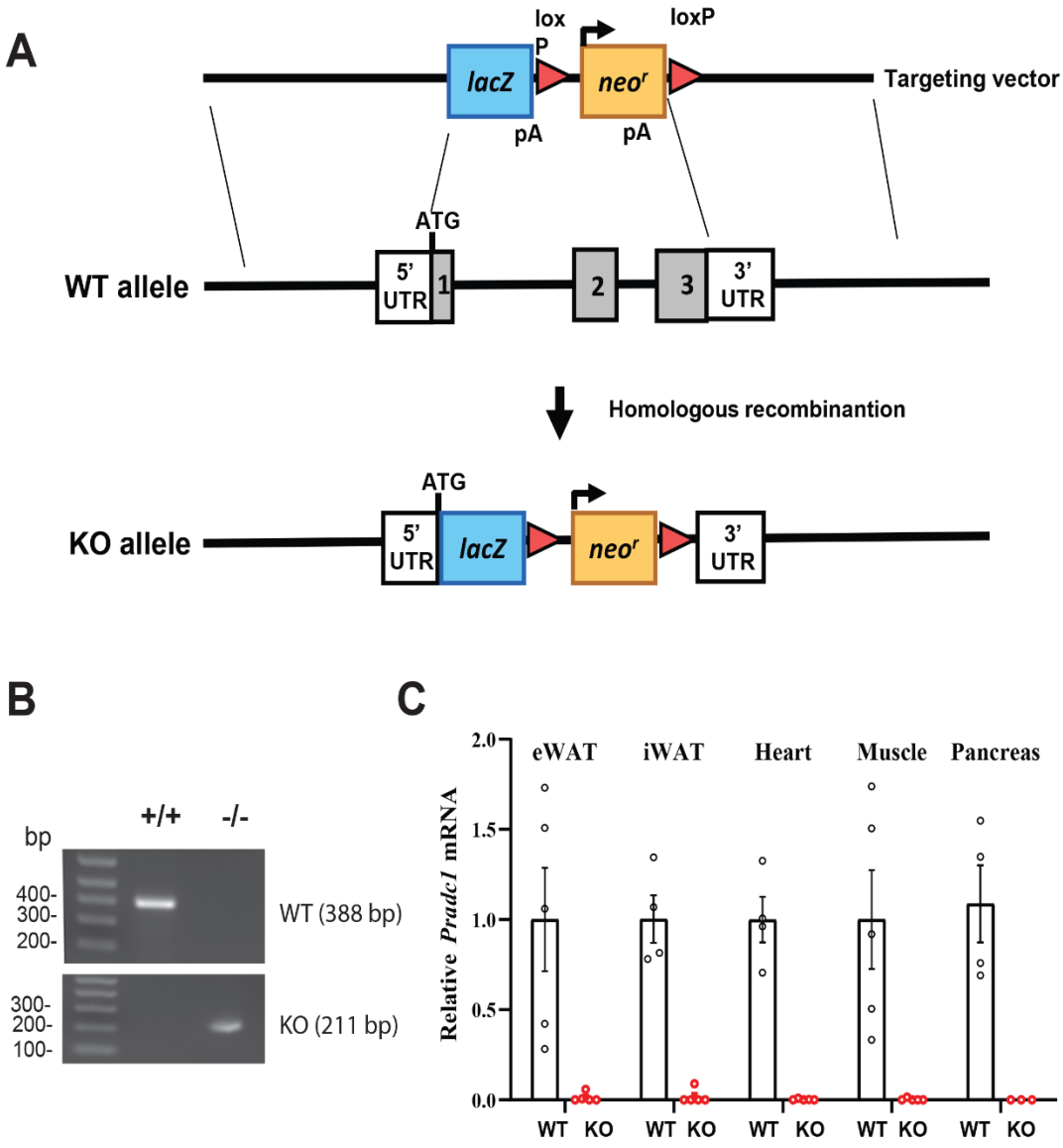

Figure 2. Generation of *Pradc1* knockout (KO) mice. ***A***, Schematic showing the gene targeting strategy used to generate *Pradc1* KO mice. ***B***, PCR genotyping results showing the successful generation of wild-type (WT; +/+) and homozygous knockout (-/-) mice. ***C***, The absence of *Pradc1* mRNA in mouse tissues of KO mice was confirmed by real-time PCR. eWAT, epididymal white adipose tissue; iWAT, inguinal white adipose tissue; LacZ, β-galactosidase; Neo^r, neomycin resistant; UTR, untranslated region; WT, wild-type; KO, knockout.

Loss of PRADC1 reduces weight gain in KO female mice fed a high-fat diet by elevating physical activity and energy expenditure

Next, we addressed whether loss of PRADC1 affects the physiologic response to a high-fat diet (HFD) induced obesity. In male mice fed an HFD, body weight over time, glucose and insulin tolerance tests, and fasting blood glucose and serum triglyceride, cholesterol, non-esterified free fatty acids, and ketone (β-hydroxybutyrate) levels were not significantly different between WT and *Pradc1* KO animals (Supplemental Fig. S3 and Table 1). In striking contrast, *Pradc1* KO female mice gained significantly less body weight over time when fed an HFD (Fig. 3A, B and Table 1). Reduced body weight was attributed to reduced fat mass (Fig. 3C,D) and not due to changes in lean mass (Fig. 3E). When normalized to body weight, *Pradc1* KO female mice had a higher percentage of lean mass (Fig. 3F). Food intake was not significantly different between WT and *Pradc1* KO female mice (Fig. 3G, H). Decreased adiposity seen in the *Pradc1* KO mice was due to increased metabolic rate as measured by the rate of oxygen consumption (Fig. 3I,J), enhanced physical activity (Fig. 3K), and enhanced energy expenditure (Fig. 3L). These data indicate that PRADC1 deficiency impacted whole-body energy balance in a sex-dependent manner. Altered thyroid hormones, stress hormone, and FGF-21 could potentially increase physical activity and/or energy expenditure in *Pradc1* KO female mice. However, serum T3, T4, thyroid stimulating hormone (TSH), corticosterone, and FGF-21 levels were not significantly different between WT and *Pradc1* KO female mice (Supplemental Fig. S4A-E). Since *Pradc1* was expressed in BAT and its expression was reduced in BAT in diet-induced obese

mice (Fig. 1), we determined whether there are any changes in uncoupling activity that could lead to greater energy expenditure. Increased BAT thermogenic activity would be reflected in increased body temperature. Measurements of body temperature did not reveal significant differences between genotypes (Supplemental Fig. S4F). The expression of *Ucp-1* in BAT and iWAT was in fact lower in the KO mice relative to WT littermates (Supplemental Fig. S4G); thus, BAT activation or “browning” of iWAT is unlikely to be the mechanism responsible for increased energy expenditure and reduced body weight seen in the HFD-fed KO female mice

	Male (45 weeks)			Female (47 weeks)		
	WT	KO	*P*-Value	WT	KO	*P*-Value
Low-fat diet (LFD)	*N* = 8	*N* = 10		*N* = 10-15	*N* = 10-13	
Body weight (g)	35.97 ± 1.154	36.23 ± 1.197	0.8804	27.83 ± 1.073	28.52 ± 1.258	0.6778
Gonadal fat mass (g)	0.83 ± 0.081	0.70 ± 0.063	0.2145	0.68 ± 0.069	0.77 ± 0.097	0.4386
Gonadal fat mass/body weight	0.02 ± 0.002	0.02 ± 0.002	0.261	0.02 ± 0.002	0.02 ± 0.002	0.5576
Inguinal fat mass (g)	0.68 ± 0.0651	0.69 ± 0.069	0.8791	0.35 ± 0.048	0.35 ± 0.049	0.9657
Inguinal fat mass/body weight	0.02 ± 0.001	0.02 ± 0.001	0.8853	0.012 ± 0.001	0.01 ± 0.001	0.7582
Liver weight (g)	1.41 ± 0.110	1.73 ± 0.234	0.271	0.96 ± 0.064	1.17 ± 0.112	0.1094
Liver weight/body weight	0.04 ± 0.002	0.05 ± 0.005	0.1877	0.03 ± 0.002	0.04 ± 0.004	0.0928
Kidney (g)	0.15 ± 0.006	0.17 ± 0.006	0.0341	0.10 ± 0.015	0.10 ± 0.011	0.9007
Kidney/body weight	0.004 ± 0.000	0.005 ± 0.000	0.108	0.004 ± 0.000	0.004 ± 0.000	0.8996
Fed blood glucose (mg/dL)	134.60 ± 9.371	144.2 ± 6.625	0.4039	112.3 ± 6.854	119.3 ± 8.735	0.5303

	Male (38 weeks)			Female (45 weeks)		
	WT	KO	*P*-Value	WT	KO	*P*-Value
High-fat diet (HFD)	*N* = 10	*N* = 6		*N* = 9	*N* = 12	
Body weight (g)	49.9 ± 1.342	47.24 ± 2.225	0.291	55.17 ± 2.214	46.94 ± 1.831	0.0095
Gonadal fat mass (g)	0.66 ± 0.066	0.52 ± 0.092	0.2502	3.67 ± 0.234	2.94 ± 0.209	0.0324
Gonadal fat mass/body weight	0.01 ± 0.001	0.01 ± 0.002	0.2964	0.07 ± 0.002	0.06 ± 0.002	0.2382
Inguinal fat mass (g)	1.25 ± 0.066	1.11 ± 0.134	0.2925	1.54 ± 0.084	1.23 ± 0.088	0.0205
Inguinal fat mass/body weight	0.03 ± 0.001	0.02 ± 0.002	0.3365	0.03 ± 0.001	0.026 ± 0.002	0.3811
Liver weight (g)	2.73 ± 0.136	2.68 ± 0.268	0.8766	1.51 ± 0.081	1.46 ± 0.085	0.6713
Liver weight/body weight	0.05 ± 0.002	0.06 ± 0.005	0.6674	0.03 ± 0.001	0.03 ± 0.002	0.0761
Kidney (g)	0.20 ± 0.005	0.21 ± 0.014	0.4527	NA	NA	NA
Kidney/body weight	0.004 ± 0.000	0.004 ± 0.001	0.2239	NA	NA	NA
Fed blood glucose (mg/dL)	162.2 ± 5.251	169.5 ± 15.48	0.599	178.8 ± 7.59	178 ± 5.451	0.9327

Table 1. Body weight, organ weight, and fed glucose levels in WT and *Pradc1* KO male and female mice fed a low-fat or high-fat diet.

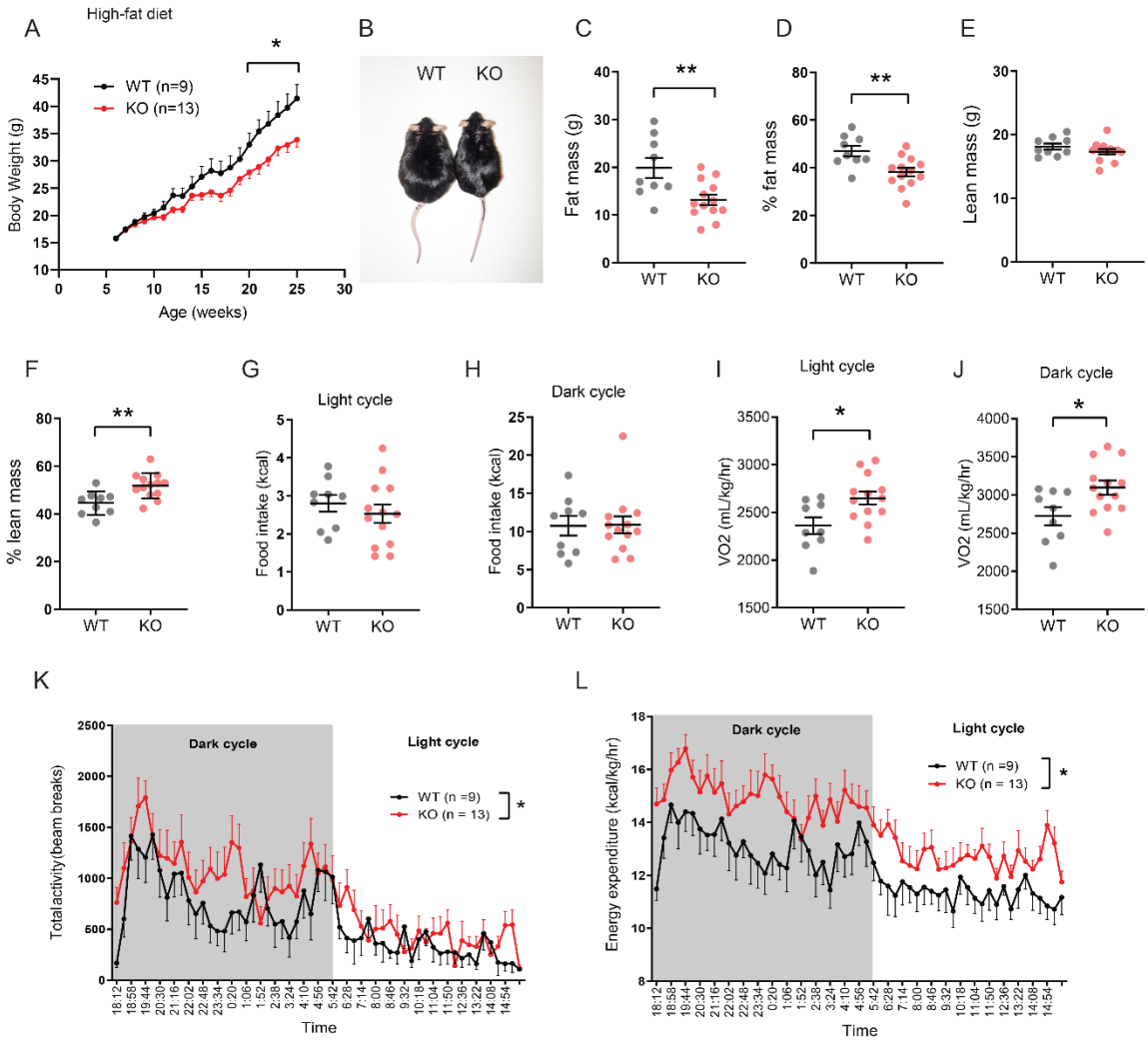

Figure 3. Reduced adiposity and enhanced physical activity and energy expenditure in *Pradc1* KO female mice fed a high-fat diet. ***A***, Body weight gain over time in WT and *Pradc1* KO female mice fed a high-fat diet. ***B***, Representative image of WT and KO female mice at 25 weeks old. ***C***, Whole-body fat mass of WT and KO female mice as determined by Echo-MRI. ***D***, Percent fat mass relative to body weight. ***E***, Whole-body lean mass of WT and KO female mice as determined by NMR. ***F***, Percent lean mass relative to body weight. ***G-H***, Food intake during the light (G) and dark (H) cycle. ***I-J***, Rate of oxygen consumption (VO_2) as a measure of metabolic rate in WT and KO female mice during the light (I) and dark (J) cycle. **K**, Total physical activity as measured by beam breaks in WT and KO female mice during the light and dark cycle. ***L***, Energy expenditure of WT and KO female mice during the light and dark cycle. Female mice: WT, n=9; KO, n=13. Mice were at 25-26 weeks of age when indirect calorimetry analyses were performed. Data are expressed as mean ± SEM. **P* < 0.05, ***P* < 0.01.

Reduced body weight and adiposity in *Pradc1* KO female mice did not alter whole-body glucose or lipid metabolism

Given that *Pradc1* KO female mice had significantly reduced body weight and adiposity, and an increase in physical activity and energy expenditure, we reasoned that they might have improved metabolic profiles. Contrary to expectation, insulin sensitivity as measured by glucose and insulin tolerance tests, as well as fasting and refed blood glucose, and serum triglyceride, cholesterol, non-esterified free fatty acid, and ketone (β-hydroxybutyrate) levels were not significantly different between HFD-fed WT and *Pradc1* KO female mice (Fig. 4A-G). Hepatic triglyceride and cholesterol levels were also not significantly different between WT and KO female mice (Fig. 4H,I). We also measured the circulating levels of two major adipocyte-derived adipokines, leptin and adiponectin. Serum levels of leptin and adiponectin in both the fed and fasted state were not significantly different between genotypes (Fig. 4J,K).

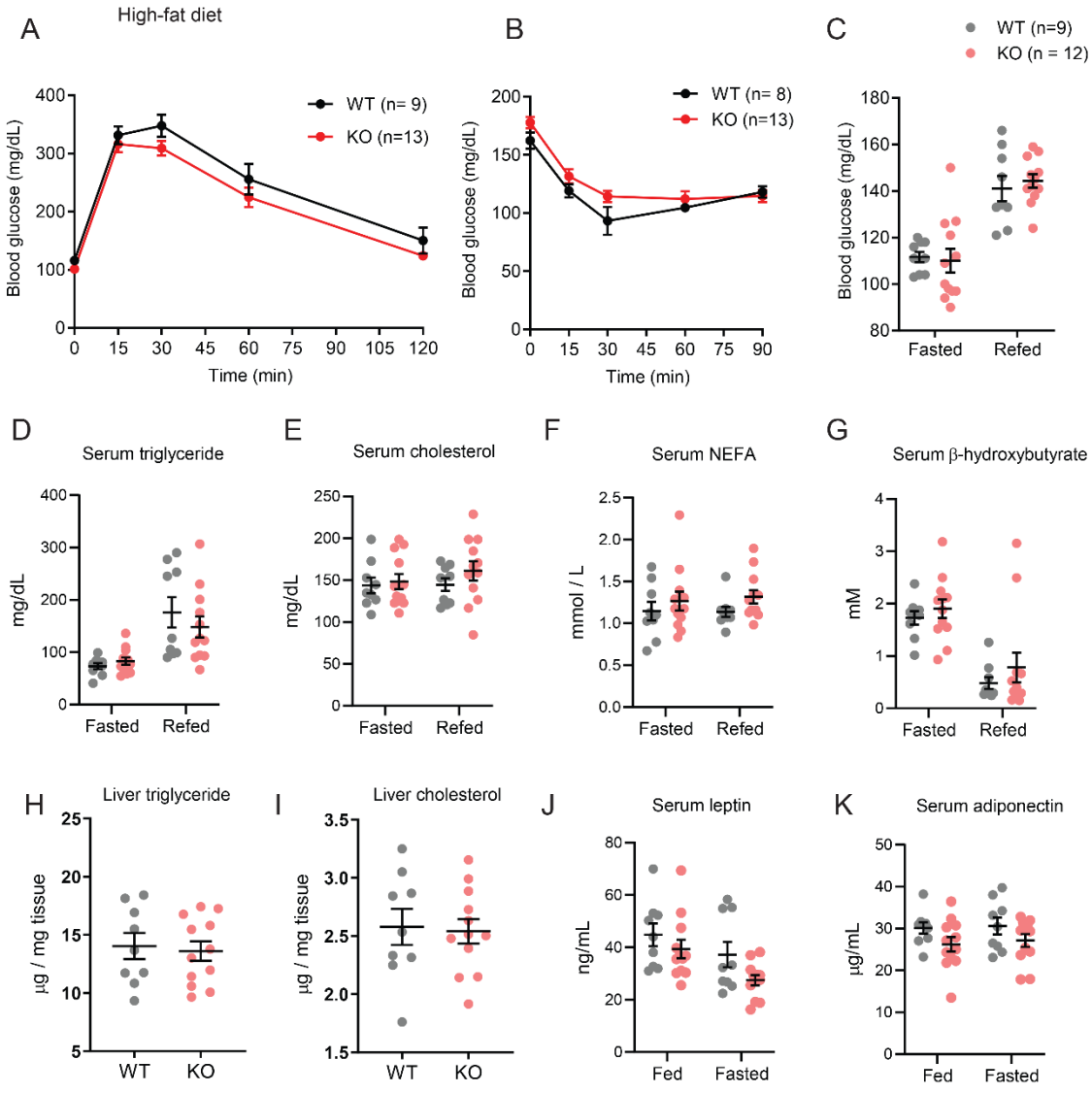

Figure 4. Glucose and lipid metabolism in WT and *Pradc1* KO female mice fed a high-fat diet. ***A-B***, Glucose tolerance **(A)** and insulin tolerance **(B)** tests in WT (n=8-9) and KO (n=13) female mice at 18 and 19 weeks of age. ***C-G***, Overnight fast and refed blood glucose, serum triglyceride, cholesterol, non-esterified free fatty acids (NEFA), and β-hydroxybutyrate in WT (n=9) and KO (n=12) female mice. ***H-I***, liver triglyceride and cholesterol levels in WT (n=9) and KO (n=12) female mice. ***J-K***, Serum leptin and adiponectin levels in fed and overnight fasted WT (n=9) and KO (n=12) female mice. Animals were at 43-45 weeks of age when serum metabolite and adipokines were measured. Data are expressed as mean ± SEM.

Impact of PRADC1 deficiency on adipose tissue histology, function, and gene expression in female mice

It is known that high-fat diet induced obesity leads to adipocyte hypertrophy and macrophage infiltration (11-13). Since *Pradc1* KO female mice had reduced adiposity, we therefore determined the impact of PRADC1 deficiency on adipose tissue structure and function. Histological analysis of visceral (gonadal) and subcutaneous (inguinal) fat depots between HFD-fed WT and *Pradc1* KO female mice revealed comparable adipocyte cell size and no significant difference in the number of crown-like structures that marked apoptotic adipocytes surrounded by infiltrating macrophages (Fig. 5A-E). We next determined whether there were any functional differences in fat mobilization in adipose tissue between WT and KO mice in response to β_3-adrenergic receptor agonist (CL 316243) stimulation. The extent of adipose tissue lipolysis, as judged by glycerol release into plasma, was reduced in *Pradc1* KO female mice (Fig. 5F). Serum levels of non-esterified free fatty acids (NEFA) were not significantly different between genotypes in response to CL stimulation (Fig. 5G). The expression of fatty acid synthesis, triglyceride synthesis, and fat oxidation genes were largely unchanged in WT and *Pradc1* KO female mice (Table 2). Seven out of the fifteen inflammation-related genes profiled by real-time PCR were altered between WT and KO female mice in a depot-specific manner (Table 2). Specifically, the expression of *Tnf-α, F4/80*, and *Il-10* was reduced in the visceral fat depot of KO female mice relative to WT controls. In the subcutaneous fat depot, the expression of *Tnf-α, Mcp-1*, *Ccl3*, *Ccl4*, *F4/80*, and *Cd68* was decreased in KO female mire compared to WT controls. Reduced

inflammatory gene expression in the white adipose tissue, however, did not appear to affect serum adipokine (adiponectin and leptin) levels, nor whole-body lipid profiles and glucose metabolism (Fig. 4). Genes involved in ER stress (e.g., *Atf4*), oxidative stress (e.g., *Nqo1*), and fibrosis (e.g., *Tgf-β*) were also downregulated in the visceral or subcutaneous fat depot of *Pradc1* KO female mice relative to WT littermates.

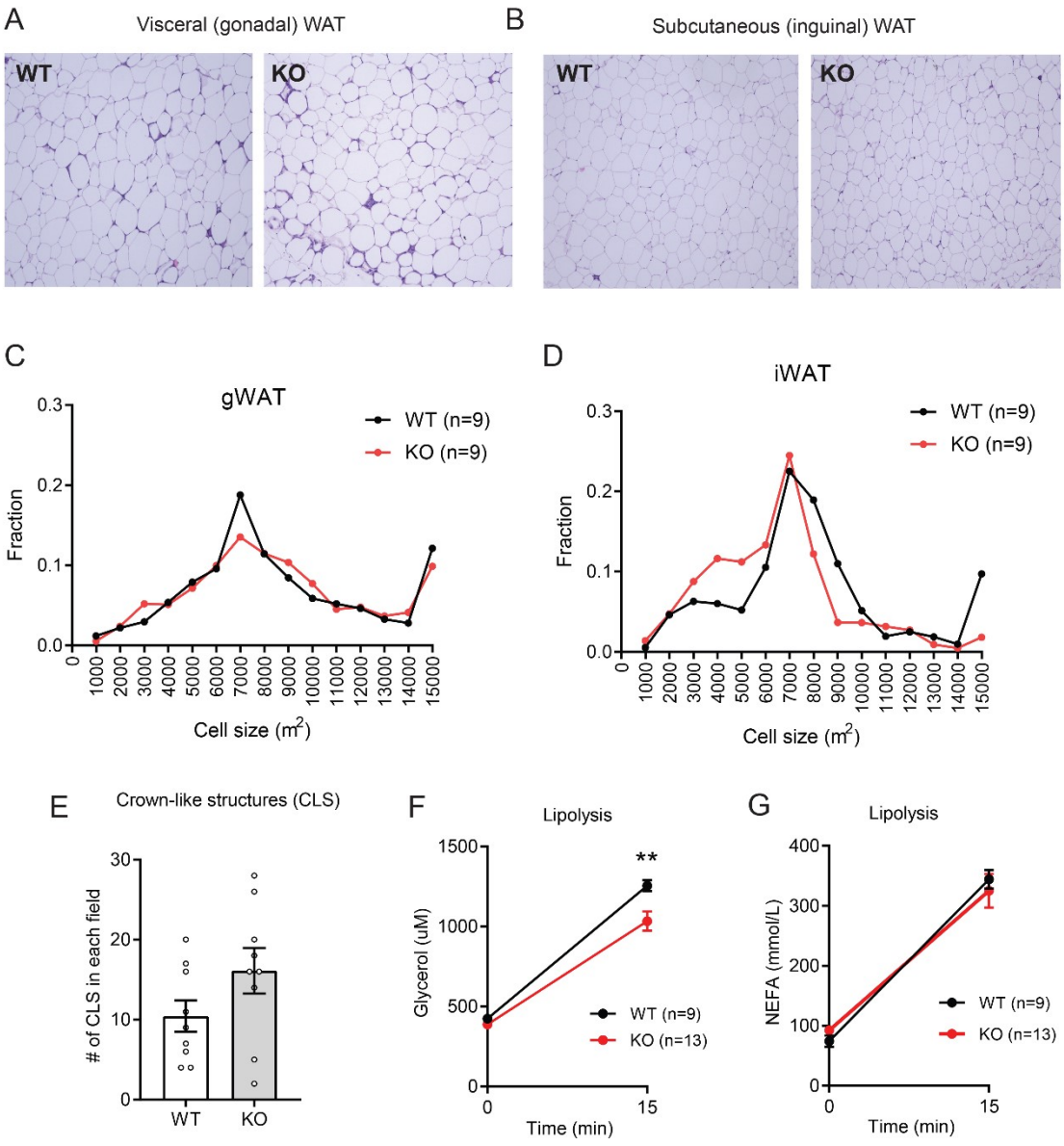

Figure 5. Impact of PRADC1 deficiency on adipocyte size, crown-like structures, and adipose lipolysis in female mice fed a high-fat diet. ***A-B***, Representative histology (H&E stained; 100X magnification) of visceral (gonadal) and subcutaneous (inguinal) white adipose tissue (WAT) of WT and KO female mice at 45 weeks of age. ***C-D***, Quantification of adipocyte cell size in gonadal (gWAT) and inguinal (iWAT) white adipose tissue of WT (n=9) and KO (n=9) female mice. ***E***, Quantification of crown-like structures in gWAT of WT (n=9) and KO (n=9) female mice. ***F-G***, Serum glycerol and non-esterified free fatty acids (NEFA) levels in 31-week-old WT (n=9) and KO (n=13) female mice injected with a β_3-adrenergic receptor agonist (CL 316243) to induce adipose lipolysis. Data are expressed as mean ± SEM. $^{**}P < 0.01$.

	Visceral (gonadal) WAT			Subcutaneous (inguinal) WAT		
	WT	KO	*P*-value	WT	KO	*P*-value
Fatty acid synthesis	*N*=8	*N*=8		*N*=8	*N*=8	
Fasn	1.00 ± 0.26	1.28 ± 0.41	0.574	1.00 ± 0.31	0.58 ± 0.19	0.3044
Acc1	1.00 ± 0.22	0.74 ± 0.16	0.385	1.00 ± 0.16	0.89 ± 0.32	0.768
Scd1	1.00 ± 0.16	0.92 ± 0.26	0.816	1.00 ± 0.09	0.62 ± 0.10*	0.022
Srebp-1c	1.00 ± 0.11	1.01 ± 0.22	0.946	1.00 ± 0.34	0.54 ± 0.16	0.291
Ppar-γ	1.00 ± 0.16	0.74 ± 0.13	0.247	1.00 ± 0.20	0.55 ± 0.19	0.146
Triglyceride synthesis						
Gpat1	1.00 ± 0.11	1.08 ± 0.12	0.635	1.04 ± 0.08	0.82 ± 0.18	0.545
Gpat2	1.00 ± 0.20	0.68 ± 0.16	0.256	N/A	N/A	
Agpat1	1.00 ± 0.08	0.89 ± 0.14	0.534	1.00 ± 0.08	1.47 ± 0.38	0.260
Agpat2	1.00 ± 0.20	1.13 ± 0.26	0.698	1.00 ± 0.22	0.41 ± 0.05*	0.046
Dgat1	1.00 ± 0.08	0.89 ± 0.16	0.586	1.00 ± 0.15	0.71 ± 0.24	0.337
Dgat2	1.00 ± 0.12	1.16 ± 0.26	0.560	1.00 ± 0.19	0.42 ± 0.07*	0.032
Lipolysis						
Atgl	1.00 ± 0.17	0.91 ± 0.09	0.663	1.00 ± 0.14	0.90 ± 0.31	0.776
Hsl	1.00 ± 0.17	0.78 ± 0.16	0.389	1.00 ± 0.13	0.72 ± 0.22	0.317
Fat oxidation						
Ppar-α	1.00 ± 0.26	0.87 ± 0.15	0.708	1.00 ± 0.16	0.84 ± 0.31	0.672
Cpt-1a	1.00 ± 0.12	0.75 ± 0.14	0.205	1.00 ± 0.16	0.59 ± 0.17	0.112
Acox1	1.00 ± 0.14	0.90 ± 0.11	0.600	1.00 ± 0.19	0.72 ± 0.31	0.479
Lcad	1.00 ± 0.08	0.69 ± 0.12	0.061	1.00 ± 0.12	0.88 ± 0.33	0.757
Mcad	1.00 ± 0.16	0.78 ± 0.19	0.415	1.00 ± 0.13	0.89 ± 0.30	0.766
Hadha	1.00 ± 0.11	0.58 ± 0.07*	0.010	1.00 ± 0.13	0.82 ± 0.27	0.562
Inflammation						
Tnf-α	1.00 ± 0.11	0.58 ± 0.09*	0.013	1.00 ± 0.16	0.51 ± 0.05*	0.021
IL-1β	1.00 ± 0.15	1.38 ± 0.40	0.397	1.00 ± 0.15	3.34 ± 1.11	0.073
IL-6	1.00 ± 0.17	0.78 ± 0.13	0.352	1.00 ± 0.32	0.87 ± 0.23	0.767
Mcp-1	1.00 ± 0.15	1.11 ± 0.28	0.719	1.00 ± 0.12	0.55 ± 0.05**	0.005
Ccr2	1.00 ± 0.12	1.16 ± 0.27	0.598	1.00 ± 0.13	1.00 ± 0.20	0.980
Ccl3	1.00 ± 0.12	0.65 ± 0.12	0.072	1.00 ± 0.12	0.37 ± 0.03***	0.001
Ccl4	1.00 ± 0.10	0.92 ± 0.14	0.687	1.00 ± 0.16	0.51 ± 0.05*	0.021
Nos2	1.00 ± 0.23	1.19 ± 0.33	0.647	1.00 ± 0.15	0.81 ± 0.26	0.550
F4/80	1.00 ± 0.11	0.62 ± 0.08*	0.025	1.00 ± 0.09	0.55 ± 0.07**	0.002
Mgl2	1.00 ± 0.19	1.20 ± 0.27	0.554	1.00 ± 0.13	1.37 ± 0.33	0.307

Cd206	1.00 ± 0.17	1.57 ± 0.35	0.171	1.00 ± 0.14	0.62 ± 0.11	0.055
IL-10	1.00 ± 0.07	0.63 ± 0.11*	0.019	1.00 ± 0.11	1.18 ± 0.24	0.491
Arg1	1.00 ± 0.22	0.82 ± 0.17	0.556	1.00 ± 0.13	0.85 ± 0.24	0.646
Cd68	1.00 ± 0.12	0.66 ± 0.13	0.100	1.00 ± 0.16	0.46 ± 0.11*	0.016
Retnl	1.00 ± 0.44	1.70 ± 0.46	0.295	1.00 ± 0.13	1.21 ± 0.41	0.641
Fibrosis						
Tgf-β	1.00 ± 0.13	0.44 ± 0.08**	0.004	1.00 ± 0.14	0.58 ± 0.16	0.081
Col3a1	1.00 ± 0.19	0.80 ± 0.14	0.4414	1.00 ± 0.16	0.60 ± 0.17	0.112
Col6a1	1.00 ± 0.10	0.99 ± 0.11	0.988	1.00 ± 0.10	0.78 ± 0.20	0.391
Hif-1α	1.00 ± 0.08	1.04 ± 0.11	0.763	1.00 ± 0.24	0.81 ± 0.27	0.617
ER stress						
Xbp-1s	1.00 ± 0.08	0.83 ± 0.13	0.329	1.00 ± 0.13	0.74 ± 0.13	0.201
Xbp-1t	1.00 ± 0.07	0.81 ± 0.08	0.115	1.00 ± 0.07	0.90 ± 0.07	0.393
Chop	1.00 ± 0.05	0.87 ± 0.07	0.212	1.00 ± 0.18	0.59 ± 0.13	0.098
Atf4	1.00 ± 0.06	0.78 ± 0.06*	0.037	1.00 ± 0.06	0.81 ± 0.10	0.167
Oxidative stress						
Sod1	1.00 ± 0.14	0.97 ± 0.12	0.892	1.00 ± 0.08	0.94 ± 0.11	0.740
Sod2	1.00 ± 0.10	1.06 ± 0.12	0.713	1.00 ± 0.15	0.80 ± 0.18	0.468
Cox2	1.00 ± 0.21	1.05 ± 0.24	0.860	1.00 ± 0.18	0.86 ± 0.22	0.636
Nox4	1.00 ± 0.12	0.94 ± 0.10	0.762	1.00 ± 0.11	0.87 ± 0.16	0.539
Nqo1	1.00 ± 0.21	0.50 ± 0.13	0.077	1.00 ± 0.10	0.51 ± 0.05**	0.001

Table 2. Real-time PCR analysis of the expression of metabolic, inflammatory, and oxidative stress genes in visceral and subcutaneous fat depots of WT and *Pradc1* KO female mice fed a high-fat diet.

Discussion

PRADC1, as a novel metabolic regulator and secretory protein, is significantly suppressed in metabolically active tissues (liver, adipose, skeletal muscle, kidney, and heart), as well as in different brain regions (hypothalamus and cortex) during the refeeding phase following an overnight fast. The striking nutritional regulation of *Pradc1* expression suggests a metabolic function for this protein. We used a genetic loss-of-function mouse model to determine if PRADC1 is required for maintaining energy homeostasis.

Under non-stressed basal conditions when mice were fed a control low-fat diet, PRADC1 was dispensable for metabolic control. None of the major metabolic parameters—body weight, insulin sensitivity, fasting glucose, or serum lipid profiles—were significantly different between genotypes of either sex. However, significant sex-dependent phenotypes were revealed when *Pradc1* KO mice were challenged with a high-fat diet to induce obesity and metabolic dysfunction, underscoring the importance of sex as a significant biological variable in the physiologic response to high caloric intake (14-16). Obese male *Pradc1* KO mice consuming a high-fat diet appeared indistinguishable from WT littermates in whole-body glucose and lipid metabolism. In striking contrast, female *Pradc1* KO mice gained significantly less body weight and fat mass relative to WT littermates when fed a high-fat diet. Reduced adiposity is not due to any differences in food intake; rather, we attribute it, at least in part, to increased physical activity and energy

expenditure in *Pradc1* KO animals. We ruled out changes in thyroid or stress hormones, or circulating FGF-21 levels, as the possible cause of elevated physical activity and energy expenditure; none of these were significantly different between genotypes. Increased BAT thermogenic activity could result in greater energy dissipation; however, the body temperature was not significantly different between genotypes. Expression of *Ucp1* was, in fact, lower in BAT and iWAT of *Pradc1* KO mice compared to WT controls, thus ruling out uncoupling or "browning" of iWAT as a possible contributor to increased energy expenditure and lower adiposity seen in the KO animals. Sympathetic input via the adrenergic pathway can promote lipolysis in WAT and BAT, as well as BAT activation (17,18). Loss of PRADC1 could potentially lead to greater lipid turnover in adipose tissue. In fact, we observed reduced lipolysis in *Pradc1* KO female mice in response to a β_3-adrenergic receptor agonist (CL 316243) stimulation compared to WT controls. Thus, our data point to increased physical activity as a likely contributor to increased energy expenditure in *Pradc1* KO female mice fed a high-fat diet.

Excess adiposity is tightly linked to metabolic dysfunction (19). In the obese state, adipose tissue undergoes significant remodeling that impairs its functions; these include low-grade inflammation due to immune cells infiltration (11-13) and fibrosis (20). Due to elevated physical activity and marked reduction in body weight (~15%) between genotypes, we expected to see significant improvements in glucose and lipid metabolism in the female *Pradc1* KO mice relative to WT littermates. Surprisingly, the metabolic profiles—insulin sensitivity, fasting blood glucose and

serum lipid profiles, extent of hepatic steatosis, and adipose tissue inflammation—were largely indistinguishable between WT and *Pradc1* KO female mice. It appears that in this mouse model, physical activity and adiposity are uncoupled from metabolic health, and that enhanced locomotor activity and reduced fat mass are insufficient to improve local inflammatory milieu within the adipose tissue, as well as systemic glucose and lipid metabolism in the context of an obesogenic diet. The integrative nature of energy balance and whole-body metabolism entails complex regulatory mechanisms that remain poorly understood. While elevated physical activity generally confers significant health benefits in humans and animal models (21), there are subsets of humans where regular exercise appears to have only limited improvements in metabolic health (22). Increased adiposity due to obesity is known to be a major risk and contributing factor to impaired insulin action and metabolic health (19); conversely, reducing fat mass through exercise or surgical interventions often significantly improves insulin sensitivity and systemic glucose and lipid profiles (23-25). Thus, the uncoupling of physical activity and fat mass from systemic metabolic health seen in the *Pradc1* KO female mice sheds lights on the complex regulation of energy balance.

In summary, our effort to identity novel metabolically responsive secretory proteins led to the functional characterization of PRADC1. Future studies will help address whether the combination of phenotypes we observed in KO female mice are primarily due to the lack of PRADC1's action in peripheral tissues and/or brain where it is expressed. In light of how little is known about this evolutionarily

conserved protein, our studies lay the groundwork and provide a context to further interrogate PRADC1's function and mechanisms of action.

Supplemental Figures

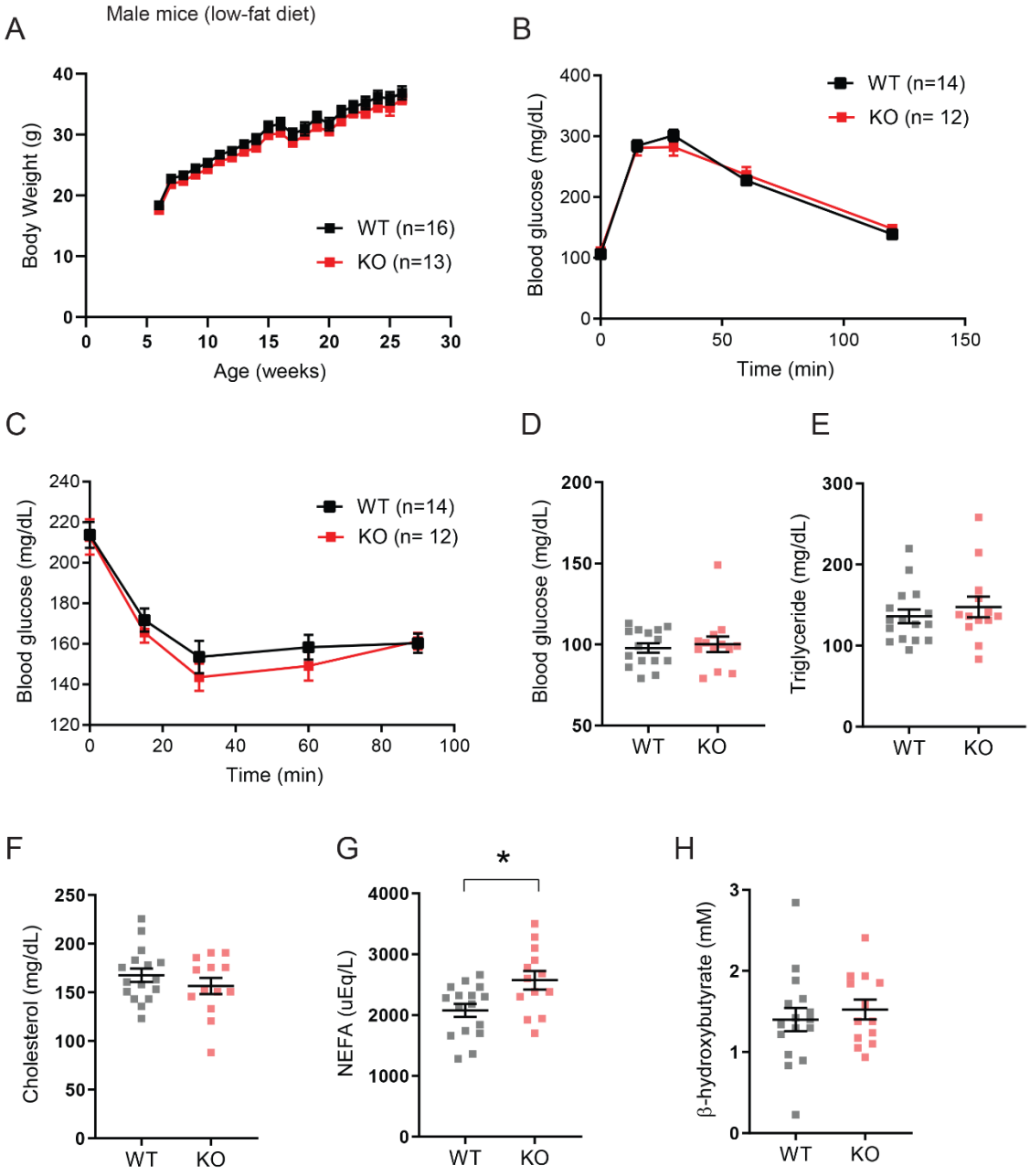

Supplemental Figure S1. Metabolic parameters of WT and Pradc1 KO male mice fed a control low-fat diet. ***A***, Body weight gain over time in WT (n=16) and KO (n=13) male mice. ***B-C***, Glucose tolerance **(B)** and insulin tolerance **(C)** tests in WT (n=14) and KO (n=12) male mice at 18 and 19 weeks of age. ***D-H***, Overnight fasting blood glucose, serum triglyceride, cholesterol, non-esterified free fatty acids (NEFA), and β-hydroxybutyrate in 17-week-old WT (n=16) and KO (n=13) male mice. Data are expressed as mean ± SEM. *P<0.05

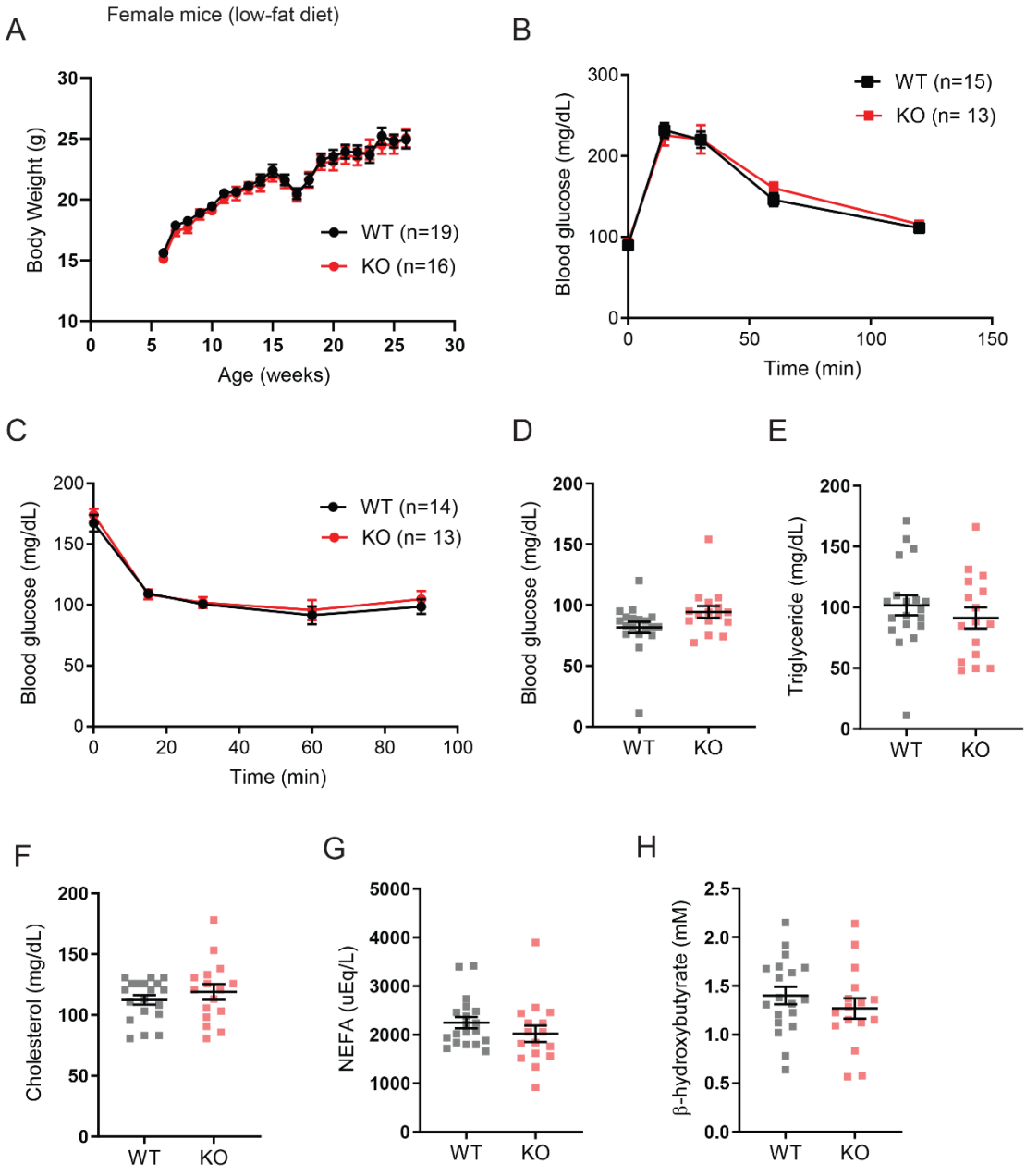

Supplemental Figure S2. Metabolic parameters of WT and Pradc1 KO female mice fed a control low-fat diet. ***A***, Body weight gain over time in WT (n=19) and KO (n=16) female mice. ***B-C***, Glucose tolerance **(B)** and insulin tolerance (C) tests in WT (n=14 or 15) and KO (n=13) female mice at 18 and 19 weeks of age. ***D-G***, Overnight fasting blood glucose, serum triglyceride, cholesterol, non-esterified free fatty acids (NEFA), and β-hydroxybutyrate in 17- week-old WT (n=19) and KO (n=16) female mice. Data are expressed as mean ± SEM.

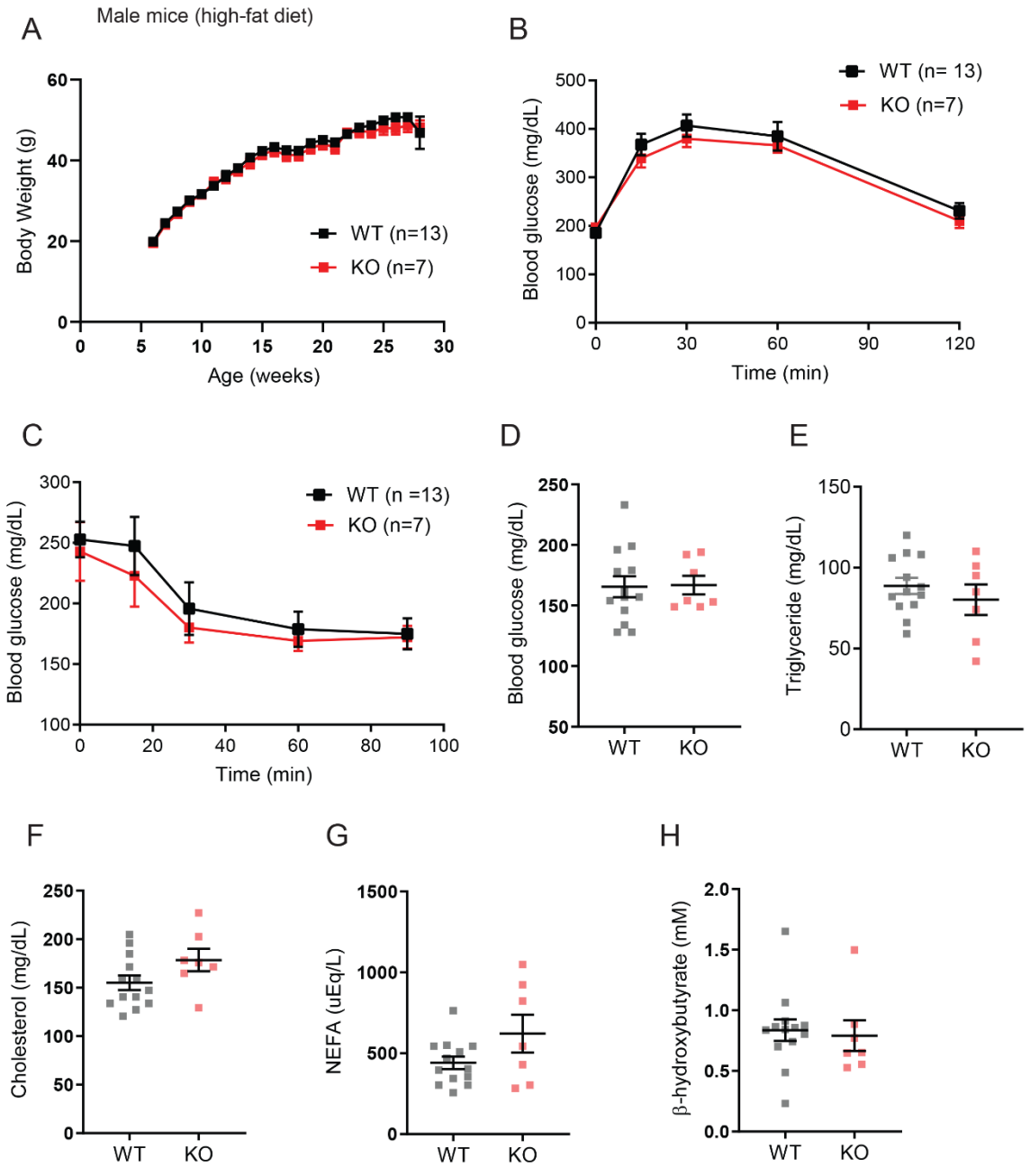

Supplemental Figure S3. Metabolic parameters of WT and Pradc1 KO male mice fed a high-fat diet. ***A***, Body weight gain over time in WT (n=13) and KO (n=7) male mice. ***B-C***, Glucose tolerance **(B)** and insulin tolerance **(C)** tests in WT (n=13) and KO (n=7) male mice at 18 and 20 weeks of age. ***D-H***, Overnight fasting blood glucose, serum triglyceride, cholesterol, non-esterified free fatty acids (NEFA), and β-hydroxybutyrate in 17-week-old WT (n=13) and KO (n=7) male mice. Data are expressed as mean ± SEM.

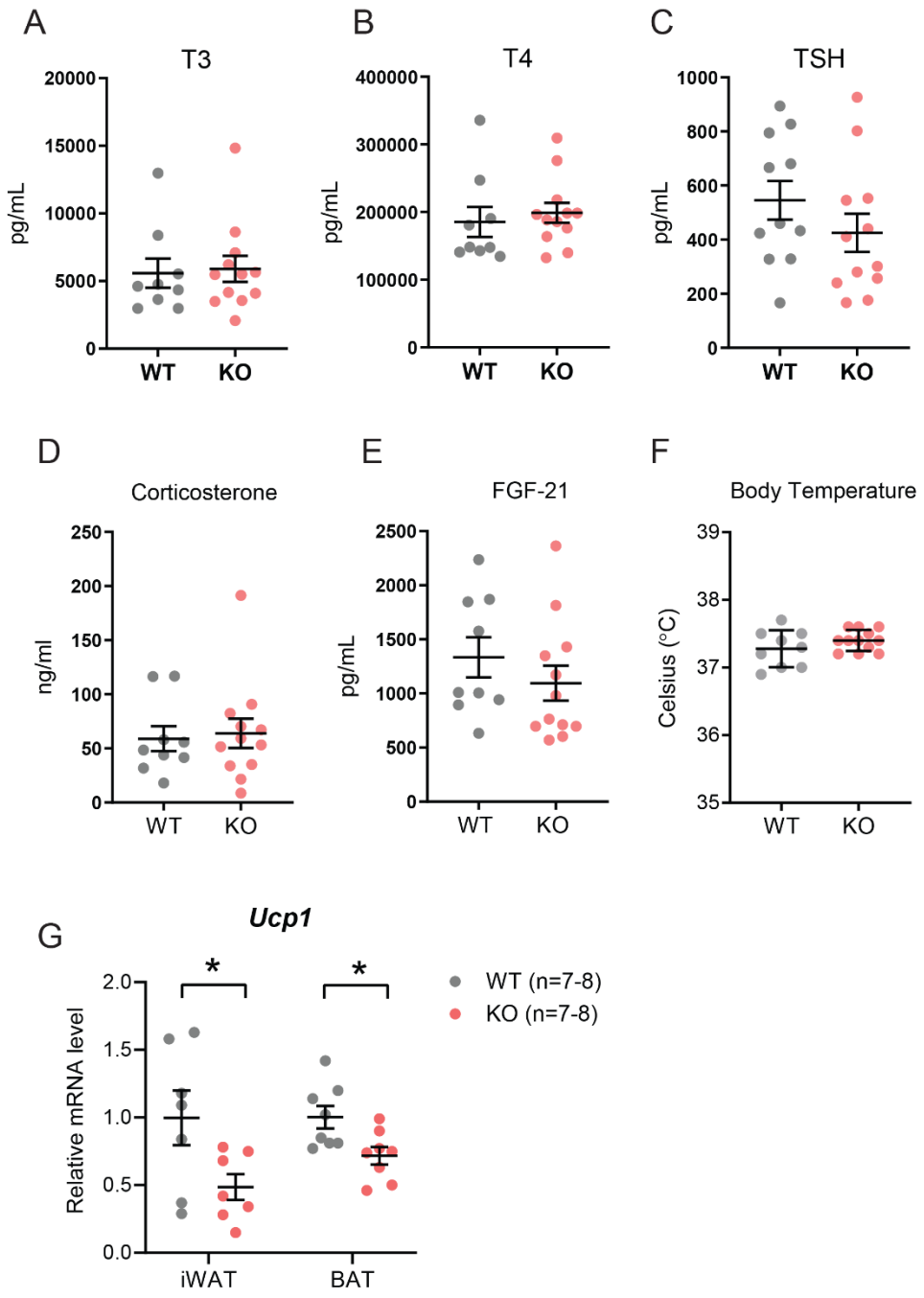

Supplemental Figure S4. Serum levels of thyroid hormones, corticosterone, FGF-21, and body temperature of WT and Pradc1 KO female mice fed a high-fat diet. ***A-E***, Serum T3, T4, thyroid stimulating hormone (TSH), corticosterone, and FGF-21 levels in 40-week-old WT (n=9-11) and KO (n=12) female mice. ***F***, Body temperature of WT and KO female mice as measured by a rectal probe (Physitemp; model BAT-12). ***G***, Real-time PCR analysis of Ucp-1 expression in inguinal white adipose tissue (iWAT) and interscapular brown adipose tissue (BAT) of WT and KO female mice. Data are expressed as mean ± SEM. *P<0.05

References

1. Clark, H. F., Gurney, A. L., Abaya, E., Baker, K., Baldwin, D., Brush, J., Chen, J., Chow, B., Chui, C., Crowley, C., Currell, B., Deuel, B., Dowd, P., Eaton, D., Foster, J., Grimaldi, C., Gu, Q., Hass, P. E., Heldens, S., Huang, A., Kim, H. S., Klimowski, L., Jin, Y., Johnson, S., Lee, J., Lewis, L., Liao, D., Mark, M., Robbie, E., Sanchez, C., Schoenfeld, J., Seshagiri, S., Simmons, L., Singh, J., Smith, V., Stinson, J., Vagts, A., Vandlen, R., Watanabe, C., Wieand, D., Woods, K., Xie, M. H., Yansura, D., Yi, S., Yu, G., Yuan, J., Zhang, M., Zhang, Z., Goddard, A., Wood, W. I., Godowski, P., and Gray, A. (2003) The secreted protein discovery initiative (SPDI), a large-scale effort to identify novel human secreted and transmembrane proteins: a bioinformatics assessment. *Genome Res* **13**, 2265-2270
2. Uhlen, M., Fagerberg, L., Hallstrom, B. M., Lindskog, C., Oksvold, P., Mardinoglu, A., Sivertsson, A., Kampf, C., Sjostedt, E., Asplund, A., Olsson, I., Edlund, K., Lundberg, E., Navani, S., Szigyarto, C. A., Odeberg, J., Djureinovic, D., Takanen, J. O., Hober, S., Alm, T., Edqvist, P. H., Berling, H., Tegel, H., Mulder, J., Rockberg, J., Nilsson, P., Schwenk, J. M., Hamsten, M., von Feilitzen, K., Forsberg, M., Persson, L., Johansson, F., Zwahlen, M., von Heijne, G., Nielsen, J., and Ponten, F. (2015) Proteomics. Tissue-based map of the human proteome. *Science* **347**, 1260419
3. Nanjappa, V., Thomas, J. K., Marimuthu, A., Muthusamy, B., Radhakrishnan, A., Sharma, R., Ahmad Khan, A., Balakrishnan, L., Sahasrabuddhe, N. A., Kumar, S., Jhaveri, B. N., Sheth, K. V., Kumar Khatana, R., Shaw, P. G., Srikanth, S. M., Mathur, P. P., Shankar, S., Nagaraja, D., Christopher, R., Mathivanan, S., Raju, R., Sirdeshmukh, R., Chatterjee, A., Simpson, R. J., Harsha, H. C., Pandey, A., and Prasad, T. S. (2014) Plasma Proteome Database as a resource for proteomics research: 2014 update. *Nucleic Acids Res* **42**, D959-965
4. Zhou, Y. B., Liu, F., Zhu, Z. D., Zhu, H., Zhang, X., Wang, Z. Q., Liu, J. H., and Han, Z. G. (2004) N-glycosylation is required for efficient secretion of a novel human secreted glycoprotein, hPAP21. *FEBS Lett* **576**, 401-407
5. Rodriguez, S., Lei, X., Petersen, P. S., Tan, S. Y., Little, H. C., and Wong, G. W. (2016) Loss of CTRP1 disrupts glucose and lipid homeostasis. *American Journal of Physiology - Endocrinology And Metabolism* **311**, E678-E697
6. Lei, X., Seldin, M. M., Little, H. C., Choy, N., Klonisch, T., and Wong, G. W. (2017) C1q/TNF-related protein 6 (CTRP6) links obesity to adipose tissue inflammation and insulin resistance. *Journal of Biological Chemistry* **292**, 14836-14850
7. Livak, K. J., and Schmittgen, T. D. (2001) Analysis of Relative Gene Expression Data Using Real-Time Quantitative PCR and the 2−ΔΔCT Method. *Methods* **25**, 402-408
8. Lei, X., Seldin, M. M., Little, H. C., Choy, N., Klonisch, T., and Wong, G. W. (2017) C1q/TNF-related protein 6 (CTRP6) links obesity to adipose tissue inflammation and insulin resistance. *J Biol Chem* **292**, 14836-14850
9. Petersen, P. S., Lei, X., Wolf, R. M., Rodriguez, S., Tan, S. Y., Little, H. C., Schweitzer, M. A., Magnuson, T. H., Steele, K. E., and Wong, G. W. (2017) CTRP7 deletion attenuates obesity-linked glucose intolerance, adipose tissue inflammation, and hepatic stress. *Am J Physiol Endocrinol Metab* **312**, E309-E325

10. Rodriguez, S., Lei, X., Petersen, P. S., Tan, S. Y., Little, H. C., and Wong, G. W. (2016) Loss of CTRP1 disrupts glucose and lipid homeostasis. *Am J Physiol Endocrinol Metab* **311**, E678-E697
11. Harman-Boehm, I., Bluher, M., Redel, H., Sion-Vardy, N., Ovadia, S., Avinoach, E., Shai, I., Kloting, N., Stumvoll, M., Bashan, N., and Rudich, A. (2007) Macrophage infiltration into omental versus subcutaneous fat across different populations: effect of regional adiposity and the comorbidities of obesity. *J Clin Endocrinol Metab* **92**, 2240-2247
12. Weisberg, S. P., McCann, D., Desai, M., Rosenbaum, M., Leibel, R. L., and Ferrante, A. W., Jr. (2003) Obesity is associated with macrophage accumulation in adipose tissue. *J Clin Invest* **112**, 1796-1808
13. Xu, H., Barnes, G. T., Yang, Q., Tan, G., Yang, D., Chou, C. J., Sole, J., Nichols, A., Ross, J. S., Tartaglia, L. A., and Chen, H. (2003) Chronic inflammation in fat plays a crucial role in the development of obesity-related insulin resistance. *J Clin Invest* **112**, 1821-1830
14. Mauvais-Jarvis, F. (2015) Sex differences in metabolic homeostasis, diabetes, and obesity. *Biology of sex differences* **6**, 14
15. Palmer, B. F., and Clegg, D. J. (2015) The sexual dimorphism of obesity. *Mol Cell Endocrinol* **402**, 113-119
16. Varlamov, O., Bethea, C. L., and Roberts, C. T., Jr. (2014) Sex-specific differences in lipid and glucose metabolism. *Front Endocrinol (Lausanne)* **5**, 241
17. Duncan, R. E., Ahmadian, M., Jaworski, K., Sarkadi-Nagy, E., and Sul, H. S. (2007) Regulation of lipolysis in adipocytes. *Annu Rev Nutr* **27**, 79-101
18. Cannon, B., and Nedergaard, J. (2004) Brown adipose tissue: function and physiological significance. *Physiol Rev* **84**, 277-359
19. Rosen, E. D., and Spiegelman, B. M. (2014) What we talk about when we talk about fat. *Cell* **156**, 20-44
20. Sun, K., Tordjman, J., Clement, K., and Scherer, P. E. (2013) Fibrosis and adipose tissue dysfunction. *Cell Metab* **18**, 470-477
21. Hawley, J. A., Hargreaves, M., Joyner, M. J., and Zierath, J. R. (2014) Integrative biology of exercise. *Cell* **159**, 738-749
22. Pandey, A., Swift, D. L., McGuire, D. K., Ayers, C. R., Neeland, I. J., Blair, S. N., Johannsen, N., Earnest, C. P., Berry, J. D., and Church, T. S. (2015) Metabolic Effects of Exercise Training Among Fitness-Nonresponsive Patients With Type 2 Diabetes: The HART-D Study. *Diabetes Care* **38**, 1494-1501
23. Poirier, P., Giles, T. D., Bray, G. A., Hong, Y., Stern, J. S., Pi-Sunyer, F. X., and Eckel, R. H. (2006) Obesity and cardiovascular disease: pathophysiology, evaluation, and effect of weight loss: an update of the 1997 American Heart Association Scientific Statement on Obesity and Heart Disease from the Obesity Committee of the Council on Nutrition, Physical Activity, and Metabolism. *Circulation* **113**, 898-918
24. Vitola, B. E., Deivanayagam, S., Stein, R. I., Mohammed, B. S., Magkos, F., Kirk, E. P., and Klein, S. (2009) Weight loss reduces liver fat and improves hepatic and skeletal muscle insulin sensitivity in obese adolescents. *Obesity (Silver Spring)* **17**, 1744-1748
25. Bradley, D., Magkos, F., and Klein, S. (2012) Effects of bariatric surgery on glucose homeostasis and type 2 diabetes. *Gastroenterology* **143**, 897-912

CURRICULUM VITAE

Ashley N. Stewart

Education

Johns Hopkins School of Medicine // Baltimore, MD
Ph.D. in Cellular and Molecular Physiology
2015-2020

University of the Sciences // Philadelphia, PA
B.S. in Microbiology, 3.64/4.0 GPA, *magna cum laude*
2011-2015

Research Experience

Graduate Researcher 2015-2020
Johns Hopkins School of Medicine, Department of Physiology
Principal Investigator: G. William Wong, PhD
Research Interests: 1) The role of N-linked glycosylation, disulfide linkages, and protein hydroxylation in regulating proteolytic processing, structure, and function of C1q/TNF-related proteins (CTRPs); 2) The role of CTRP4 in ulcerative colitis pathophysiology

Microbiology Intern 2014
GlaxoSmithKline, Consumer Healthcare
Principal Investigator: Linda Skowronski
Research Interests: 1) Develop an optimal preservative formulation to prevent growth of Burkholderia cepacian complex (*Bcc*) in aqueous consumer healthcare products; 2) Study growth requirements of *Bcc* under various manipulated environmental conditions

Undergraduate Researcher 2011-2015
University of the Sciences, Department of Biological Sciences
Principal Investigator: Peter Berget, PhD
Research Interests: Develop four modular protease biosensors for the detection of enzymes involved in hemostasis in human plasma

Publications

Sarver DC, **Stewart AN**, Rodriguez S, Little HC, Aja S, Wong GW. Loss of CTRP4 alters adiposity and food intake behaviors in obese mice. Am J Physiol Endocrinol Metab. 2020 Oct 5. doi: 10.1152/ajpendo.00448.2020. Epub ahead of print. PMID: 33017221.

Stewart AN, Little HC, Clark DJ, Zhang H, Wong GW. Protein Modifications Critical for Myonectin/Erythroferrone Secretion and Oligomer Assembly. Biochemistry. 2020 Jul 28;59(29):2684-2697.

Rodriguez S*, **Stewart AN*,** Lei X, Cao X, Little HC, Fong V, Sarver DC, Wong GW. PRADC1: a novel metabolic-responsive secretory protein that modulates physical activity and adiposity. FASEB J. 2019 Dec; 33(12):14748-14759.
*Both authors contributed equally to this work

Little HC, Rodriguez S, Lei X, Tan SY, **Stewart AN**, Sahagun A, Sarver DC, Wong GW. Myonectin deletion promotes adipose fat storage and reduces liver steatosis. FASEB J. 2019 Jul; 33(7):8666-8687.

Stewart AN, Tan SY, Clark DJ, Zhang H, Wong GW. N-Linked Glycosylation-Dependent and -Independent Mechanisms Regulating CTRP12 Cleavage, Secretion, and Stability. Biochemistry. 2019 Feb 12; 58(6):727-741.

Andrisse S, Childress S, Ma Y, Billings K, Chen Y, Xue P, **Stewart A**, Sonko ML, Wolfe A, Wu S. Low-Dose Dihydrotestosterone Drives Metabolic Dysfunction via Cytosolic and Nuclear Hepatic Androgen Receptor
Mechanisms. Endocrinology. 2017 Mar 1;158(3):531-544.

Other Professional Experience

Business Analyst 2020
EpiWatch Inc.
- Developed and executed competitive analysis strategy to identify lucrative consumer segments, determine unmet needs, and inform commercialization strategy
- Built concise and compelling materials for investor pitches highlighting the company's unique value proposition

Corporate Partnerships Fellow 2018-2020
Johns Hopkins Technology Ventures
- Analyze requests for proposals submitted by industry partners and develop catered research decks, resulting in over $3M of secured startup seed funding
- Assist with alliance management between Hopkins faculty and a Fortune 500 pharmaceutical company on a $20M research partnership focused on back of the eye diseases

Faculty Senate Representative 2017-2020
Johns Hopkins School of Medicine
- Represent >700 graduate students as the graduate student ambassador and liaison on a committee of 54 faculty
- Negotiated with faculty to enact policy changes that benefit students and trainees, resulting in the acceptance of 2 new faculty-student relationship policies

President, Biomedical Scholars Association 2016-2018
Johns Hopkins School of Medicine

- Facilitated development of the inaugural Accepted Applicants Visit program for prospective underrepresented minority (URM) PhD students, resulting in a significant increase in the URM population within one year
- Managed a $6000 annual budget and organized over 40 career development, community service, and social events per year to foster a sense of community and promote professional success among URM graduate students

Human Capital Director and Partnership Director, Shine Foundation 2015-2017

- Secured partnerships with 5 domestic abuse shelters and 2 financial service providers in Baltimore, and oversaw the development of 3 financial literacy programs
- Recruited and trained client-facing team members, leading to a 4.5-fold increase in the number of volunteers

Honors and Awards

2020 Bouchet Honor Society Inductee
2019 Maria del Carmen Vitery Graduate Student Award
2019 McKinsey Diversity Connect Participant
2018 Graduate Student Association Citizen of the Year
2018 Scientist Mentoring & Diversity Program for Biotech Scholarship
2018 JHU-CASSS Pharma and Biotech Industry Mentorship Program
2017 Ford Foundation Predoctoral Fellowship ($78,000)
2017 NSF Graduate Research Fellowship, Honorable Mention
2015 Norman F. Ramsey Commencement Research Award
2014 United Negro College Fund-Merck Research Science Initiative Fellowship ($25,000)